New Approaches to Optical Code-Division Multiple Access

Raymond Yim

Department of Electrical and Computer Engineering
McGill University
Montreal, Canada

September 2002

A thesis submitted to the Faculty of Graduate Studies and Research in partial fulfillment of the requirements for the degree of Master of Engineering

National Library of Canada

Acquisitions and Bibliographic Services

395 Wellington Street
Ottawa ON K1A 0N4
Canada

Bibliothèque nationale du Canada

Acquisisitons et services bibliographiques

395, rue Wellington
Ottawa ON K1A 0N4
Canada

Your file Votre référence
ISBN: 0-612-85902-9
Our file Notre référence
ISBN: 0-612-85902-9

Abstract

This thesis focuses on new strategies of designing Optical Code-Division Multiple Access (OCDMA) networks. Specifically, two new spreading code families of 2-dimensional (2D) wavelength-time system are considered: Depth-First Search Codes (DFSC) and Balanced Codes for Differential Detection (BCDD). DFSC utilizes a depth-first search algorithm to generate unipodal codes with maximum unit auto- and cross-correlation properties that are suitable for direct detection. These codes have similar interference-limited bit error rate (BER) performance as most 2D wavelength-time codes, but the algorithm can generate more codes, enabling the full potential of Forward Error Correction (FEC). BCDD defines a new set of high weight antipodal codes with relaxed correlation constraints that is suitable for differential detection. These codes can support approximately twice as many users as the other previously published OCDMA systems. Using a system with 32 wavelengths and 16 time chips operating at OC-12 transmission rates (622Mbps), BCDD can support an aggregate throughput of approximately 136Gbps when proper FEC is applied.

Furthermore, studies on the information theoretical capacity of chip synchronous OCDMA channel with Single User Detection (SUD) is conducted to obtain the ultimate throughput that can be achieved. Calculations are done under three assumptions: (i) interference-limited channel, (ii) interference-limited channel with Gaussian noise; or (iii) Gaussian approximated interference channel. In additions, system specific DFSC and BCDD capacity is obtained. These results are used as the basis for comparison among DFSC, BCDD and other previously proposed OCDMA systems. It is found that the maximum throughput of an OCDMA system is limited to about 0.7 bits per OCDMA chip. With the application of turbo code, BCDD can support an aggregate throughput of about 0.42 bits per OCDMA chip.

Sommaire

Cette thèse se concentre sur de nouvelles stratégies de conception des accès multiples à répartition des codes optiques (OCDMA). Spécifiquement, deux nouvelles familles sequences d'étalements de système à deux dimensions (2D) longueur d'onde-temps sont considérées: codes de recherche en profondeur (DFSC) et codes équilibrés pour la détection différentielle (BCDD). DFSC utilise un algorithme de recherche en profondeur pour produire des codes unipolaires avec autocorrélation et corrélation en retard unitaire convenant à la détection directe. Ces codes démontrent un taux d'erreur sur les bits (BER) limitée par interférence comparable à la plupart des codes 2D longueur d'onde-temps, l'avantage de cette méthode étant de générer plus de codes, ce qui permet une meilleure utilisation des techniques de correction d'erreurs sans voie de retour (FEC). BCDD définit un nouvel ensemble de codes antipolaires à poids élevé possédant des contraintes de corrélation relaxées qui convient à la détection différentielle. Ces codes peuvent soutenir deux fois plus d'utilisateurs que les systèmes d'OCDMA précédemment publiés. En utilisant un système avec 32 longueurs d'onde et 16 bribes de temps fonctionnant au taux de la transmission OC-12 (622Mbps), BCDD peut soutenir un débit global d'approximativement 136Gbps quand des techniques FEC appropriées sont appliquées.

De plus, des études sur la capacité théorique de canaux OCDMA asynchrones avec détection d'utilisateur simple (SUD) sont entreprises pour déterminer le débit maximum pouvant être réalisé. Les calculs sont effectués sous trois présuppositions: (i) canal limité par interférence, (ii) canal limité par interférence avec bruit gaussien; et (iii) canal à interférence gaussienne approximative. De plus, la capacité spécifique du DFSC et du BCDD est obtenue. Ces résultats sont employés comme base de comparaison entre le DFSC, BCDD et certains systèmes OCDMA précédemment proposés. On constate que la débit maximum d'un système d'OCDMA est limité à environ 0.7 bits par bribe d'OCDMA. Avec l'application de turbo-codes, BCDD atteint un débit global d'environ 0.42 bits par bribe d'OCDMA.

Acknowledgements

I would like to take this opportunity to show my sincere appreciation to my two supervisors: Prof. Jan Bajcsy and Prof. Lawrence Chen. It has been an extremely rewarding experience for me to be able to perceive communications in both the theory and practical point of view. On the practical side, Prof. Chen has given me a head start in understanding the OCDMA technology and optical hardware limitations, and he has proposed the use of balanced receiver, which is at the heart of this thesis. On the other hand, Prof. Bajcsy has enabled me to see the importance of coding in relations to the channel capacity. In many discussions, he has inspired me to touch on the fundamental issues that are keys to understand and expand on my observations. I am extremely thankful for their time and effort to instill me the many sides of research.

I would like to extend my thanks to my peers in McConnell Room 820. First of all, I thank Charif Beainy for his idea of chip analysis for the asynchronous capacity and for reviewing my thesis. Secondly, I want to thank Patrick Mitran for explaining the turbo decoding scheme, providing the srand interleaver for my turbo code simulations and reviewing my thesis. Additionally, I want to thank Naveen Mysore for the word template of this thesis. Finally, I want to thank all of them and Prof. Bajcsy for their development of the BCJR decoder that I have utilized for this thesis. I would also like to thank the other reviewers of this thesis, Julien Faucher and Xu Bo, for their many valuable suggestions. Also, I would like to thank Isabel Deslauriers for helping me to translate the thesis abstract to French.

Finally, I am thankful for the funding provided by the *Natural Science and Engineering Research Council* (NSERC) and the support that I have received from my family, so I can focus my efforts in the research. Also, I am grateful for the support from Annie Chau, who has stimulated me for a diverse and balanced growth.

I honor God, the First Cause of all, who has kept me up all days trying to seek the many mysteries that He has laid. Seek on...

Contents

Chapter 1 Introduction **1**

1.1 Demand for OCDMA Technology 1
1.2 Advantages and Evolution of OCDMA Technology 2
1.3 Thesis Overview 4
1.4 Contributions of this Thesis 4
1.5 Thesis Organization 5

Chapter 2 Preliminaries **6**

2.1 Fundamental Concepts of OCDMA 6
2.2 Progress in OCDMA Technology 7
2.2.1 Direct Detection 7
2.2.2 Differential Detection 11
2.2.3 Major Challenges in Current OCDMA Systems 13
2.3 Channel Capacity Concept 14
2.4 Forward Error Correction 15
2.4.1 Reed-Solomon Codes 16
2.4.2 Turbo Codes 17
2.4.3 Super Orthogonal Codes 19
2.4.4 Practicality Issues of FEC in Optical System 20

Chapter 3 Depth-First Search Direct Detection Codes **21**

3.1 Design Constraints and Algorithm 23

3.2 Code Generation Results 24
3.2.1 Effects of Changing the Code Size m and n 25
3.2.2 Effects of Changing the Hamming Weight 26
3.2.3 Comparison to Previously Proposed Systems 27
3.3 Performance Analysis 27
3.3.1 Average Variance Estimation 28
3.3.2 Binary Statistics Calculation 31
3.3.3 Comparison with existing 2D codes 35
3.3.4 The Impact of Forward Error Correction 37
3.4 Optical Simulation Example 37
3.4.1 Simulation Setup 37
3.4.2 Simulation Results 39

Chapter 4 Balanced Code for Differential Detection 44

4.1 Design Constraints and Algorithm 46
4.2 Code Generation Results 47
4.3 Performance Analysis 49
4.3.1 Average Variance Estimation 49
4.3.2 Binary Statistics Calculation 51
4.3.3 Forward Error Correction 54
4.4 Optical Simulation Results 55
4.4.1 Simulation Setup 55
4.4.2 Simulation Results 56

Chapter 5 Asynchronous OCDMA Channel Capacity 59

5.1 System Model of Asynchronous OCDMA 59
5.2 Capacity of Asynchronous OCDMA Transmission 61
5.2.1 Interference-Limited Channel without Noise 61
5.2.2 Capacity in the presence of AWGN Noise 63
5.2.3 Capacity under Gaussian Multiuser Interference Approximation 65
5.3 Comparison of Proposed 2D-OCDMA Systems 68
5.4 Spreading Sequence Specific Channel Capacity 70

5.4.1 DFSC Capacity 71
5.4.2 BCDD Capacity 72
5.5 Attempts to Reach the Channel Capacity 72
5.6 Chapter Summary 76

Chapter 6 Conclusion 77

6.1 Summary of Presented Work 77
6.2 Future Research Directions 79
6.2.1 Enhanced Coding Strategy for OCDMA 79
6.2.2 Multi Access Interference Cancellation and Detection 79
6.2.3 Synchronous and Fully Asynchronous OCDMA Capacity 82

Appendix A – Reed Solomon Codes 84

Appendix B – Turbo Codes 86

References 90

List Of Figures

Fig. 2.1 Schematic block diagram of an OCDMA network.................................. 6
Fig. 2.2 Common components used for OCDMA encoding/decoding: (a) spectral mask (b) optical tapped delay (c) fiber bragg grating. 8
Fig. 2.3 Schematic View of Balanced Receiver.. 11
Fig. 2.4 Graphical representation of differences between channel output distribution of (a) unipolar direct detection and (b) antipodal differential detection OCDMA. 12
Fig. 2.5 Input/output bit error probability of Reed-Solomon codes.................. 17
Fig. 2.6 Turbo-coded OCDMA network (a) encoder and (b) decoder................ 18
Fig. 2.7 Input/output bit error probability of rate 1/2 turbo code by Berrou *et al.* with interleaver size of 65536 bits [66]. 19
Fig. 2.8 Transmitted signals for (a) OOK-OOC with bit "1" and bit "0" are sent; (b) OOK-SOC with output of the convolutional encoder is "1010" (pulses in dash line are not transmitted).. 20
Fig. 3.1 Encoding of 2D MPPR/MPPC OCDMA code..................................... 22
Fig. 3.2 Decoding of 2D wavelength-time direct detection code when (a) sequence matches and (b) sequence mismatches. 22
Fig. 3.3 Schematic illustration of DFSC algorithm. 24
Fig. 3.4 Maximum number of codes generated as a function of (a) m with $n =$ 16 and (b) n with $m = 16$ for $w = 4$, 6 and 8. 26
Fig. 3.5 Maximum number of codes generated as a function of w for $n = 16$ and $m = 16, 24, 32, 48$... 26

Fig. 3.6 Calculated BER as a function of the number of simultaneous (active) users for (a) $n = 16$, $w = 6$ and m as a parameter; (b) $m = 16$, $w = 6$ and n as a parameter; (c) $m = 16$, $n = 16$ and w as a parameter.................................... 30
Fig. 3.7 Comparison of Gaussian approximated MAI distribution and results from binary statistics for DFSC(32,16,0.125) when the number of active users are (a) 10, (b) 40, (c) 80, and (d) 120. 33
Fig. 3.8 Comparison between estimated MAI variance (thick line) and results obtained from binary statistics (dots) for DFSC(32,16,0.125)............................ 34
Fig. 3.9 Comparison of BER performance of DFSC(32,16,0.125) using variance estimation (thick line) and binary statistics (dots). 35
Fig. 3.10 Comparing the BER as a function of simultaneous users for DFSC, YP and FFH. 36
Fig. 3.11 Spreading codes used for 8-user DFSC(16,16,0.125) system. Code number: (a) 1, (b) 2, (c) 3, (d) 10, (e) 12, (f) 20, (g) 26, (h) 30......................... 38
Fig. 3.12 8-User Optical Simulation Model. 39
Fig. 3.13 Two consecutive bit "1" for OCDMA signal for user with code 30. 40
Fig. 3.14 Decoded electrical signal (voltage versus time) for 8-user OCDMA system: (a) code 1, (b) code 2, (c) code 3, (d) code 10, (e) code 12, (f) code 20, (g) code 26 and (h) code 30.. 41
Fig. 3.15 Decoder output for user 10 with transmitted pattern "0011000100110000" and interference due to: (a) no other user; (b) user 12; (c) user 12 and 20; (d) user 2, 3, 12 and 20; (e) user 1, 2, 3, 12, 20, 26 and 30. 42
Fig. 4.1 Decoding of 2D wavelength-time differential detection code: (a) sequence matches; (b) sequence mismatches (In the figure, underlined number represent negative: $\underline{1}$ = -1)... 45
Fig. 4.2 High-level implementation of BCDD decoder....................................... 46
Fig. 4.3 Ratio of maximum number of generated codes to code size subject to different correlation constraints.. 48
Fig. 4.4 Performance comparison of the BCDD and DFSC............................... 51
Fig. 4.5 MAI distribution from binary statistics for BCDD(41,32,0.0991) when the number of active users is (a) 10, (b) 40, (c) 80 and (d) 120......................... 52

Fig. 4.6 Comparison between estimated MAI vairance (thick line) and results obtained from binary statistics (dots) for BCDD(41,32,0.0991). 53
Fig. 4.7 Comparison of BER performance of BCDD(41,32,0.0991) using variance estimation (thick line) and binary statistics (dots). 54
Fig. 4.8 BCDD(41,32) code generation and users supported at 10^{-9} with and without forward error correcting code. 55
Fig. 4.9 Decoded electrical signal (voltage versus time) for 8-user OCDMA system: (a) code 1, (b) code 2, (c) code 3, (d) code 4, (e) code 5, (f) code 6, (g) code 7 and (h) code 8. 57
Fig. 4.10 Decoder output for user 1 with transmitted pattern “101100111000” and interference due to: (a) no other user; (b) 1 user; (c) 2 users; (d) 4 users; and (e) 7 users 58
Fig. 5.1 Discrete memoryless channel model of a 3-user asychronous OCDMA system with SUD. 60
Fig. 5.2 Fundamental limits on asynchronous OCDMA transmission in a noise-free environment. 62
Fig. 5.3 Aggregate OCDMA throughput for different values of input probability 63
Fig. 5.4 Aggregate OCDMA throughput limits for equiprobable input distribution and different values of noise variance. 64
Fig. 5.5 OCDMA throughput at different noise variance with different input distribution for noise variance (a) $\sigma^2 = 0.09$ and (b) $\sigma^2 = 0.25$ 65
Fig. 5.6 OCDMA channel model using a Gaussian approximation for the MAI.. 66
Fig. 5.7 Aggregate OCDMA throughput for actual and approximated channel at different noise variance. 67
Fig. 5.8 Mean square error between the ideal OCDMA channel output density and the approximate output density. 68
Fig. 5.9 Comparison of the performance and the bound for the proposed 2D-OCDMA schemes in the interference-limited case. 69
Fig. 5.10 Channel models for (a) DFSC and (b) BCDD 70
Fig. 5.11 DFSC capacity for DFSC(32,16,0.167). 71

Fig. 5.12 BCDD capacity for BCDD(32,16,0.156)... 72
Fig. 5.13 Channel coding strategy for BCDD.. 73
Fig. 5.14 BER performance of BCDD(32,16,0.156) as a function of active users using (a) Berrou's turbo code with rate 1/2, and srand interleaver of length 10000 bits; (b) Berrou's turbo code with RS(255,239). 74
Fig. 5.15 BER as a function of the numbers of iterations for different numbers of active users.. 75
Fig. 5.16 BER performance of BCDD(32,16,0.156) as a function of active users using (a) Berrou's turbo code with rate 1/3, and srand interleaver of length 10000 bits; (b) Berrou's turbo code with RS(255,239). 75
Fig. 6.1 Signal vector representation for MAI cancellation: (a) before cancellation; (b) after cancellation. 80
Fig. 6.3 Multi-user multiple access channel (a) channel model (b) capacity region [59]... 82
Fig. 6.2 Two-user fully asynchronous OCDMA model (a) physical meaning (b) channel model. 83

List of Tables

Table 3.1 Percentage difference in Gaussian-approximated and calculated BER for DFSC.......... 32
Table 4.1 Differences between Gaussian approximated and calculated BER for BCDD.......... 52
Table 4.2 Spreading sequence of BCDD(48,4,0.125) used in demonstration.......... 56
Table 5.1 Channel characteristics with respect to the noise and MAI variance.......... 65

List of Terms

APD	Avalanche Photodiode
AWGN	Additive White Gaussian Noise
BCDD	Balanced Codes for Differential Detection
BCJR	Algorithm by Bahl, Cocke, Jelinek and Raviv
BER	Bit Error Rate
BPPM	Binary Pulse-Position Modulation
CDMA	Code-Division Multiple Access
CLT	Central Limit Theorem
CSMA/CD	Carrier-Sense Multiple Access with Collision Detection
DFSC	Depth-First Search Algorithm
DMC	Discrete Memoryless Channel
DSP	Digital Signal Processing
DWDM	Dense Wavelength Division Multiplexing
EOM	Electro-Optic Modulator
FBG	Fiber Bragg Grating
FEC	Forward Error Correction
FFH	Fast Frequency Hop Code
Gbps	Gigabits per second
i.i.d.	Independent Identically Distributed
ITU-T	International Telecommunication Union – Telecommunication Standardization

LAN	Local Area Network
LMS	Least Mean Square
MAC	Multi Access Channel
MAI	Multiple Access Interference
Mbps	Megabits per second
MMSE	Minimum Mean Square Error
MPPC	Multiple Pulse Per Column
MPPR	Multiple Pulse Per Row
MUD	Multiuser Detection
MVDR	Minimum Variance Distortionless Response
OCDMA	Optical Code-Division Multiple Access
OOC	Optical Orthogonal Codes
OOK	On-Off Keying
PH	Prime-Hop
PIN	P - Intrinsic material – N diode
pmf	Probability Mass Function
PRBS	Pseudo Random Binary Sequence
RS	Reed-Solomon
RSC	Recursive Systematic Code
SIR	Signal-to-Interference Ratio
SNR	Signal-to-Noise Ratio
SONET	Synchronous Optical Network
SOC	Super Orthogonal Codes
SOVA	Soft Output Viterbi Algorithm
SUD	Single User Detection
TPC	Turbo Product Codes
WDM	Wavelength Division Multiplexing
xDSL	Digital Subscriber Line
YP	Yu-Park Direct Detection Code

Chapter 1 Introduction

1.1 Demand for OCDMA Technology

With the explosion of Internet technology and the ever-increasing popularity of data networks, the demand for high bandwidth, low latency, secure and scalable communication systems has pushed the limit of current telecommunication technology. While Synchronous Optical Network (SONET) over Dense-Wavelength Division Multiplexing (DWDM) in optical fiber systems may provide terabit solutions in the long-haul backbone network, the same can not be said for the access point of the network, where conventional transmission media – twisted pair of copper wires and coaxial cable – lay an ultimate limit in delivering high-speed data. Nonetheless, the triumph of the photonic technology in high bit-rate long haul systems suggests that this limit may be removed by introducing optical fiber in the local area access network. A local area network (LAN) scenario is shown in Fig. 1.1.

A question remains: what is the best way of constructing an efficient high bit-rate optical local area access network? Traditional frequency and time division multiple-access (FDMA/TDMA) schemes have rather cumbersome protocols to deal with synchronization, slot allocation and other issues that occur in a multiple access user environment [1]-[2]. Furthermore, existing multiple access schemes (protocols), such as Ethernet and Token Ring, can only achieve a relatively low efficiency in terms of the traffic throughput and depend heavily on data processing in order to function properly [2]. These drawbacks have led one to envision the use of Code-Division Multiple-Access (CDMA) [3],[9],[21] as a mean to increase capacity in local area access networks. Optical Code-Division Multiple Access (OCDMA) has the potential of implementing transparent all-optical networks where multiple users transmit signal simultaneously without any coordination.

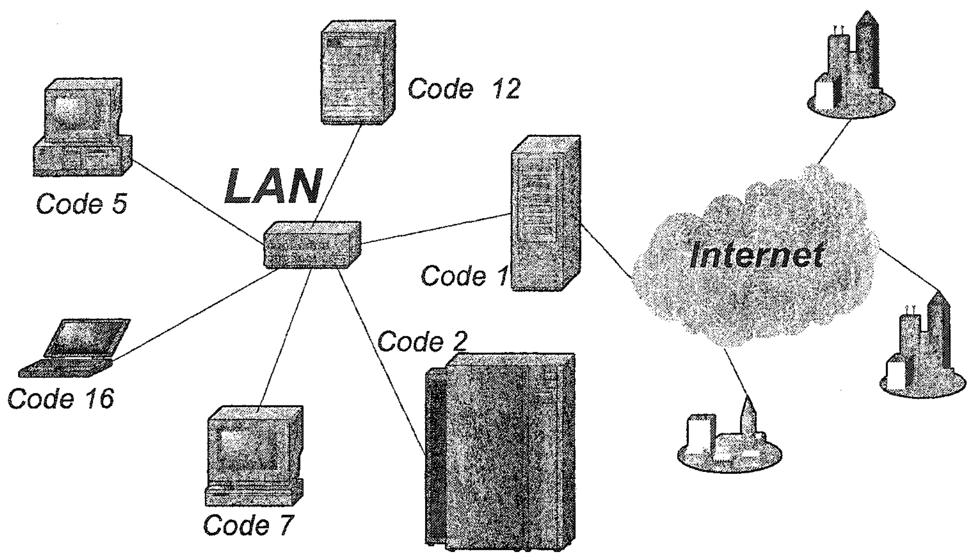

Fig. 1.1 A local area network communication system scenario.

1.2 Advantages and Evolution of OCDMA Technology

The major advantage of using CDMA technology in a local area access network environment is the ability to accommodate simultaneous information exchange among multiple users on the same medium without any coordination between users. Specifically, using a different signature pattern, or code as shown in Fig. 1.1, each user transmits on a common channel without the knowledge of the states of other active users. In traditional FDMA and TDMA systems, a specific frequency or time slot must be assigned either statically or dynamically by a centralized control system. This introduces additional overhead and latency in communication due to the use of protocol and circuit switching. The same holds true for other multiple access schemes, such as Aloha and Carrier-Sense

Multiple Access with Collision Detection (CSMA/CD, commonly known as Ethernet), where their aggregate throughput is closely tied to the latency of the system [4].

Traditional CDMA, on the other hand, can minimize the delay by allowing users to transmit information in an asynchronous fashion. Furthermore, unlike other multiple access schemes, in which a protocol is needed to communicate the destination address of the broadcast signal, CDMA embeds the address in the signature sequence. This not only increases the efficiency of transmission, but it adds security as another important advantage of CDMA systems. Without the knowledge of the signature sequence, it is much more difficult for an intruder to extract the encoded bit stream when compared to TDMA/FDMA systems. Other advantages of CDMA include soft user capacity, high noise tolerance and robustness to signal jamming.

The success of CDMA technology in wireless communications has inspired research into the use of this technique for asynchronous all-optical communication networks. In the past two decades, many researchers have laid the foundations for making the OCDMA technology feasible. Overall, the code design and performance analysis of one-dimensional time or spectral direct detection spreading sequences have been well studied. However, the performance of such systems is restricted due to the need for long spreading sequences. This requirement forces the system to run either at a low bit rate, or at super high chip rate, and such systems can only support a limited number of users.

Moreover, the limited ability to perform signal processing in optics due to the lack of optical registers, multipliers and memory, has been a stumbling block for creating low bit error rate (BER) systems. Nevertheless, the advancement of WDM technology and photonic device technologies, such as the introduction of fiber gratings and variable delay lines, opens a new area of research in two-dimensional wavelength-time OCDMA spreading sequences. The use of balanced receivers can offer a new strategy in differentially detecting OCDMA-encoded signals [39]-[53]. Furthermore, the advancement in Digital Signal Processing (DSP) technology has enabled the use of channel coding for high bit-rate communication systems [70],[76],[81]. These changes in technology enable fundamental changes and improvements in the design of OCDMA systems.

1.3 Thesis Overview

This thesis focuses on new theoretical and practical techniques to increase the throughput in OCDMA networks. We propose two new ways of designing 2D wavelength-time spreading sequences for OCDMA systems, one for direct detection and one for differential detection. Specifically, the Depth-First Search Code (DFSC) algorithm for direct detection has comparable performance with other existing systems, but it allows an increased number of spreading sequences to be generated. Also, Balanced Codes for Differential Detection (BCDD) employ a new set of constraints in their design and demonstrate a dramatic improvement in performance compared with all existing direct or differential detection systems. Furthermore, this is achieved without degradation in the maximum number of codes that can be generated – a highly desirable parameter when forward error correcting codes (FEC) are introduced in the system. In addition, we investigate the information theoretical capacity limit of an asynchronous OCDMA channel. This result gives both a basis for comparing various OCDMA schemes and possible directions for future OCDMA research. In the attempt to reach the calculated capacity, we apply turbo codes and Reed-Solomon codes to the proposed spreading sequences. Finally, various other feasibility studies have been conducted on novel concepts that can be applied to OCDMA systems, such as interference cancellation techniques and multiuser detection.

1.4 Contributions of this Thesis

This thesis presents three novel contributions to the communication engineering community. The Depth-First search algorithm has been published in the *IEEE Photonics Technology Letters* under the title "Design and Performance of 2-D Codes for Wavelength-Time Optical CDMA" [5]. The work on Balanced Codes for Differential Detection has been presented at the *5th International Conference on Application of Photonic Technology (Photonic North 2002)* under the title "2D Wavelength-Time Codes for Optical Code-Division Multiple-Access with Differential Detection" [6], and has been submitted to the *IEEE Photonics Technology Letters* under the title "A New Family of 2D Wavelength-Time Codes for Optical CDMA with Differential Detection" [7]. Finally, the investigation on the capacity of OCDMA channel has been presented at the *21st Biennial Symposium on Communications* under the title "On the Capacity Limit of Asynchronous OCDMA with Single User Detection" [8], and an extended work will be submitted under the title "On the Use of Channel Coding in Approaching the Optical CDMA Capacity".

1.5 Thesis Organization

The remainder of this thesis is organized as follows. Chapter 2 will present the fundamentals of CDMA in a multiple access channel, the progress of OCDMA technology during the past two decades and the power of channel coding in delivering a high performance data network. In Chapter 3, the design, analysis and performance of 2D wavelength-time DFSC for direct detection systems are presented, and comparisons are made to existing 2D wavelength-time codes. In Chapter 4, the design, analysis and performance of 2D wavelength-time BCDD are presented. For both DFSC and BCDD, simulation results are shown to assess the basic physical impairments of such systems. In Chapter 5, the asynchronous OCDMA transmission is modeled in a noiseless and noisy environment. Channel capacity calculations are performed, and the obtained results are used to compare the performance of existing 2D wavelength-time systems against the fundamental limits. Furthermore, an initial exploration of channel code to reach the channel capacity has been conducted. Finally, Chapter 6 summarizes our results and proposes possible directions to extend this work.

Chapter 2 Preliminaries

2.1 Fundamental Concepts of OCDMA

Optical Code Division Multiple Access (OCDMA) operates as a multi access channel (MAC) in which all users transmit and receive encoded signals on the same fiber. Diagrammatically, Fig. 2.1 shows the block diagram of a generic physical channel model. Note that this diagram can be applied to any of the OCDMA systems that will be discussed in this thesis by modifying the content of the components listed. In the figure, dashed lines represent electric signals, and solid lines represent optical signals.

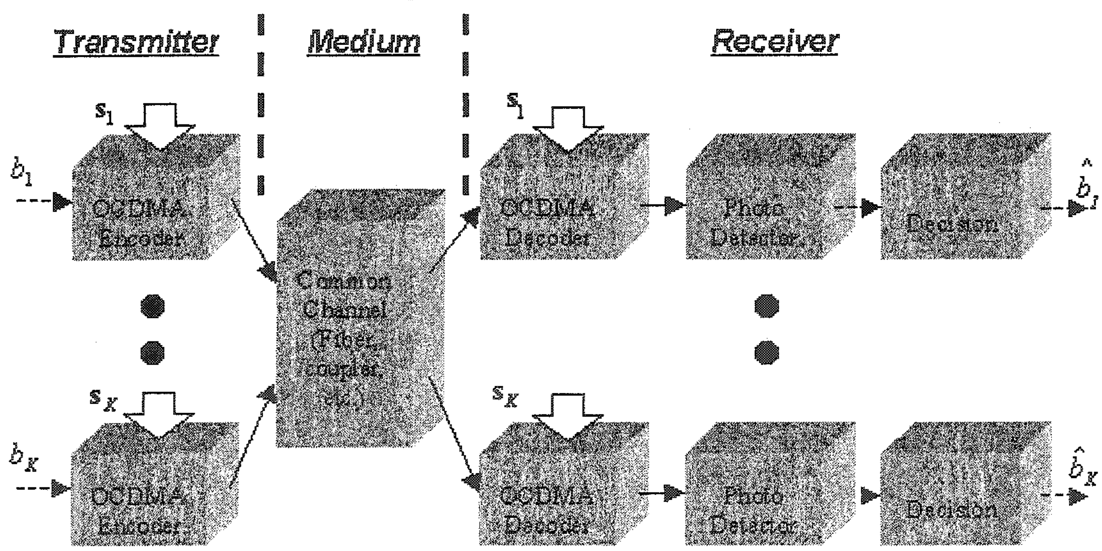

Fig. 2.1 Schematic block diagram of an OCDMA network.

On the transmitter side of an OCDMA system, an OCDMA encoder is used to encode the input data bit stream ($\mathbf{b}_j$) into an optical signal depending on the signature sequence ($\mathbf{s}_j$) that is distinct for each user on the system. This encoded signal is multiplexed with the signals generated from all other users, and it is redistributed to each user using the same fibers. At the receiver side, an OCDMA decoder uses a matched filter that matches to the signature sequence of the desired user. Depending on the technology of choice, this decoded optical signal is then passed into a direct detection photo-detector (e.g., InGaAs PIN, Ge APD, etc.) or a differential detection balanced receiver, which generates an electrical signal. The binary sstream ($\hat{\mathbf{b}}_j$) can be obtained from the electrical signal by properly setting the threshold for hard decision, or by performing soft decision decoding depending on the channel code.

2.2 Progress in OCDMA Technology

Ever since its introduction in 1983 by Shaar and Davis [9], many approaches for realizing an all-optical OCDMA network have been considered. In general, OCDMA technology can be classified into six major categories: (i) Incoherent Pulse Amplitude Encoding, (ii) Coherent Pulse Phase Encoding, (iii) Spectral Phase Encoding, (iv) Spectral Amplitude Encoding, (v) Spatial Encoding, and (vi) Hybrid Encoding such as wavelength-time codes. Among these six categories, direct and differential detection can be applied. Other classifications involve coherent and incoherent encoding, as well as synchronous and asynchronous transmission. This section provides a literature survey of the current OCDMA technology.

2.2.1 Direct Detection

Most direct detection OCDMA systems employ on-off keying (OOK) modulation, where optical power is sent following the spreading sequence of choice when the user transmits bit "1", while nothing is sent for bit "0". After the encoded signal passes through the OCDMA decoder, the photo-detector picks up all the power within the detection chip window. For hard decision, due to the unipolar nature of the transmitted signal, the electrical output signal is then passed into a decision circuit with threshold set at a point determined by the Hamming weight (w), i.e., the number of chips used to transmit bit "1", and the average of total multiple access interference (μ) caused by other users in the system.

In general, assuming synchronization at the chip level and setting the detection threshold at $\mu + w/2$, the Gaussian-approximated average interference-limited bit error rate (BER) performance for K active users is [10]:

$$BER = Q\left(\frac{1}{2}\sqrt{\frac{w^2}{(K-1)\bar{\sigma}_{pq}^2}}\right) = Q\left(\frac{1}{2}\sqrt{SIR}\right), \qquad (2.1)$$

where $\bar{\sigma}_{pq}^2$ represents the average aperiodic cross-correlation variance between each code pair p and q over the four possible 2-bit combinations "00", "01", "10" and "11", and $Q(x) = \frac{1}{\sqrt{2\pi}}\int_x^{\infty}\exp(-t^2/2)dt$.

Some common components for performing encoding and decoding for OCDMA include spectral mask [11], optical tapped delay [21], and Fiber Bragg Grating (FBG) [12] as shown in Fig. 2.2 (a), (b) and (c) respectively.

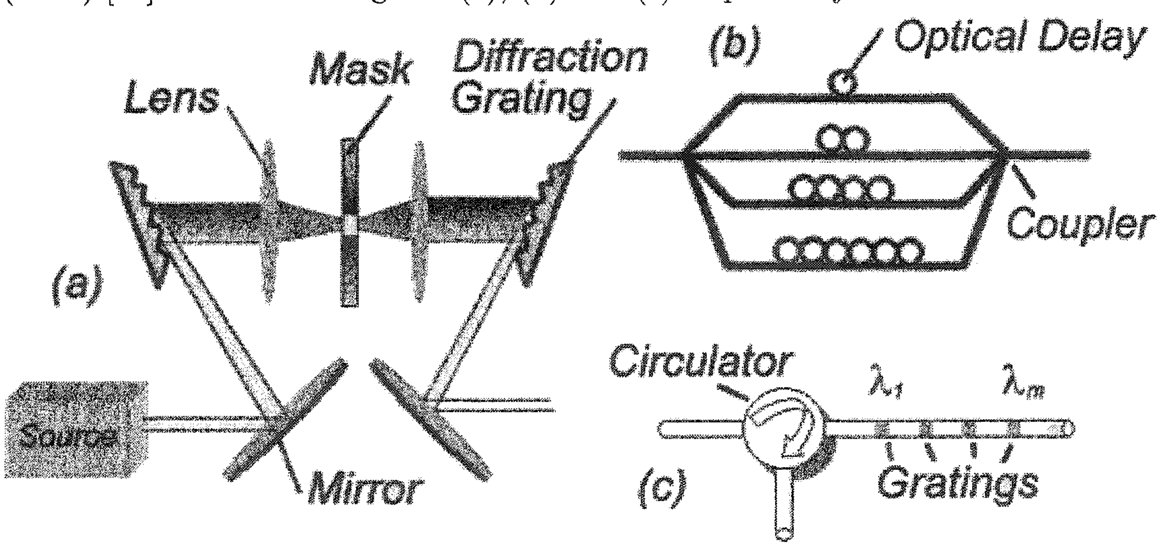

Fig. 2.2 Common components used for OCDMA encoding/decoding: (a) spectral mask (b) optical tapped delay (c) fiber bragg grating.

2.2.1.1 Incoherent Pulse Amplitude Encoding

Any optical source has a finite coherence length, which governs the duration that the phase of a wave is relatively unchanged. For instance, a broadband white light source has a coherence length of about 900nm, a Fabry Perot laser has a coherence length of approximately 100μm, and an ultra stabilized He-Ne laser has a coherence length of 15,000km [13]. In general, components with long coherence length are more expensive to manufacture. For an economical system, incoherent pulse amplitude encoding detection neglects any phase information of the encoded signal, and it directly detects optical power in a particular chip window. Since the cross-correlation between each code pair directly affects the received interference power, and thus the performance of a system, in the past, many spreading code families have been developed for such types of systems in the attempts to minimize the aperiodic cross-correlation between user codes. These include prime codes [9], m-sequences [14], gold sequences [15] and optical orthogonal codes [16]-[24]. For such systems, optical signals are encoded at points beyond the coherence length of the optical source using optical tapped delay lines as shown Fig. 2.2(b). The signature sequences are sparsely spaced (low Hamming weight) pseudo-orthogonal codes, thus the aperiodic cross correlation between codes can be made to be less than or equal to some small value (either 1 or 2 depending on the code families).

2.2.1.2 Spectral Phase Encoding

For spectral phase encoding, a grating is used to diffract a unipolar sub-picosecond pulse onto a pseudorandom spatially patterned phase mask inserted between two confocal lens pair as shown in Fig. 2.2(a) [24]-[29]. This introduces pseudorandom phase shifts among different spectral components of the transmitted signal. At the decoder, a phase conjugate mask is used to extract the encoded signal. When the decoding mask is properly matched, the spectral phase shifts are removed and the original sub-picosecond pulse is reconstructed. Otherwise, the decoder simply spectrally re-spreads the encoded signal, and the pulse cannot be reconstructed. A threshold device (usually a nonlinear optical device) is used to detect if a peak occurs in the decoded signal.

2.2.1.3 Spatial Encoding

In contrast with wireless CDMA where only one communication medium exists for transmitting the signal, multiple fibers can be laid to create parallel communication channels for OCDMA systems. Other spatial encoding systems employ free-space optics to achieve parallel channels. Many implementations of such systems have been considered, such as two-dimensional Optical Orthogonal Signature Pattern Codes (OOSPC) [30]-[31] and spatial OCDMA codes [32]-[34].

2.2.1.4 Hybrid Encoding

There are many types of hybrid encoding schemes, such as wavelength-time and space-wavelength-time codes. We focus the discussion on wavelength-time codes in this thesis. The paradigm of wavelength-time direct detection encoding is very similar to the one-dimensional (1D) temporal codes. For 1D codes, the code size is directly affected by the number of time chips that it has in a bit period. This results in the use of either extremely short pulses, which is very difficult to match and detect, or a very slow bit rate for sending data. For wavelength-time encoding, it exploits an additional degree of freedom by using multiple wavelengths together with time spreading in the design of the spreading sequences. The advantage is that a higher bit rate can be accommodated with the same code size. Furthermore, it is also easier to design user codes that satisfy specific auto- and cross-correlation constraints. Note that the aperiodic cross-correlation should only be considered in the time-domain. Some examples include Fast Frequency Hopping (FFH) [35], wavelength-time prime-hop (PH) sequences [36], and Yu-Park (YP) code construction (which defines a mapping algorithm to produce 2D OCDMA spreading sequences from 1D prime sequences) [37]. Most of these constructions are based on the use of FBG technology, as shown in Fig. 2.2(c), and array waveguide gratings. The performance analysis of such 2D OCDMA codes is the same as the 1D counterpart.

2.2.2 Differential Detection

Differential detection is enabled by the use of a balanced receiver. For such receivers, two photo-detectors are placed at the output of the OCDMA decoder as shown in Fig. 2.3. Depending on the encoding scheme, the output of the decoder is directed to the positive or negative terminal based on the wavelength, time-chip or phase information. At the output of the balanced receiver, the power detected on the negative terminal is subtracted from the power detected on the positive terminal, and a bipolar electrical signal can be obtained at the output. The hard decision threshold is set to zero for such systems.

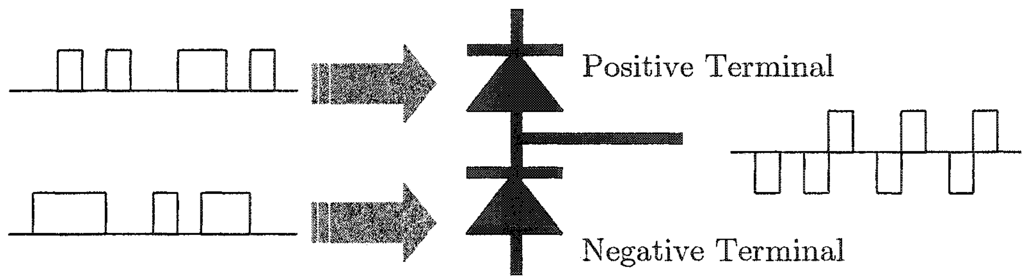

Fig. 2.3 Schematic View of Balanced Receiver.

Usually, two distinct optical signals are employed to transmit the bit "1" and "0" to be used for differential detection. In general, the interference-limited BER performance of an OCDMA system employing antipodal signaling [38] is (derivation shown in section 4.3.1.1):

$$BER = Q\left(\sqrt{\frac{w^2}{(K-1)\bar{\sigma}_{pq}^2}}\right) = Q\left(\sqrt{SIR}\right), \tag{2.2}$$

where, as stated previously, $\bar{\sigma}_{pq}^2$ represents the average aperiodic cross correlation variance between each code pair p and q over the four possible 2-bit combinations "00", "01", "10" and "11". As one can see from the equation, for the same signal-to-interference (SIR) ratio, the BER of a differential detection system performs better than direct detection systems. In Fig. 2.4, the differences between the channel output distributions of the two detection schemes are demonstrated when Gaussian approximations are used to model the multiple access interference (MAI) for a large number of active users in the system.

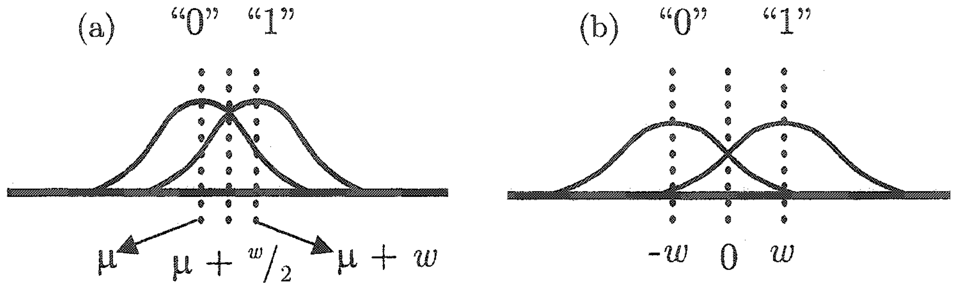

Fig. 2.4 Graphical representation of differences between channel output distribution of (a) unipolar direct detection and (b) antipodal differential detection OCDMA.

2.2.2.1 Coherent Pulse Phase Encoding

There have been two generations of coherent OCDMA systems. The very first form employed the use of a ladder network, in which two fibers were employed to provide parallel spatial channels for the encoded signal [39]-[41]. For such schemes, all transmitted power can be rerouted onto the same chip when the spreading sequences match, thus increasing the signal power, and hence the BER performance, at the output.

A later form of coherent pulse phase encoding emits phase-modulated narrow optical pulses using an Electro-Optic Modulator (EOM). The pulse is then encoded by an optical tapped delay line with different delays and predetermined phase shifts on each branch [42]-[46]. This effectively creates optical bipolar codes. At the receiver, a phase lock loop is employed to recover the carrier phase information for demodulation purposes, and a balanced detector is employed to extract the bipolar signal depending on the phase of the incoming signal.

2.2.2.2 Spectral Amplitude Encoding

Instead of using the phase information of the optical signal, which depends directly on the coherence length of an optical source and can be expensive to implement, spectral amplitude encoding uses the wavelength of an encoded signal to route optical power into the positive and negative terminals of the balanced receiver. Some examples of spectral amplitude encoding include Walsh-Hadamard [11], bipolar [47]-[51] and m-sequence [52].

2.2.2.3 Wavelength-time Encoding

Differential detection can also be employed in wavelength-time encoding. An optical tapped delay line can be used when the wavelengths of an optical signal are separated. The balanced receiver can then pick up the appropriate power in the positive and negative terminals depending on the spreading sequence. An example of such a code is the prime/OOC [53]. Two distinct optical orthogonal codes (OOC) are used for each user to transmit the "1" and "0" bits. At the decoder, the positive terminal picks up the power corresponding to the spreading sequence for bit "1, and negative terminal for bit "0".

2.2.3 Major Challenges in Current OCDMA Systems

In contrast with wireless CDMA systems, which are traditionally used for voice and low data rate communication, OCDMA can exploit the high bandwidth available in a fiber to achieve high data rate communication. Hence, a more stringent BER requirement is needed. Typically, a benchmark BER requirement for such a system is at 10^{-9}, or one errant bit in a billion. Due to the inference-limited nature of CDMA, it is extremely difficult to achieve a low BER when a large number of users are present. Previously, designs of most OCDMA systems have focused on reducing the cross-correlation between each code pair in a sequence family. It is true that such systems can enhance the BER performance by limiting the amount of interference between each user; however, it also limits the maximum number of codes that can be generated, thus only a limited number of users can be supported even when good channel coding strategies are employed. For example, prime sequences force the cross-correlation between each code pair to be less than or equal to two [9], but it can generate only p spreading sequences in a time spread system with p^2 time chips. This restricts the efficiency of the channel throughput to be at most $1/p$. Similarly, for a system employing OOCs, the cross-correlation between each code pair is less than or equal to one, but for time spread systems with n time chips and a Hamming weight w, the cardinality Φ of any set of OCDMA codes with unit auto- and cross-correlation is limited by the Johnson bound [54]:

$$\Phi_{OOC} \leq \frac{n-1}{w(w-1)}. \qquad (2.3)$$

In other words, the maximum efficiency of a 1D OOC system will always be less than approximately $1/w^2$. For 2D wavelength-time codes, the maximum number of users that a Fast Frequency Hop (FFH) system can support is equal to the number of wavelengths available in the system. Finally, the only existing 2D differential system Prime/OOC has a maximum number of codes equal to mp when m wavelength and p^2 time chips are used, which corresponds to an efficiency of $1/p$.

It is a significant challenge to increase the number of codes that a code family can accommodate while maintaining a relatively low BER performance. This involves the use of suitable spreading sequences, detection techniques, and channel coding strategies.

2.3 Channel Capacity Concept

As one seeks ways of improving the throughput of an OCDMA system, it is important to know the absolute maximum throughput. This gives insight in finding a suitable channel coding strategy to allow reliable communication. The concepts in information theory [57] can be applied to any channel model to determine the maximum rate at which data can be sent across a channel with error probability approaching zero as the block length is made arbitrary large. Fundamentally, the channel capacity is given by the source probability that maximizes the mutual information of the channel. For a discrete-memoryless channel, the channel capacity C in bits per channel use is given by [58]:

$$C = \max_{p(x)} I(X;Y) = \max_{p(x)}[H(Y) - H(Y \mid X)] = \max_{p(x)}[H(X) - H(X \mid Y)], \qquad (2.4)$$

where $I(X;Y)$ denotes the mutual information between the input X and the output Y of the channel. $H(.)$ and $H(.|.)$ are the entropy and the conditional entropy. They measure the uncertainty of X and X given Y and are defined by [58]:

$$H(X) = -\sum_{x\in X} p(x)\log p(x); \quad (2.5)$$

$$H(Y \mid X) = -\sum_{x\in X}\sum_{y\in Y} p(x,y)\log p(y \mid x). \quad (2.6)$$

For a Gaussian Channel, where input X is corrupted by Additive White Gaussian Noise (AWGN) Z with variance σ^2, the channel capacity is given by the differential entropy [59]:

$$C = \max_{p(x)} H(Y) - \frac{1}{2}\log\left(2\pi e\sigma^2\right). \quad (2.7)$$

With respect to the channel signal-to-noise ratio ($\mathrm{SNR_c}$), the capacity of a discrete-time AWGN channel is given by the following expression [59]:

$$C = \frac{1}{2}\log\left(1 + SNR_c\right), \quad (2.8)$$

where SNR_c is defined by the ratio of signal power to the noise power.

In a broadcast network, the total aggregate capacity of the network, or the sum capacity, is sum of individual capacities that are available to each user in the system.

2.4 Forward Error Correction

It is extremely rare that information can be transmitted reliably over a noisy or interference-limited channel near the capacity without the aid of clever channel coding strategies. Forward Error Correction (FEC) coding has been proven to be an excellent way of lowering the BER performance of any system. The general idea of FEC involves the addition of redundant symbols into the user data. At the receiver, due to the existence of noise and interference, some of the transmitted bits will be corrupted. However, since the transmitter has sent more bits than necessary, the redundant information can be used to identify and correct the errant received bits.

The most basic error correcting code is a 3-bit repetition code, where each user bit is transmitted over three bit periods with the same information. If one of the three bits transmitted is damaged, the other two bits can be used to recover the desired signal with a higher probability. One drawback to such an approach is the lower information bit rate. A 3-bit repetition code sacrifices 67% of the channel throughput to transmit redundant information. Over the past sixty years, coding theorists have discovered many FEC codes that can lower the BER while maximizing the efficiency of transmission. Some of the major ones include Hamming Codes [59], Reed-Solomon codes [61], convolutional codes [62]-[64] and turbo codes [65]. FEC has previously been considered for use in OCDMA systems [70],[76],[77]. In the scope of this thesis, Reed-Solomon and turbo codes are used.

2.4.1 Reed-Solomon Codes

Reed-Solomon codes are a type of non-binary cyclic codes that are suitable for correcting burst noise. Such codes are used in modern storage devices such as compact disks (CDs) and Digital Video Disks (DVDs), in high-speed modems such as Digital Subscriber Line (xDSL) [66]-[67], in space communications, in submarine systems [68] and in high-speed optical backbone networks [69]. In OCDMA, Reed-Solomon codes have also been considered in conjunction with OOK-OCDMA signalling [70]. Fundamentally, Reed-Solomon codes are composed of symbols over a Galois Field GF(2^m), where m is a positive integer that is larger than 2. In general, for a Reed-Solomon code composed of $n = 2^m - 1$ code symbols with k data symbols, RS(n,k) has an input/output bit error probability (P_{in}/P_{out}) relationship as follows [72]:

$$P_{out} \approx \frac{1}{2n} \sum_{j=t+1}^{n} j \binom{n}{j} \left[1 - (1 - P_{in})^m\right]^j (1 - P_{in})^{m(n-j)}, \qquad (2.9)$$

where $t = (n\text{-}k)/2$ is the symbol-error correcting capability of the code. For Reed Solomon code over GF(2^8), the input/output bit error rate performance at different redundancy symbol size is shown in Fig. 2.5.

For the benchmark BER of OCDMA systems at 10^{-9}, RS(255,239) lowers a channel BER of $3.5\text{x}10^{-4}$ to 10^{-9}, and RS(255,223) improves a channel BER of $1.6\text{x}10^{-3}$ to 10^{-9}. For details regarding the encoding and decoding process of Reed-Solomon codes, please refer to the Appendix A.

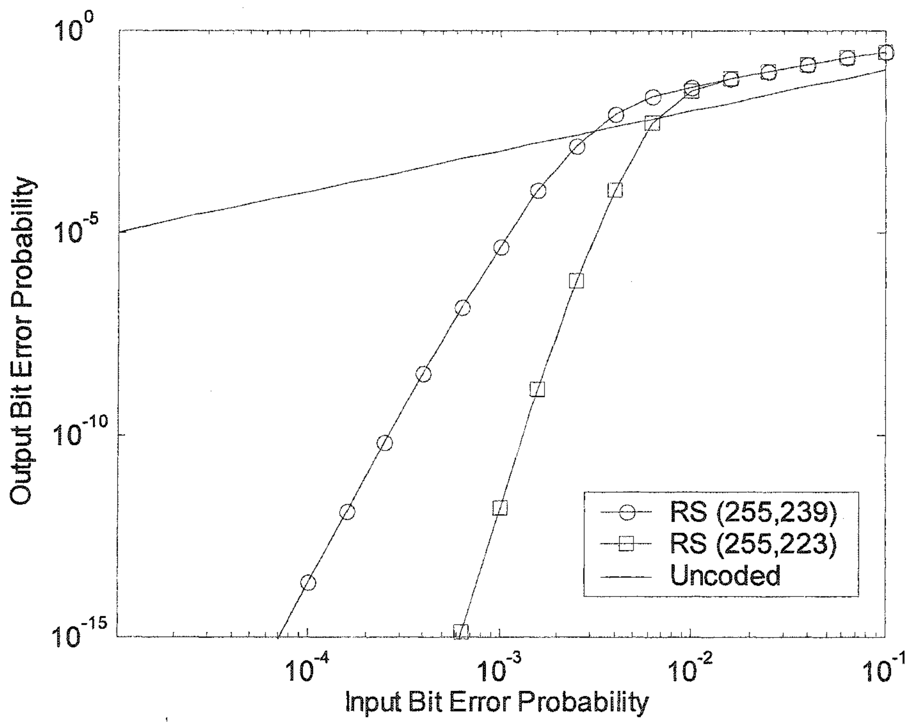

Fig. 2.5 Input/output bit error probability of Reed-Solomon codes.

2.4.2 Turbo Codes

The basic idea of turbo codes involves the use of parallel concatenation of two convolutional codes separated by an interleaver, and perhaps with the systematic bit information. Convolution codes alone have been considered previously in the OCDMA systems [70]. Convolutional codes are essentially made up of cleverly designed linear shift registers with certain feedback and feed-forward coefficients to create a finite state machine. At the receiver side, an iterative procedure is used to decode the noise corrupted information using a soft decision output algorithm, such as the BCJR algorithm, which is named after its inventor Bahl, Cocke, Jelinek and Raviv [73], or the Soft Output Viterbi Algorithm (SOVA) [74]-[75].

The application of turbo codes in OCDMA networks has recently been considered [76]-[77]. One example is turbo-coded packet transmission using Binary Pulse-Position Modulation (BPPM) proposed by Kim and Poor [76]. In their system, two identical recursive systematic convolutional codes with rate ½ are used in the turbo encoder. The OCDMA encoding and decoding block is shown in Fig. 2.6.

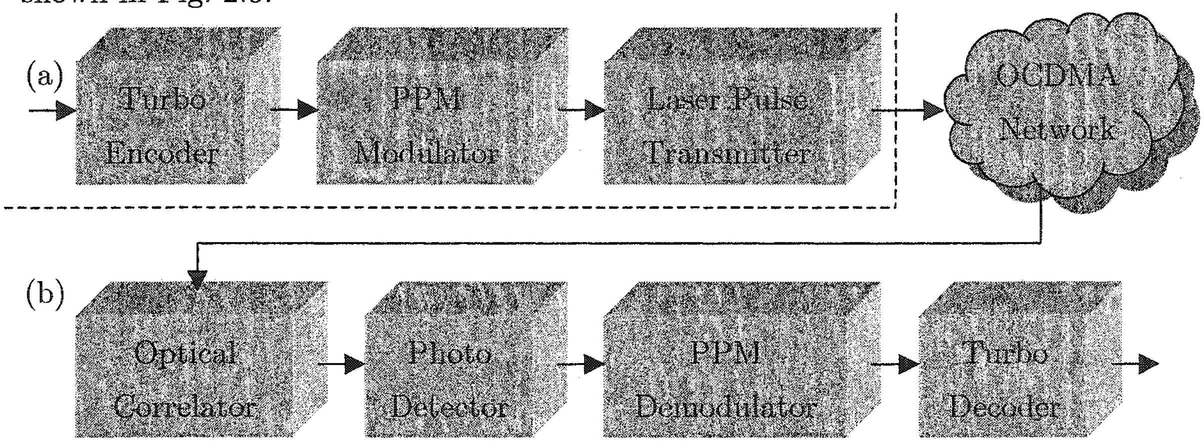

Fig. 2.6 Turbo-coded OCDMA network (a) encoder and (b) decoder.

In their simulations, 1D time spread OCDMA codes with spreading length of 500 and a Hamming weight of 5 are used in the transmission. For the turbo encoder, two convolutional encoders using generator polynomials $1+D^2$ and $1+D+D^2$ are used. With an interleaver length of 100, this setup cannot support any user at BER of 10^{-9} using BPPM. However, the authors claim that some users can be supported when higher-order PPM modulation is used.

In the research in channel coding, however, turbo codes have been shown to achieve performance that is as close as 0.03dB from the Shannon capacity [78]. The original work by Berrou *et al.* achieves 0.7dB from the Shannon limit using a rate ½ code with interleaver size of 65536 bits after 18 iterations [65]. It employs a 16-state recursive systematic code with generator (37, 21) in octal representation. The input/output bit error probability of such a turbo code is shown in Fig. 2.7. Although a typical turbo code cannot bring the BER below 10^{-9} as required by OCDMA systems, it may be used in conjunction with a Reed-Solomon code to achieve such performance. Using Berrou's turbo code scheme, as observed in Fig. 2.7, it is possible to lower the BER from $4x10^{-2}$ to 10^{-5} using only 3 iterations. For further information about the encoding and decoding process of turbo codes, refer to Appendix B.

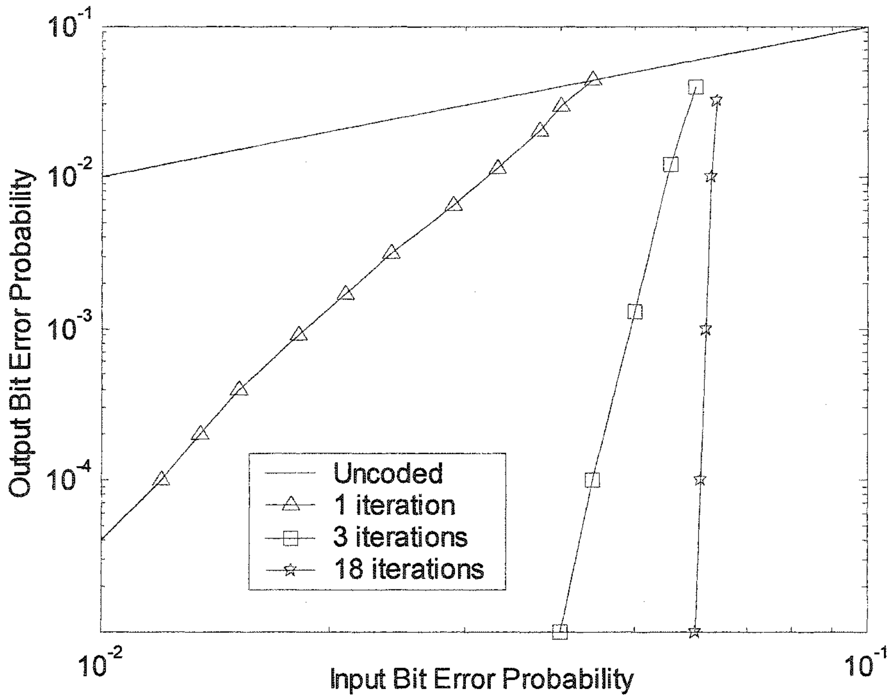

Fig. 2.7 Input/output bit error probability of rate 1/2 turbo code by Berrou *et al.* with interleaver size of 65536 bits [65].

2.4.3 Super Orthogonal Codes

In addition to Reed-Solomon, convolutional and turbo codes, which are concatenated serially with the OCDMA encoders and decoders, Super Orthogonal Codes (SOC) have been proposed recently that combine channel coding with the OCDMA spreading sequence [79]-[80]. SOC employs a convolutional encoder with rate $1/w$ for the input data stream, where w corresponds to the Hamming weight of the OOC. Instead of transmitting the w output bits of the convolutional encoder in w bit periods, SOC transmits the output bits internally in the w active chips of the spreading sequence. Fig. 2.8 (a) and (b) demonstrate the difference in the transmitted signals of OOK-OOC and SOC respectively. Effectively, SOC improves the BER performance by employing channel coding on the chip level, resulting in a bandwidth efficient transmission. However, it also requires the decoder to sample every chip in the bit period, and it also requires very high speed signal processing.

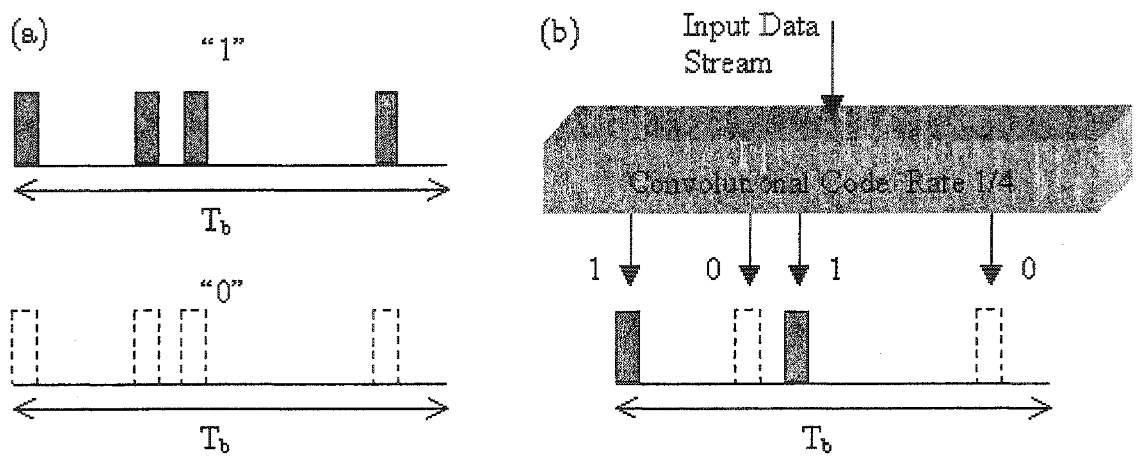

Fig. 2.8 Transmitted signals for (a) OOK-OOC with bit "1" and bit "0" are sent; (b) OOK-SOC with output of the convolutional encoder is "1010" (pulses in dash line are not transmitted).

2.4.4 Practicality Issues of FEC in Optical System

The concept of FEC coding has always been considered difficult to use in optical networks due to the high-speed nature of optical systems and the latency introduced by FEC. However, the speed advancement of DSP chips has enabled the possibility of employing FEC in optical systems. In fact, the next generation 40Gbps networks employ RS(255,239) in the system [69]. Also, commercial products based on turbo codes have been introduced that can handle optical traffic at OC-3 transmission rates (155Mbps) [81]. Hence, it is practically feasible to employ FEC in OCDMA systems.

Chapter 3 Depth-First Search Direct Detection Codes

The Depth-First Search Code (DFSC) uses a search algorithm to discover a new set of spreading sequences for 2D wavelength-time direct detection OCDMA. In theses cases, respectively, multiple pulses of different wavelengths can occur within the same time chip and multiple pulses can occupy different time chips with the same wavelength within a bit period.

An illustration of a possible encoding process of such a 2D wavelength-time code is shown in Fig. 3.1. A broadband source is modulated with the transmitted bit so that power is only sent when bit “1” is transmitted. The pulse first undergoes wavelength encoding in which unnecessary wavelengths are filtered out with respect to the spreading sequence. The remaining pulses are then encoded in the temporal domain. After compensating for coupling loss so that each transmitted chip contain the same amount of power, the output 2D wavelength-time signal is sent to the network.

For the decoder, the same components are used with a time-reverse order to serve as a matched filter for the encoded signal. It is worthy to note that power compensation is required for each wavelength since they may undergo different number of delay lines (thus splitters). Fig. 3.2 demonstrates the scenarios when the spreading sequence is matched and mismatched. When the spreading sequence matches, the transmitted power is regrouped into the same time chip.

When a mismatched code is received, the encoded signal effectively gets re-spread by the decoder. Since the various spreading sequences are only pseudo-orthogonal to each other, there may be a non-zero cross-correlation between two users. Furthermore, as shown in Fig. 3.2, even when the decoding sequence matches, the auto-correlation side lobes are not completely zero. This has implications on the difficulties of locking to the sampling location at the receiver. However, this is beyond the scope of this thesis.

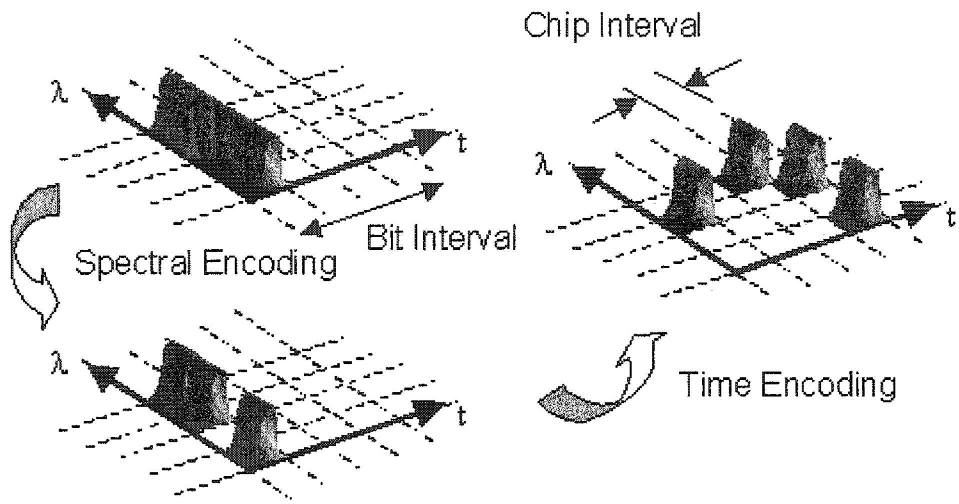

Fig. 3.1 Encoding of 2D MPPR/MPPC OCDMA code.

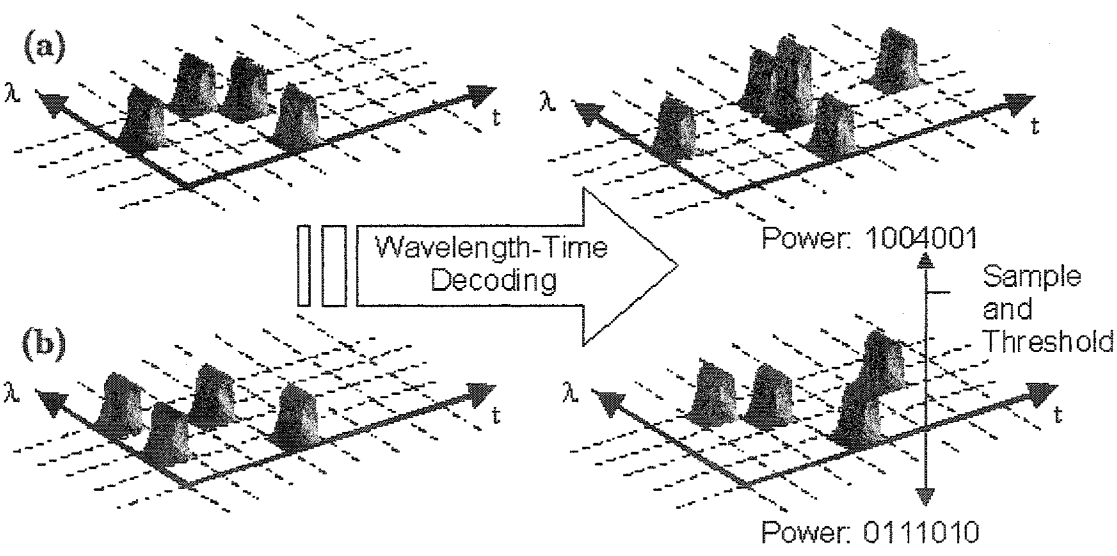

Fig. 3.2 Decoding of 2D wavelength-time direct detection code when (a) sequence matches and (b) sequence mismatches.

3.1 Design Constraints and Algorithm

In order to minimize interference, DFSCs employ similar design constraints as OOCs, where the aperiodic cross-correlation and auto-correlation side lobes are restricted to be less than or equal to one. However, for most previously proposed systems, the Hamming weight w is related to a parameter defining the code size. For example, PH codes have $w = p$, $m = p$ and $n = p^2$ where p is a prime number. Each DFSC family can arbitrary choose its Hamming weight. Mathematically, the Hamming weight w, auto-correlation κ_a and cross-correlation κ_c constraints can be described respectively as follows:

$$\langle \mathbf{s}_p, \mathbf{s}_p \rangle = w, \tag{3.1}$$

$$\langle \mathbf{s}_p, \mathbf{s}_p(\tau) \rangle \leq \kappa_a \quad \tau \in \{1, \cdots, n-1\}, \tag{3.2}$$

$$\langle \mathbf{s}_p, \mathbf{s}_q(\tau) \rangle \leq \kappa_c \quad \tau \in \{0, \cdots, n-1\}, \tag{3.3}$$

for all p and q, where $\mathbf{s}_p$ is the spreading sequence for bit "1" of user p, $\mathbf{s}_p(\tau)$ and $\mathbf{s}_q(\tau)$ denote the modulo shifted spreading sequence for bit "1" of user p and q due to asynchronism. For DFSCs, we set $\kappa_a = \kappa_c = 1$. The inner product in the above expressions is defined by

$$\langle \mathbf{a}, \mathbf{b} \rangle = \sum_{i=1}^{m} \sum_{j=1}^{n} a_{ij} b_{ij}, \tag{3.4}$$

where $a_{ij} \in \{0,1\}$ denotes whether a chip at the i-th wavelength and j-th time chip in spreading sequence $\boldsymbol{a}$ is active.

DFSCs are based on a depth-first search algorithm [82] to generate 2D codes satifying the above three constraints. As schematically shown in Fig. 3.3, the 2D codes are represented by a binary tree where each level corresponds to an element in the 2D grid. We order the tree so that all the elements in the first time chip are placed near the tree root. As the tree is traversed along a given branch, a test for the cross-correlation condition is performed. A code is found once the number of nodes selected equals the code weight. At this point, all other routes below the path traversed are pruned. The search begins again at the root and iterates through surviving branches. After all the codes are generated, the auto-correlation properties are checked and those not satisfying the required constraint are eliminated.

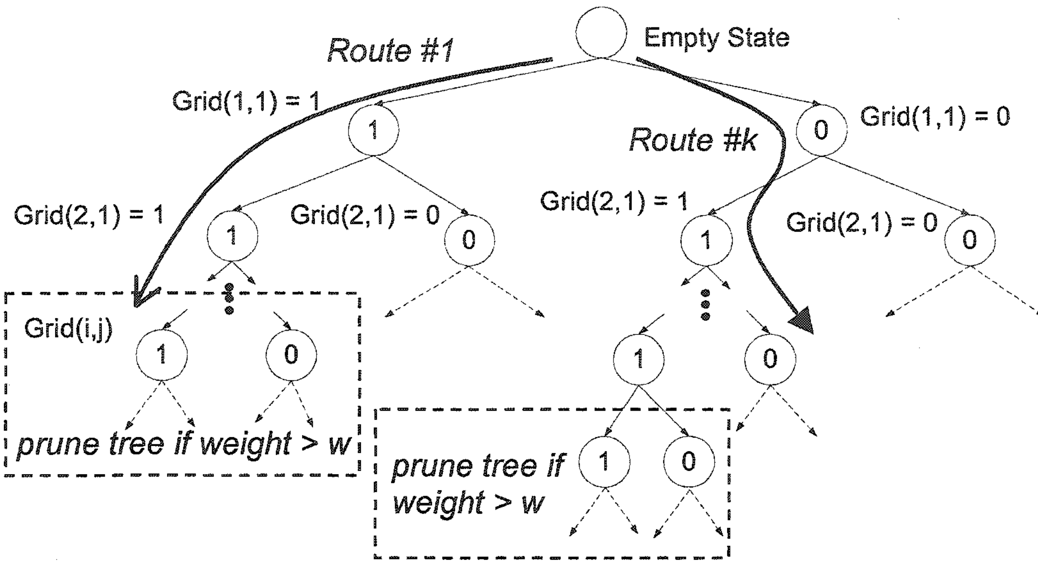

Fig. 3.3 Schematic illustration of DFSC algorithm.

3.2 Code Generation Results

The most important factor for evaluating the code generation results is the maximum number of spreading sequences Φ_{max} that can be generated given a code size (number of wavelength and time chips) and Hamming weight. In this section, we consider the impact of varying these parameters on the maximum number of DFSCs that satisfy the constraints given by (3.1) to (3.3). To distinguish the different sets of DFSC, the notation DFSC(m, n, κ_c/w) is used to denote a system with m wavelengths, n time chips and normalized correlation defined by the ratio of maximum cross-correlation $\kappa_c = 1$ to the Hamming weight w.

3.2.1 Effects of Changing the Code Size m and n

The effect on the number of codes (i.e. supported users) due to changes in the number of wavelengths and chip slots is shown in Fig. 3.4. In Fig. 3.4(a), the number of time-chips is fixed to 16, while the number of wavelengths varies from 16 to 48. Fig. 3.4(b) illustrates the reverse situation where the number of wavelengths is fixed to 16. First of all, it is obvious that the number of codes that can be generated increases as the code size increases. Furthermore, an increase in the number of wavelengths gives more codes than an equivalent increase in time chips. For instance, DFSC(48,16,0.25) supports 2493 users whereas DFSC(16,48,0.125) supports only 830 users. This feature can be easily explained in terms of the aperiodic cross-correlation constraint. Asynchronism occurs only in the time dimension; hence, by adding more time-chips, although the additional space allows code size expansion, the cross-correlation condition limits the growth factor. To understand this phenomenon fully, we may consider the existence of a set of synchronous OOCs (i.e. no time shifts in the auto- and cross-correlations). With the shifted auto- and cross-correlation conditions satisfied in our asynchronous code, at least the time-shifted version of the code, in the synchronous sense, satisfies the OOC condition. Thus,

$$\Phi_{synch} \geq n\,\Phi_{asynch} \tag{3.5}$$

where n is the number of time-chips. Hence, for asynchronous systems alone

$$\frac{\Phi_{mxn}}{\Phi_{nxm}} \approx \frac{m}{n} \tag{3.6}$$

In the case of DFSC(48,16,0.25) and DFSC(16,48,0.25), the ratio of maximum number of users is 3.0036 while the ratio of wavelength and time is exactly 3.

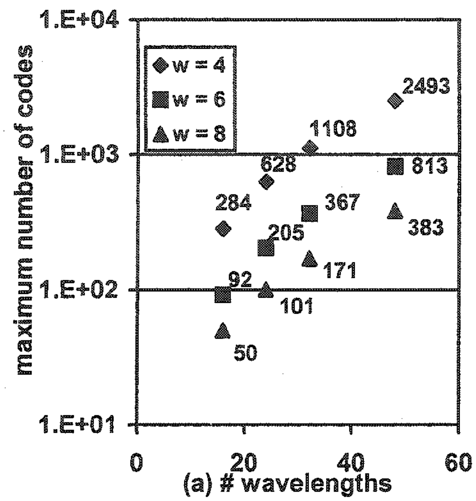

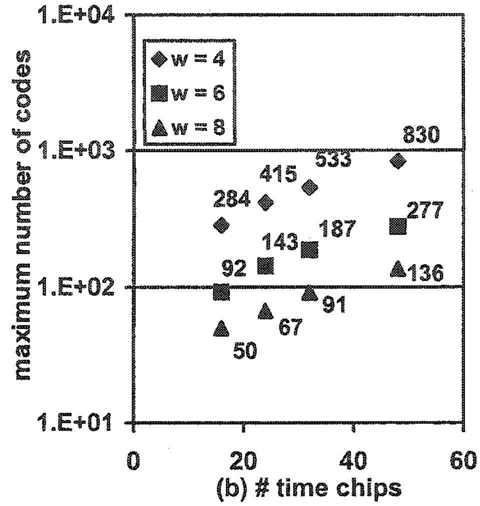

Fig. 3.4 Maximum number of codes generated as a function of (a) m with $n = 16$ and (b) n with $m = 16$ for $w = 4$, 6 and 8.

3.2.2 Effects of Changing the Hamming Weight

Fig. 3.5 shows the effect of varying the Hamming weight w of the code. As w of the code increases, the probability of correlation between different codes also increases thereby decreasing the maximum number of codes that can be generated.

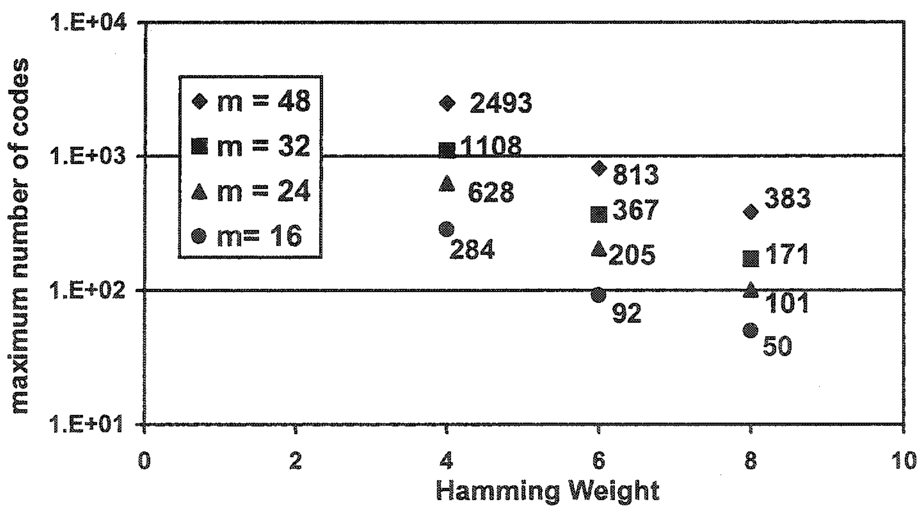

Fig. 3.5 Maximum number of codes generated as a function of w for $n = 16$ and $m = 16$, 24, 32, 48.

3.2.3 Comparison to Previously Proposed Systems

The comparison between the maximum number of codes that can be generated by DFSC and other previously proposed 2D wavelength-time systems is made based on the ratio between the number of codes generated and the code size. For DFSC(48,16,0.25), 2493 codes are generated by depth-first search algorithm, which corresponds to 3.25 times the code size. For a higher weight DFSC(48,16,0.125), the ratio is 0.3698. For Fast Frequency Hop FFH(48,16,0.0625), however, the maximum number of codes that can generated is 48 (the number of wavelengths), which corresponds to 0.0625 times the code size. For the Yu-Park construction, YP(8,127,0.125) can generate 126 distinct codes, which corresponds to a ratio of 0.124. Finally, for Prime Hop code, PH(11,121,0.0909) can generate 121 codes, which corresponds to a ratio of 0.0909. Note that for other code constructions, the Hamming weight condition cannot be modified, thus they cannot increase the generated codes to code size ratio by reducing the weight. It is clear that DFSC can definitely generate more codes than previously proposed 2D spreading sequence families. Although the additional codes tell no information about the BER performance of a system, it has a huge impact when FEC is applied, which will be discussed in section 3.3.4.

3.3 Performance Analysis

Two methods are employed to evaluate the system performance of DFSC: average variance estimation and binary statistic calculation. In the average variance estimation, the variance of the MAI is estimated based on Gaussian approximation, and obtained via a Monte-Carlo simulation. This variance governs the BER performance of the system. In binary statistic calculation, the interference statistics between each user pair are evaluated, and it is used to generate the probability mass function (pmf) of the interference. The error probability can be obtained from observing the pmf.

The following standard assumptions are made in the performance analysis: (A1) perfect time-chip synchronization between all interfering users (the system is otherwise asynchronous); (A2) ideal rectangular-shaped temporal pulses and spectral slices for the encoded and the decoded signals; (A3) incoherent superposition of MAI where a broadband source is employed as the input to the encoders; (A4) the absence of near-far problem; and (A5) the absence of channel noise and receiver noise.

3.3.1 Average Variance Estimation

3.3.1.1 Mathematical Analysis

Since there have been discrepancies in the BER expressions in previously published works [10],[18],[35], it is preferred to re-derive the expression from first principles. For a given bit slot, in direct detection OCDMA, the transmitted sequence of user u is $b_u\mathbf{s}_u$, where $b_u \in \{0, 1\}$ is the transmitted bit of user u. A spreading sequence is only sent when the user is transmitting the bit "1". At the output of the multiple access channel, the received vector $\mathbf{r}_i$ corresponds to the summation of the transmitted signals of all active users assuming asynchronous operation. The matched filter output of user u can be modeled as

$$out_u = \langle \mathbf{r}, \mathbf{s}_u \rangle + \eta, \tag{3.7}$$

where η is the receiver noise, which is neglected in the analysis due to (A5). Without loss of generality, we assume user 1 as the desired user. The output of the matched filter takes the form

$$out_1 = b_1 w + \left\langle \sum_{k=2}^{K} \mathbf{s}_k(X_k, Y_k, \tau_k), \mathbf{s}_1 \right\rangle, \tag{3.8}$$

where K is the number of active users, $\mathbf{s}_k(X_k, Y_k, \tau_k)$ denotes the spreading sequence when bits $X_kY_k = \{00,01,10,11\}$ are transmitted consecutively by user k, and asynchronism causes a time shift of τ_k time chips between user k and user 1. On an asynchronous binary symmetric channel, X_k and Y_k are independent identically distributed (i.i.d.) Bernoulli random variable with probability $p = 0.5$, and τ is i.i.d. uniform discrete random variable in the range $[0,\ldots,n\text{-}1]$. In the equation, the first term represents the desired user signal and the second term represents the MAI to the first user.

When the number of active users on the system is large, we can use Gaussian approximations to evaluate the BER performance of the system. The variance of the MAI is:

$$VAR(MAI) = (K-1)\overline{\sigma}_k^2, \tag{3.9}$$

where $\overline{\sigma}_k^2$ is the average variance of interference caused by time-shifted cross-correlation between user 1 and all other users, and is defined by

$$\overline{\sigma}_k^2 = E_k\left[VAR_{X,Y,\tau}\left(\left\langle \mathbf{s}_k(X_k, Y_k, \tau_k), \mathbf{s}_1\right\rangle\right)\right]. \tag{3.10}$$

Since the expected value of the MAI is not zero, one needs to vary the threshold of the decision rule in order to optimize the BER performance. If μ is the average variance, the threshold should be set to μ + w/2. For such a case, the BER performance takes the form

$$\begin{aligned} BER &= \Pr[b=1]\Pr[MAI < \mu - w/2] + \Pr[b=0]\Pr[MAI > \mu + w/2] \\ &= Q\left(\frac{1}{2}\sqrt{\frac{w^2}{(K-1)\overline{\sigma}_{pq}^2}}\right) \end{aligned}, \tag{3.11}$$

which corresponds to the expression in (2.1). In the expression, $\overline{\sigma}_{pq}^2$ is obtained using (3.10) except that it refers to the expected value generated from all code pairs p and q rather than between user 1 and k.

3.3.1.2 Results

For a given number of simultaneous users K, we use a Monte-Carlo simulation employing random codes to evaluate $\overline{\sigma}_{pq}^2$ and calculate the corresponding BER using (3.11). The simulation stops when the change in consecutive variance is smaller than 10^{-7} and at least 3000 trials have been considered (typical simulations involve 3000 to 50000 trials). Fig. 3.6(a) and (b) show the BER as a function of K for codes having the same w, but differing in m and n. As expected, for a given K and w, increasing m and n enhances the system performance. This is due to the fact that the probability of overlap between the spreading sequences decreases as the code size increases. For DFSC(24,16,0.167), DFSC(32,16,0.167) and DFSC(48,16,0.167), the number of simultaneous users that can be supported at the benchmark BER of 10^{-9} is 6, 8, and 12 respectively. Similar numbers are obtained for DFSC(16,24,0.167), DFSC(16,32,0.167) and DFSC(16,48,0.167). Since the codes satisfy the same auto- and cross-correlation constraints, codes with $m > n$ have the same performance as those with $n > m$. However, it is important to recall that more codes can be generated if $m > n$.

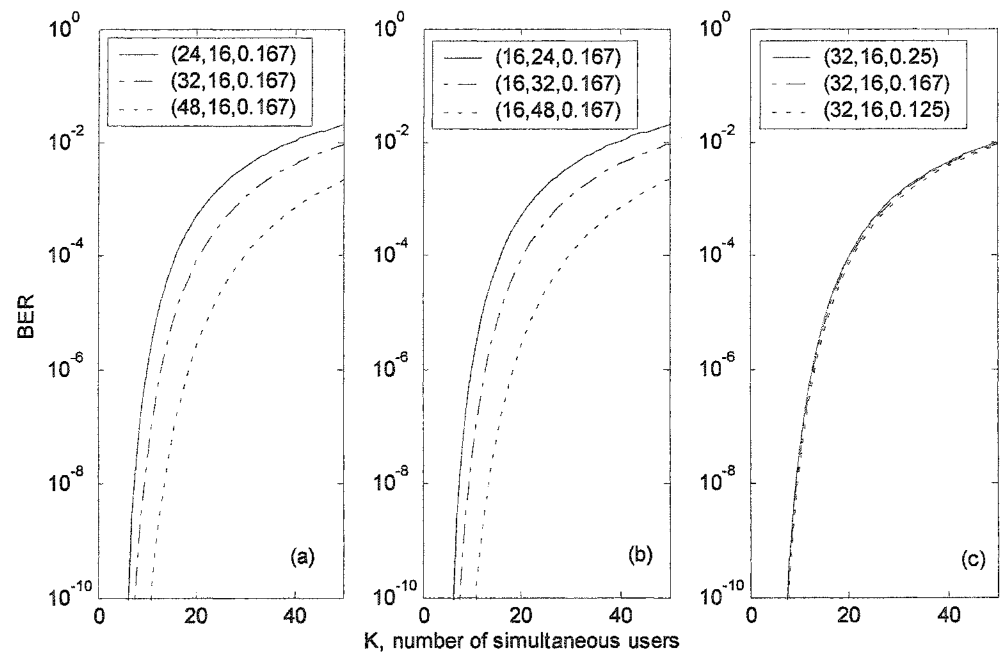

Fig. 3.6 Calculated BER as a function of the number of simultaneous (active) users for (a) n = 16, w = 6 and m as a parameter; (b) m = 16, w = 6 and n as a parameter; (c) m = 16, n = 16 and w as a parameter.

As the Hamming weight w increases, we would normally expect the BER performance to improve. However, as shown in Fig. 3.6(c), there is very little performance gain. This is because as w increases, the probability of overlapping between two spreading sequence increases. This causes the interference variance to increase with the signal strength, thus the SIR ratio exerts only marginal improvement. It is important to note that as w increases, the maximum number of codes that can be generated decreases, but the performance only improves slightly. This suggests that it is more beneficial to use low weight codes.

In general, for a given number of available wavelengths and chip slots, the average interference variance is related to the Hamming weight and the maximum number of codes Φ_{max}. As the probability of transmitting "1" on each chip approaches a uniform distribution, the average variance becomes coupled to the parameters specified, and this effectively places a bound on the performance of all OOC systems, including DFSC.

3.3.2 Binary Statistics Calculation

3.3.2.1 Mathematical Analysis

One common question that arises when evaluating the performance of an OCDMA system is the validity of the Gaussian approximation for the MAI. To answer this question, we have to consider the binary statistics of the aperiodic cross-correlation between each user pair. Let $0 \le N_c(\mathbf{s}_p(X,Y,\tau),\mathbf{s}_q) \le 4n$ be the number of occurrences of cross-correlation $c \in \{0,1,\ldots,\kappa_c\}$ between spreading sequences s_p and s_q for all combinations of $X \in \{0,1\}$, $Y \in \{0,1\}$ and $\tau \in \{0,1,\ldots,n\text{-}1\}$. The pmf of the cross-correlation between code p and q is

$$P_{pq}(\alpha) = \Pr[\alpha = c] = \frac{1}{4n} N_c(\mathbf{s}_p(X,Y,\tau),\mathbf{s}_q). \tag{3.12}$$

Without loss of generality, we assume user 1 as the desired user, and users 2 to K as the interfering users. The pmf of the MAI is

$$P_{MAI}(\alpha) = P_{21}(\alpha) * P_{31}(\alpha) * \cdots * P_{K1}(\alpha), \tag{3.13}$$

where * denotes convolution. The maximum interference for K active users is $(K\text{–}1)\kappa_c$. The average MAI μ is determined by the expected value of the pmf and is given by

$$\mu = \sum_{\alpha=0}^{(K-1)\kappa_c} \alpha P_{MAI}(\alpha). \tag{3.14}$$

When the threshold is set to $\mu + w/2$, the BER probability is

$$BER = \Pr[b=1]\Pr[MAI < \mu - w/2] + \Pr[b=0]\Pr[MAI > \mu + w/2]$$
$$= \frac{1}{2}\left(\sum_{\alpha=0}^{\mu-w/2} P(\alpha) + \sum_{\alpha=\mu+w/2}^{(K-1)\kappa_c} P(\alpha)\right) \quad (3.15)$$

for equiprobable input bit distributions. The variance of the MAI is

$$\sigma_{MAI}^2 = \sum_{\alpha=0}^{(K-1)\kappa_c} \alpha^2 P_{MAI}(\alpha) - \mu^2 \quad (3.16)$$

3.3.2.2 Results

For illustration, we use DFSC(32,16,0.125) for analyzing the probability distribution of the MAI. Fig. 3.7 shows the MAI distribution when 10, 40, 80 and 120 users transmit on the network. A total of 15 samples are taken for each calculation, where users are randomly chosen from the total of 145 spreading sequences available from the code generation. The dotted items denote the calculated pmf of the MAI, while the solid line denotes the Gaussian-approximated distribution of the MAI. As seen from the figure, when the number of users is low, the Gaussian approximation does not hold, mainly due to the non-existence of negative correlation values. Even when 80 users are transmitting on the network, the tail of the Gaussian distribution is chopped. This has an impact on evaluating the BER performance using expression (3.11) as shown in Table 3.1.

Table 3.1 Percentage difference in Gaussian-approximated and calculated BER for DFSC.

Number of User	Approx. BER	Calculated BER	% Difference
10	1.4×10^{-8}	4.7×10^{-5}	99.97%
40	3.8×10^{-3}	4.9×10^{-3}	22.43%
80	3.1×10^{-2}	2.9×10^{-2}	-4.93%
120	6.4×10^{-2}	6.2×10^{-2}	-2.12%

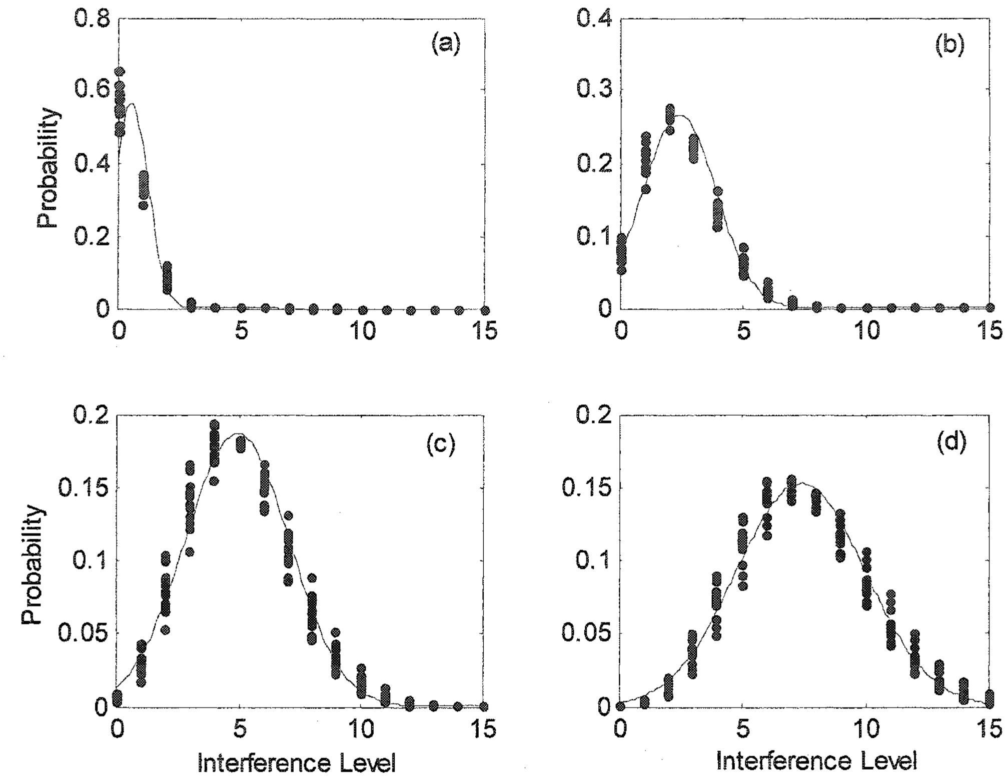

Fig. 3.7 Comparison of Gaussian approximated MAI distribution and results from binary statistics for DFSC(32,16,0.125) when the number of active users are (a) 10, (b) 40, (c) 80, and (d) 120.

It is worth noting that in a real system, asynchronism will blur the discrete nature of the binary statistics to become more Gaussian-like. This holds true also when noise is present in the system.

Fig. 3.8 shows a comparison between the estimated variance obtained from Monte-Carlo simulations (solid line) and the results obtained by considering the binary statistics (dots). We observe that as the number of active users increases, the variance of the MAI increases. However, on average, the MAI grows more or less linearly as expected from probability theory.

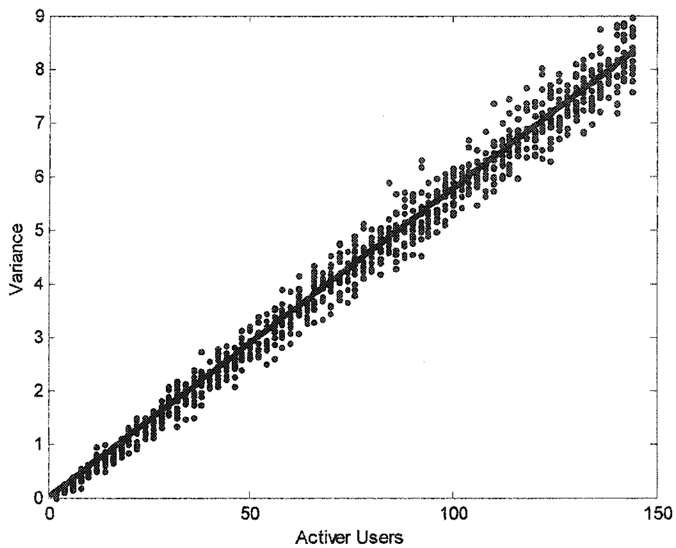

Fig. 3.8 Comparison between estimated MAI variance (thick line) and results obtained from binary statistics (dots) for DFSC(32,16,0.125).

Finally, the BER performance as a function of active users is shown in Fig. 3.9. The thick solid line in the figure denotes the BER performance obtained from the Gaussian approximation, and the dots correspond to the results from the 15 trials. For a low number of users, the BER performance does not result as expected based on the Gaussian approximation. The performance degrades to near BER $= 10^{-7}$ when 6 users are online. Hence, only 5 users can really be supported below the benchmark BER using DFSC(32,16,0.125). Nonetheless, as the number of active users in the network increases, the Gaussian approximation becomes valid, and the results from the two analyses converge. Thus, we conclude that when the number of users on the network exceeds 80, the Gaussian approximation holds (less than 5% difference). Note that this result applies to all direct detection codes.

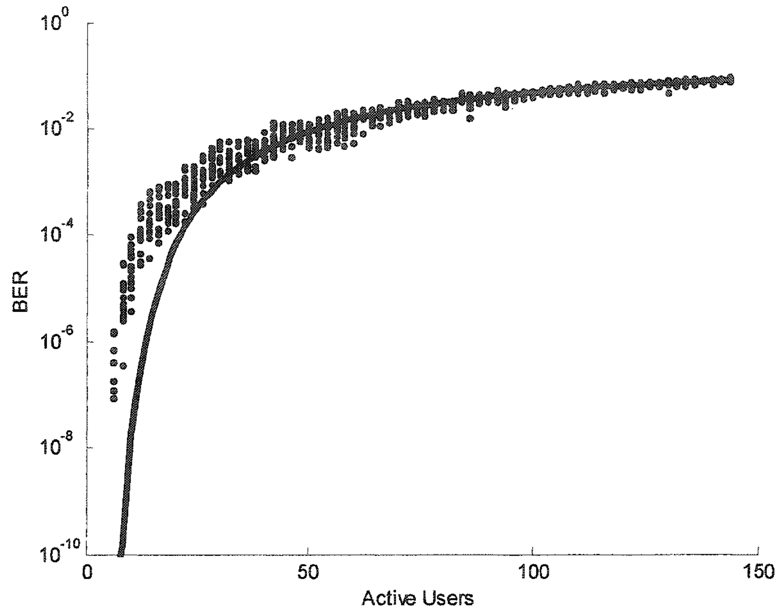

Fig. 3.9 Comparison of BER performance of DFSC(32,16,0.125) using variance estimation (thick line) and binary statistics (dots).

3.3.3 Comparison with existing 2D codes

We compare the BER performance of DFSC with previously established 2D wavelength-time codes, namely PH, FFH and YP codes. In order to ensure a fair comparison of the various codes, we use the same process to evaluate the BER performance, i.e., we first generate the code sequence using the corresponding construction algorithms and then compute the BER using variance estimation in (3.11).

For PH(11,121,0.0909) which has a code size of 11x121= 1331, 20 users with a BER below 10^{-9} can be supported. Similarly, for DFSC(42,32,0.167) which has a code size of 42x32 = 1344, it can support the same amount of users. Although the BER performance is approximately the same between the two codes, DFSC uses a Hamming weight of 6 while PH uses a Hamming weight of 11. When receiver noise is present, this implies that DFSC can achieve the same BER performance using less optical power. Furthermore, DFSC can generate 1164 codes while PH can only generate 110 codes. Thus, DFSC outperforms PH codes in this sense.

When DFSC(32,16,0.125) and DFSC(16,63,0.125) are compared to the YP construction, as shown in Fig. 3.10, the DFSC codes can support 8 and 15 users with BER $< 10^{-9}$ respectively, and YP(8,67,0.125) and YP(8,127,0.125), which have a similar code size and Hamming weight as the comparing DFSC, can support the same amount of users. While the BER performances of the codes are comparable, the number of codes that can be generated by DFSC is larger than YP. For example, DFSC(32,16,0.125) has 145 codes while YP(8,67,8) has 66 codes. Furthermore, it is also worthy to note that DFSC can design 2D codes with significantly fewer time chips than both PH and YP codes (whose time dimension aspects are based on 1D temporal sequences that are typically very long); hence, DFSC can support high data rate communication.

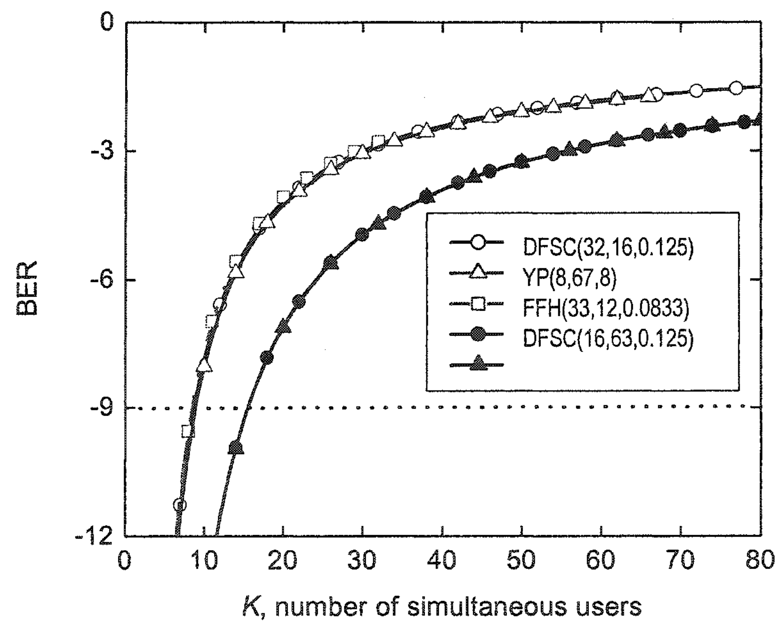

Fig. 3.10 Comparing the BER as a function of simultaneous users for DFSC, YP and FFH.

When DFSC is compared to FFH codes, as shown in Fig. 3.10, DFSC(32,16,0.125) has very similar BER as FFH(33,12,0.0833) – both can support 8 users at a BER $< 10^{-9}$. It is true that in this case, the code size of DFSC is about 1.3 times than FFH; nonetheless, the maximum number of codes that can be generated by DFSC is 4.5 times greater – 145 compared to 33. Again, the maximum number of codes that can be generated by FFH is limited to the number of wavelengths used in defining the codes.

3.3.4 The Impact of Forward Error Correction

FEC can be used to increase the number of users that can be supported at a given BER for any OCDMA system. As shown previously in Fig. 2.5, RS(255,239) may improve the channel BER from 3.5×10^{-4} to 10^{-9}, and RS(255,223) improves channel BER from 1.6×10^{-3} to 10^{-9}. As a result, when RS(255,239) or RS(255,223) are used, the effective benchmark BER becomes 3.5×10^{-4} and 1.6×10^{-3} respectively. For RS(255,223) over DFSC(42,32,0.167), the number of users that can be support at the benchmark BER almost quadruples from 20 to 78. A similar gain ratio can also be obtained for DFSCs of different sizes. However, the maximum number of codes that can be generated from other code families is much lower than that of DFSC. For example, even if FEC is applied to FFH codes with 42 wavelengths, the number of users that can be supported at the benchmark BER is 42, which is half of what can be accomplished by DFSC(42,36,0.167). Other soft decision and iterative FEC techniques may be used to further improve the performance of direct detection codes. However, we would need to consider the asymmetric distribution of the MAI. The design of such codes is beyond the scope of this thesis.

3.4 Optical Simulation Example

Simulations are performed using standard optical software *Linksim*™ to demonstrate the functionality of DFSC for OCDMA systems.

3.4.1 Simulation Setup

DFSC(16,16,0.125) is chosen for the demonstration purpose. Using the depth-first search algorithm, this DFSC system can accommodate a total of 31 codes.

Among these users, we have chosen the 8 codes listed in Fig. 3.11 for the optical simulation. The spreading codes shown correspond to code # 1, 2, 3, 10, 12, 20, 26 and 30.

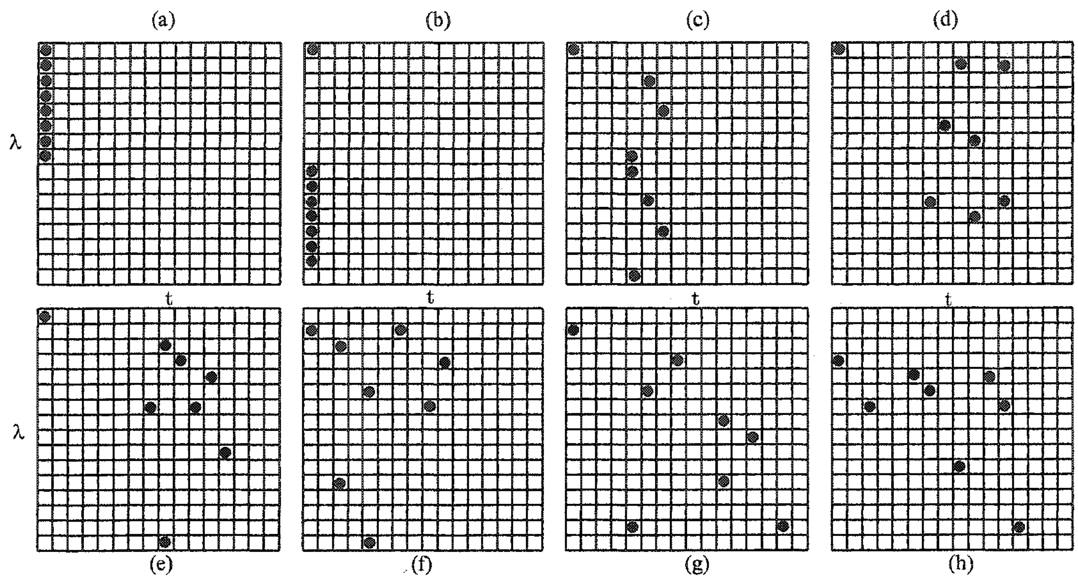

Fig. 3.11 Spreading codes used for 8-user DFSC(16,16,0.125) system. Code number: (a) 1, (b) 2, (c) 3, (d) 10, (e) 12, (f) 20, (g) 26, (h) 30.

The model used for the simulation is shown in Fig. 3.12. A pseudorandom binary sequence (PRBS) signal is sent to an OCDMA encoder, which uses multiple tunable lasers and optical delay lines to encode the optical signal depending on the spreading sequence. To model asynchronism among all users, an optical delay line is placed at the end of the encoder, and a random time delay within a bit interval is used. An optical multiplexer is employed to combine optical signals from all different users onto the same fiber, and an optical splitter is used to divide the combined signal to each decoder. The decoders perform matched-filtering using complementary optical delays for each wavelength according to the spreading sequence, and a photodiode is used to convert the signal back to electrical.

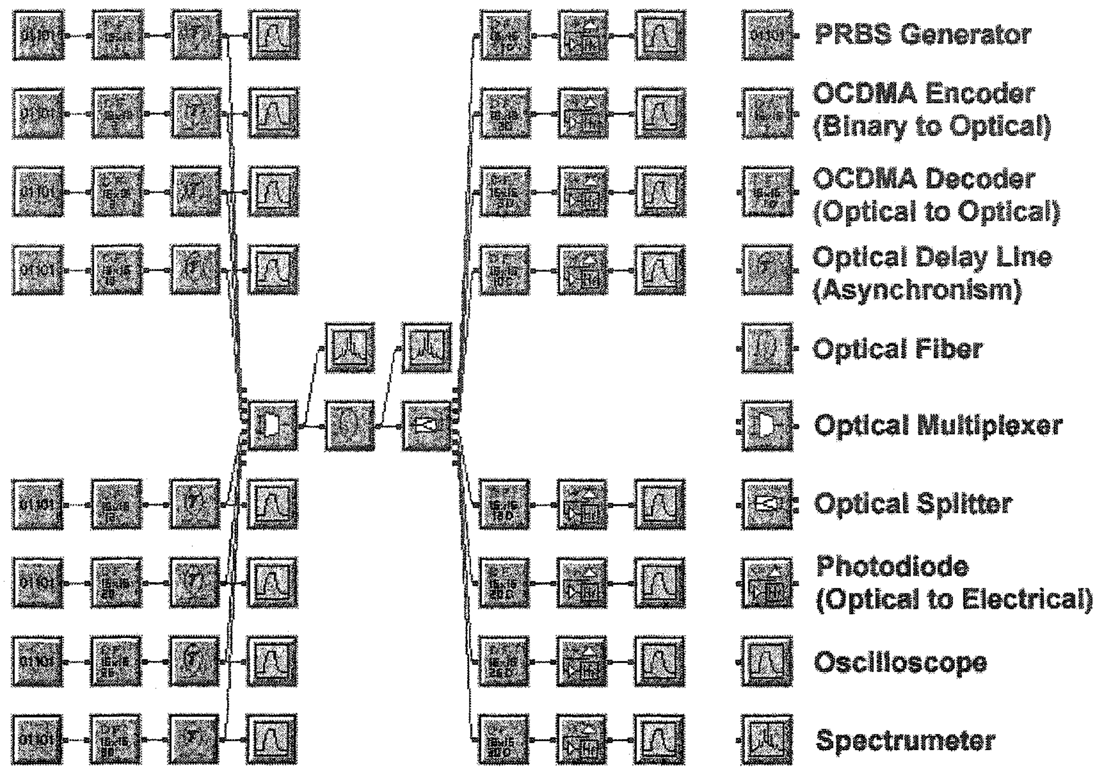

Fig. 3.12 8-User Optical Simulation Model.

3.4.2 Simulation Results

For the simulation, an OC-3 data rate (155.52Mbps, chip rate at 2.49Gbps) is used, the asynchronism delays are arbitrarily chosen to be 0.2351, 0.6291, 0.0126, 0.4000, 0.5231, 0.9502, 0.7215 and 0.1025 of a bit period respectively for the 8 users (Channel is assumed to be fully asynchronous for this simulation). Two kilometres of non-linear single-mode fiber with 8.2μm core diameter is placed between the encoders and decoders. The photo-detector is followed by a Bessel filter with a bandwidth of 625MHz.

As an illustration, the OCDMA encoded signal for a user with spreading code #30 is displayed in Fig. 3.13. Within a bit interval, eight pulses are generated at different wavelengths. For this simulation, the wavelengths have a channel spacing of 0.8nm, ranging from 1550nm to 1562nm. The bit interval is 6.43ns long, and each chip is about 402ps long.

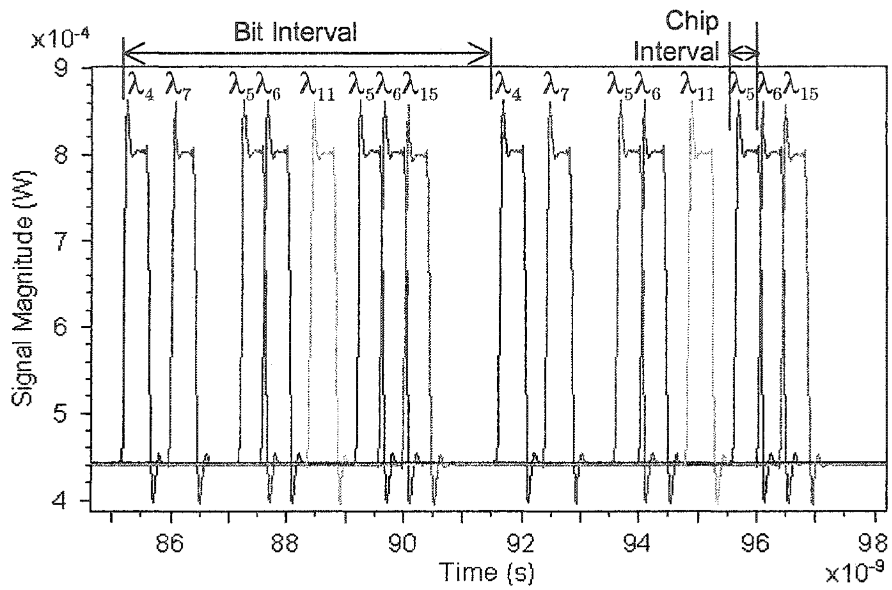

Fig. 3.13 Two consecutive bit "1" for OCDMA signal for user with code 30.

The decoded electrical signals for all users are shown Fig. 3.14. On the figure, the PRBS signals are listed with the corresponding users. In general, the auto-correlation peak stands out among the MAI for this realization of an 8-user system. This suggests that with proper threshold, the OCDMA signal can be decoded. However, a close examination reveals that the threshold cannot be set to the same value for all users. For instance, the maximum voltage amplitude for the second user in Fig. 3.14(b) is about $9\text{x}10^{-5}$V while the minimum voltage amplitude for the sixth user in Fig. 3.14(f) is about $12\text{x}10^{-5}$V. If the threshold is set to about $10\text{x}10^{-5}$V, the second user will detect a constant bit "0", while the sixth user will detect a constant bit "1". The difference between the power levels of the received signal directly reflects the average interference caused by the active users. Hence, for best performance, the threshold should not be determined by the number of users on the system (especially when the number of active users is small), but it should be estimated dynamically by each user. Finally, Fig. 3.15 shows the output of user 10 under 5 scenarios: 1, 2, 3, 5 and 8 users are online.

In the simulation, the optical signal has a bandwidth of 12nm. If the fiber dispersion is 17ps/nm/km, the signal broadening may be significant depending on the fiber length. For instance, 2km fiber will cause a broadening of 408ps. Comparing to the chip width of 402ps, one can expect the signal power at the extreme wavelengths to misalign at the receiver, causing intersymbol interference.

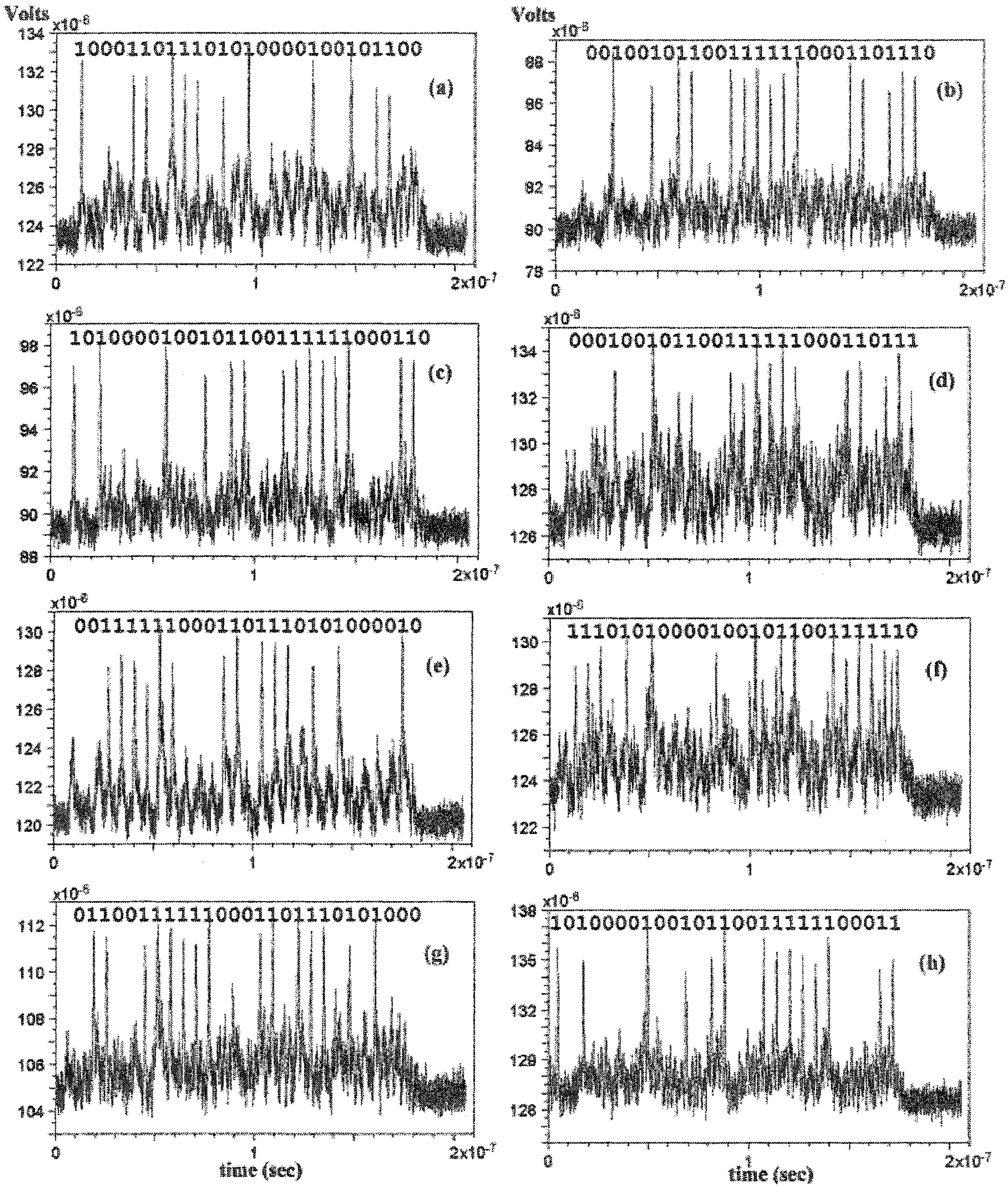

Fig. 3.14 Decoded electrical signal (voltage versus time) for 8-user OCDMA system: (a) code 1, (b) code 2, (c) code 3, (d) code 10, (e) code 12, (f) code 20, (g) code 26 and (h) code 30.

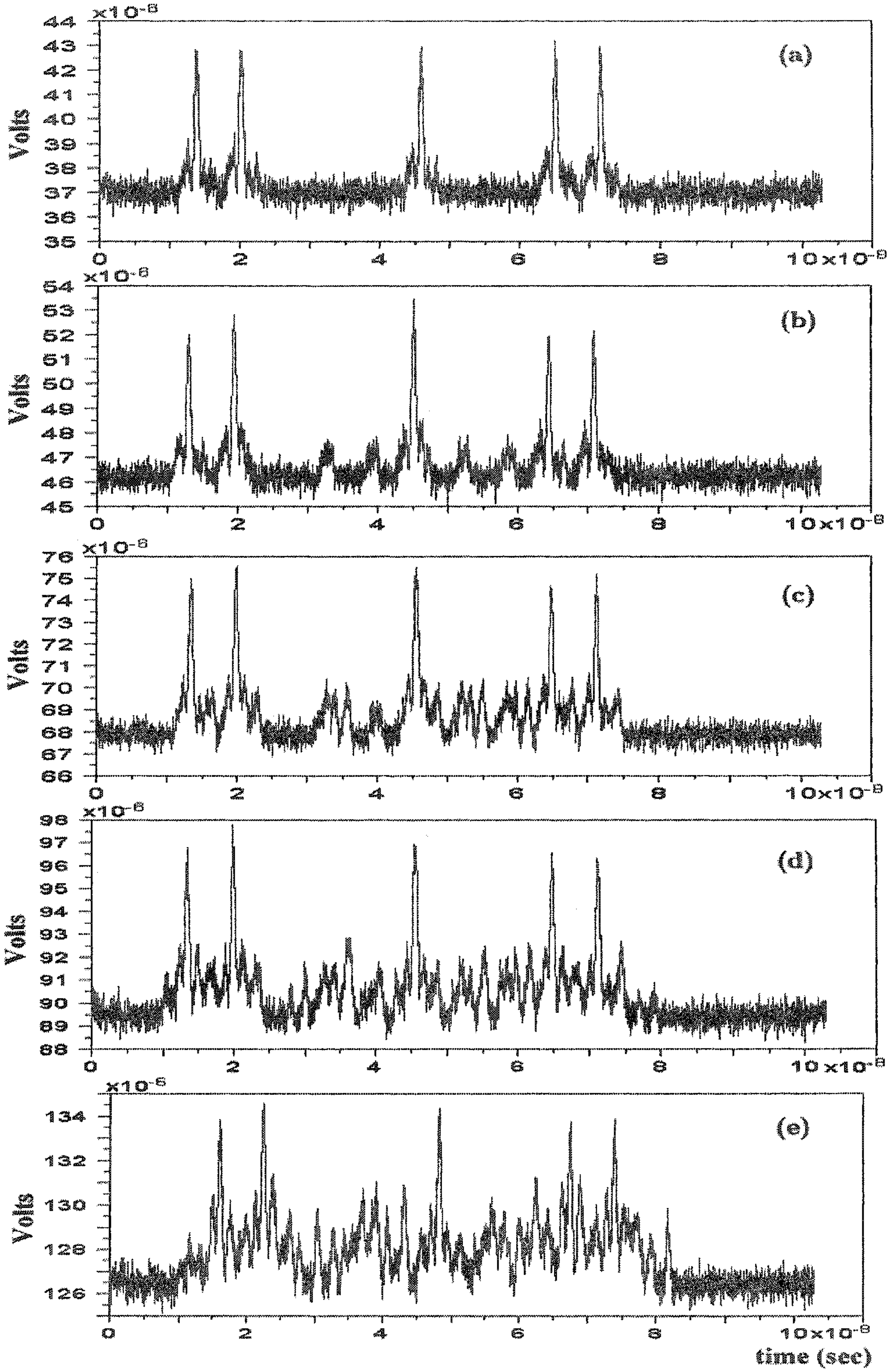

Fig. 3.15 Decoder output for user 10 with transmitted pattern "0011000100110000" and interference due to: (a) no other user; (b) user 12; (c) user 12 and 20; (d) user 2, 3, 12 and 20; (e) user 1, 2, 3, 12, 20, 26 and 30.

To study the effect of dispersion, Fig. 3.16 compares the decoder outputs of user 10 for different fiber lengths with the same MAI. Overall, between a fiber length of 1m and 2km, the decoder waveforms are similar in shape, which clearly identify the autocorrelation peaks. This hints that the dispersion effect is small. However, in Fig. 3.16(c), when a fiber length of 10km is used, the sampling peaks become blurred. This is expected since 10km of fiber will cause a broadening of 2.04ns, which spans over 5 time chips. To reduce the effect of dispersion, one may consider the use of dispersion-shifted fibers or narrowing the channel spacing of the wavelength-time encoded signal.

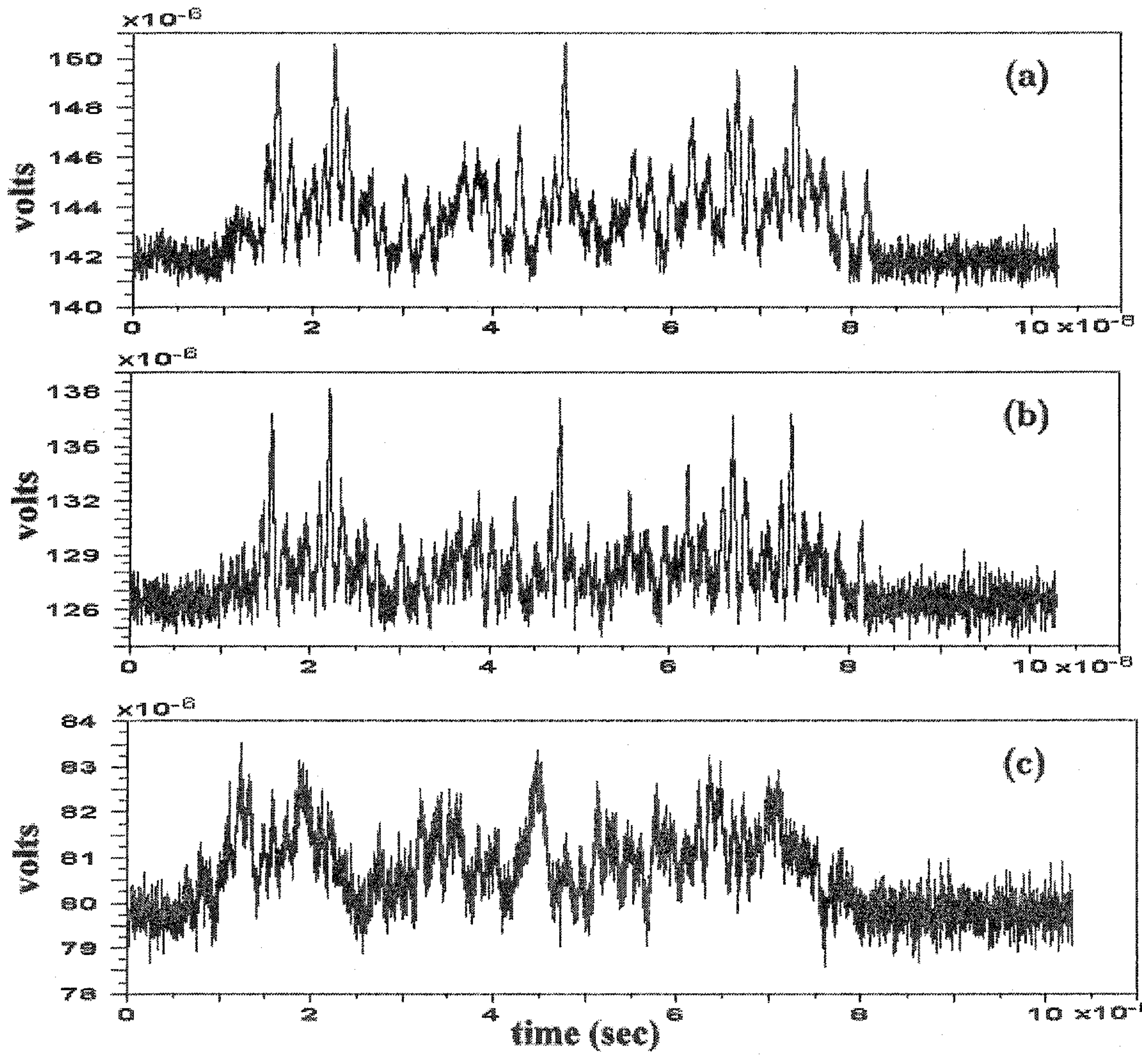

Fig. 3.16 Decoder output for user 10 with transmitted pattern "0011000100110000" with 7 other interference users when the fiber lengths are (a) 1m, (b) 2km and (c) 10km long.

Chapter 4 Balanced Code for Differential Detection

The Balanced Code for differential detection (BCDD) defines a set of new constraints for designing 2D wavelength-time OCDMA spreading codes using differential detection technology. The most important distinction between BCDD and all previously defined OCDMA codes is that it no longer limits the auto-correlation side lobes and cross-correlation to small values. In doing so, it allows more user codes to be generated with high Hamming weight. In other words, BCDDs do not employ sparse sequences, but rather it ensures each wavelength-time chip to have equal probability of transmitting one and zero on the channel. It controls the level of the MAI by varying the auto- and cross-correlation constraints.

While the encoding process of BCDDs is similar to the DFSC systems, the decoder functions differently as it incorporates the use of a balanced receiver. Fig. 4.1 illustrates the decoding process of a BCDD when the spreading sequence is matched and mismatched. Note that the power levels among figures are not drawn to scale in order to emphasize the autocorrelation peak. The positive decoder performs matched filtering to pick up signals representing the bit "1" for each wavelength, and the negative decoder performs matched filtering to pick up signals representing the bit "0". These are then fed into the positive and negative terminals of the balanced receiver. The electrical current output of the receiver is proportional to the difference of power between the two receiver terminals. For the demonstrated codes, the maximum absolute auto-correlation side lobe and cross-correlation is between ±2.

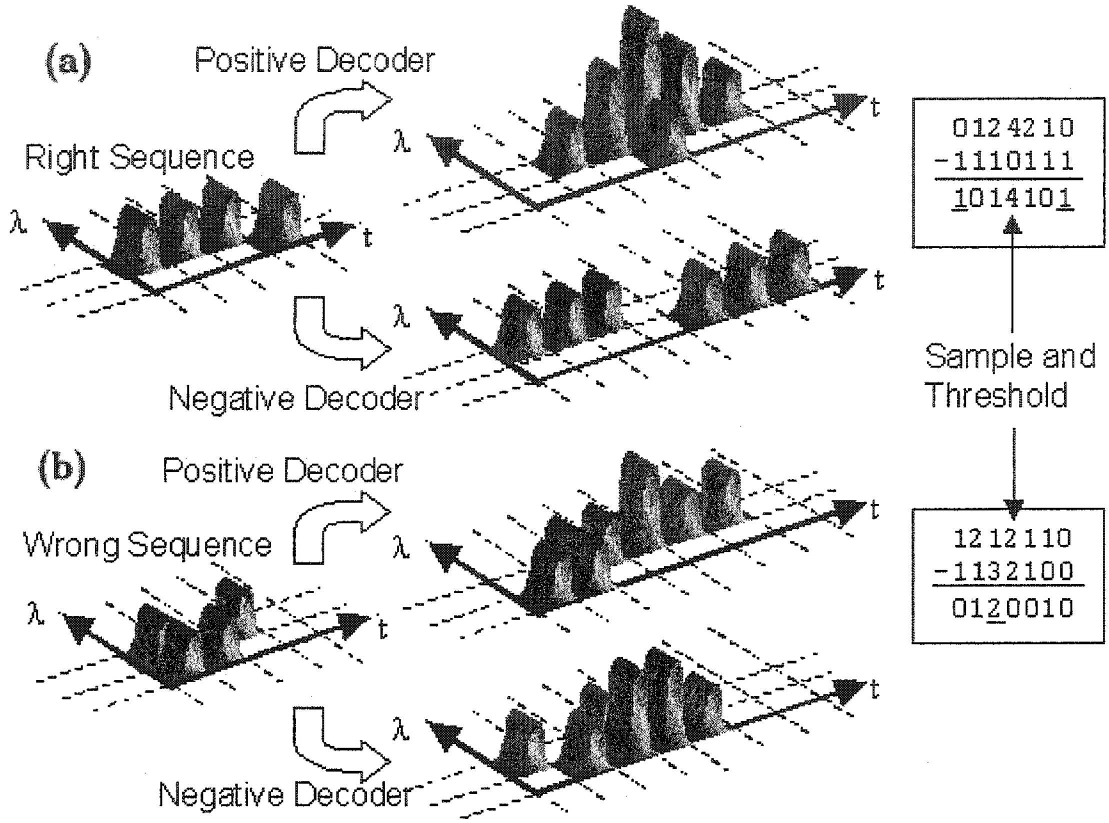

Fig. 4.1 Decoding of 2D wavelength-time differential detection code: (a) sequence matches; (b) sequence mismatches (In the figure, underlined number represent negative: $\underline{1}$ = -1).

A high-level block diagram for implementing a BCDD decoder is shown in Fig. 4.2. For the illustrated spreading code that uses 2 wavelengths and 4 time slots, the grey and white boxes denote the spreading codes used to transmit the bit "1" and "0" respectively. At the decoder, a WDM splitter is used to isolate each wavelength. A passive optical splitter is then used to obtain 4 copies of the encoded signal for realignment. A cross-connect is placed to map all the power corresponding to the "1" and "0" bits into two multiplexers that are fed into the positive and negative terminal of the balanced receiver respectively.

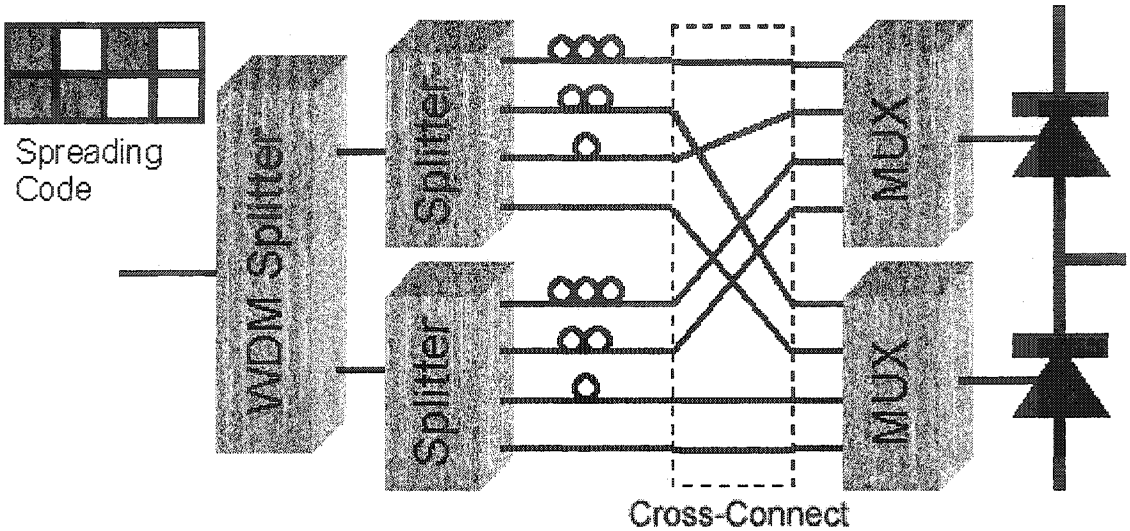

Fig. 4.2 High-level implementation of BCDD decoder.

4.1 Design Constraints and Algorithm

BCDD has revisited the code design constraints for obtaining an OCDMA spreading sequence. Unlike traditional spreading sequences with low Hamming weight, BCDD fixes the Hamming weight to the maximum meaningful value for antipodal signalling – half of the code size. This ensures the maximum distance between the signal constellation for the "1" and "0" bits. Furthermore, BCDD sets the maximum absolute aperiodic auto- and cross-correlation to variable values κ_a and κ_c respectively. For m wavelengths and n time-chips, these conditions are described mathematically as:

$$\left\langle \mathbf{s}_u^1, \mathbf{s}_u^1 \right\rangle = \left\langle \mathbf{s}_u^0, \mathbf{s}_u^0 \right\rangle = w = \frac{1}{2} m \times n \,, \tag{4.1}$$

$$\left| \left\langle \mathbf{s}_u^1 - \mathbf{s}_u^0, \mathbf{s}_u(X, Y, \tau) \right\rangle \right| \le \kappa_a \quad \tau \neq 0 \,, \tag{4.2}$$

$$\left| \left\langle \mathbf{s}_u^1 - \mathbf{s}_u^0, \mathbf{s}_v(X, Y, \tau) \right\rangle \right| \le \kappa_c \,, \tag{4.3}$$

for all distinct users u, two-bit sequences $XY \in \{00,01,10,11\}$ and $\tau \in \{0,1,\ldots,n-1\}$. s_u^1 and s_u^0 are the spreading sequences for user u when "1" and "0" are transmitted respectively. It is worth noting that $\mathbf{s}_u^0 = I - \mathbf{s}_u^1$ for all chips for BCDD. The definition of inner product is the same as previously defined for DFSC. Furthermore, we have set $\kappa_a = \kappa_c$ in the code design. For $\kappa_a \neq \kappa_c$, trials have been conducted and show that performance degrades marginally while the maximum number of codes generated remains approximately the same.

A greedy algorithm is employed to obtain a set of pseudorandom BCDDs that satisfy the conditions. The algorithm arbitrarily chooses spreading sequences that consist of w ones and w zeros. It then checks for the auto- and cross-correlation condition with the previously found codes. The algorithm stops searching when no new code is found after a prescribed number of tries – which we set to be 100 times the code size – or if a desired number of codes have been reached.

4.2 Code Generation Results

We study the effect of varying the number of wavelengths and time-chips on the maximum number of users. The notation BCDD(m,n,κ_c/w) denotes a system employing m wavelengths, n time-chips and a normalized correlation which is equal to the maximum auto- and cross-correlation value (κ_c) divided by the Hamming weight (w) of the code. From Fig. 4.3, we see that for codes of the same size (mxn) and the same normalized correlation, we can obtain a larger code ratio when $m > n$. This is due to the same reason as stated for DFSCs: since the auto- and cross-correlation values are set to be the same, the synchronous system argument in equation (3.6) also applies to BCDD. Furthermore, we can observe that a larger size in either code dimension results in the same ratio of supported users having a lower normalized correlation. A comparison is also made to DFSC (solid circles in Fig. 4.3). We see from the plot that the BCDDs can potentially generate the same number of codes with less correlation than direct detection codes. Furthermore, compared with the only other 2D differential detection codes, namely the prime/OOC [53] (solid triangle in Fig. 2), our proposed BCDD can support far more users, i.e., generate significantly more codes, given the constraints in (4.1) to (4.3).

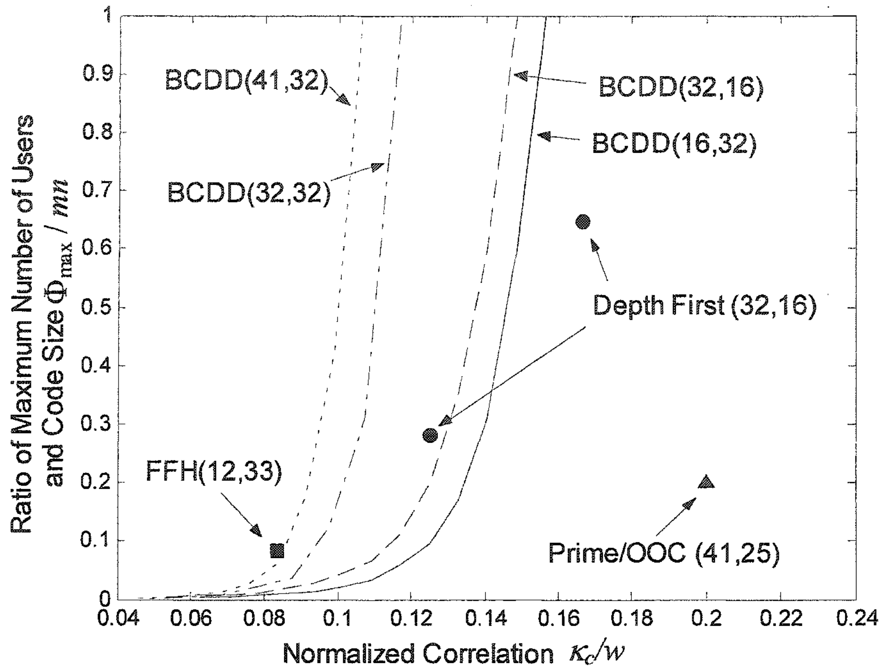

Fig. 4.3 Ratio of maximum number of generated codes to code size subject to different correlation constraints.

As observed in Fig. 4.3, by relaxing the cross-correlation constraint, we can greatly increase the amount of codes generated by the algorithm. This additional degree of freedom in code design is highly desirable as OCDMA systems may be reconfigured to accommodate more users as necessary. On the other hand, traditional direct and differential detection code design algorithms typically limit the number of maximum potential users (Φ_{max}) on a network. For instance, although at a normalized correlation of 0.0833, FFH(12,33) (solid square in Fig. 4.3) can generate about the same proportion of maximum supported users as BCDD(41,32), the FFH algorithm does not allow the flexibility of adding more users beyond such capacity. For BCDD, it is possible to generate codes beyond the code size, i.e. $\Phi_{max} > m \times n$.

4.3 Performance Analysis

The two methods for evaluating the BER performance of DFSC are also applied to BCDD. Moreover, the same assumptions (A1) to (A5) in section 3.3 also apply to the following performance analysis.

4.3.1 Average Variance Estimation

4.3.1.1 Mathematical Analysis

BCDD employs an antipodal signalling strategy, where an equal amount of signal power is used to transmit both a "0" and "1" data bit. As stated in (4.1), the Hamming weight w of the spreading sequence is $w=\langle \mathbf{s}_u^1,\mathbf{s}_u^1\rangle=\langle \mathbf{s}_u^0,\mathbf{s}_u^0\rangle$. For a given bit slot, the transmitted sequence of user u is $b_u\mathbf{s}_u^1+\bar{b}_u\mathbf{s}_u^0$, where b_u is the transmitted bit of user u, and $\bar{b}_u=1-b_u$. Using assumptions (A1) to (A4), at the balanced receiver (differential detector), the output of the differential detector for user u can be modeled as

$$out_u=\langle \mathbf{r},\mathbf{s}_u^1\rangle-\langle \mathbf{r},\mathbf{s}_u^0\rangle+\eta\,, \tag{4.4}$$

where r is the received signal corresponding to the summation of the transmitted signals of all active users assuming asynchronous operation, and η represents the overall receiver noise from both the positive and negative terminal. By assumption (A5), we neglect the effect of noise in the following analysis. Without loss of generality, we assume that user 1 is the desired user. Using the knowledge that $<s_u^1,\ s_u^0>\ =\ <s_u^0,\ s_u^1>\ =0$, the matched filter output takes the form

$$out_1=(b_1-\bar{b}_1)w+\left\langle \sum_{k=2}^{K}\mathbf{s}_k(X_k,Y_k,\tau_k),\mathbf{s}_1^1-\mathbf{s}_1^0\right\rangle, \tag{4.5}$$

where K is the number of active users, $s_k(X_k, Y_k, \tau_k)$ denotes the spreading sequence when bits $X_kY_k \in \{00,01,10,11\}$ are transmitted consecutively by user k, and asynchronism causes a time shift of τ_k time chips between user k and user u. X and Y are assumed to be i.i.d. Bernoulli random variables with probability $p =$

0.5, while τ is i.i.d. uniformly distributed on {0,1,2,...,n-1}. For BCDD, the mean value of the MAI is fairly close to zero (typically below 10^{-5}). The interference variance is caused by the time-shifted cross-correlation of all other possible users in the network when "11", "10", "01" and "00" are transmitted over two-bit periods:

$$\bar{\sigma}_k^2 = E_k\left[VAR_{X,Y,\tau}\left(\left\langle \mathbf{s}_k(X_k, Y_k, \tau_k), \mathbf{s}_1^1 - \mathbf{s}_1^0 \right\rangle\right)\right]. \tag{4.6}$$

The average interference-limited BER performance of differential detection system with antipodal signaling is obtained from

$$\begin{aligned} BER &= \Pr[b=1]\Pr[MAI < -w] + \Pr[b=0]\Pr[MAI > w] \\ &= \frac{1}{\sqrt{2\pi}\bar{\sigma}_{pq}} \int_w^\infty \exp\left(\frac{-x^2}{2\bar{\sigma}_{pq}^2}\right) dx \end{aligned}, \tag{4.7}$$

which is equivalent to the expression in (2.2). $\bar{\sigma}_{pq}^2$ is obtained using (4.6) when for all possible code pairs p and q are considered.

4.3.1.2 Results

The BER performance of BCDD is compared to DFSC in Fig. 4.4. Using 32 wavelengths, 16 time chips and a normalized correlation of 0.125, the performance of BCDD is clearly better than DFSC – BCDD can support 16 users with a BER below 10^{-9} while DFSC can support only 9 users. It is important to recall that the performance of DFSC is very similar to all other 2D direct detection codes; hence, BCDD can outperform existing 2D direct detection systems. This is expected due to the use of an antipodal signalling strategy. By increasing the code size in either the wavelength or time dimension, more users can be accommodated at the same BER as expected. BCDD(32,32,0.0977) can support 30 users, while BCDD(41,32,0.0991) can support 37 users.

To ensure fairness when comparing the BER performance to other 2D differential detection schemes, such as prime/OOC [53], we use the same performance analysis platform to calculate the interference-limited average variance for the BER calculation. We have found that prime/OOC(41,25,0.2) can support 16 users at a BER below 10^{-9}. With a similar code size, BCDD(32,32,0.0977) can support 30 users, which is almost twofold that of the other systems. This can be explained by noting that BCDD uses both antipodal signalling strategy and the maximum allowable Hamming weight in the code design.

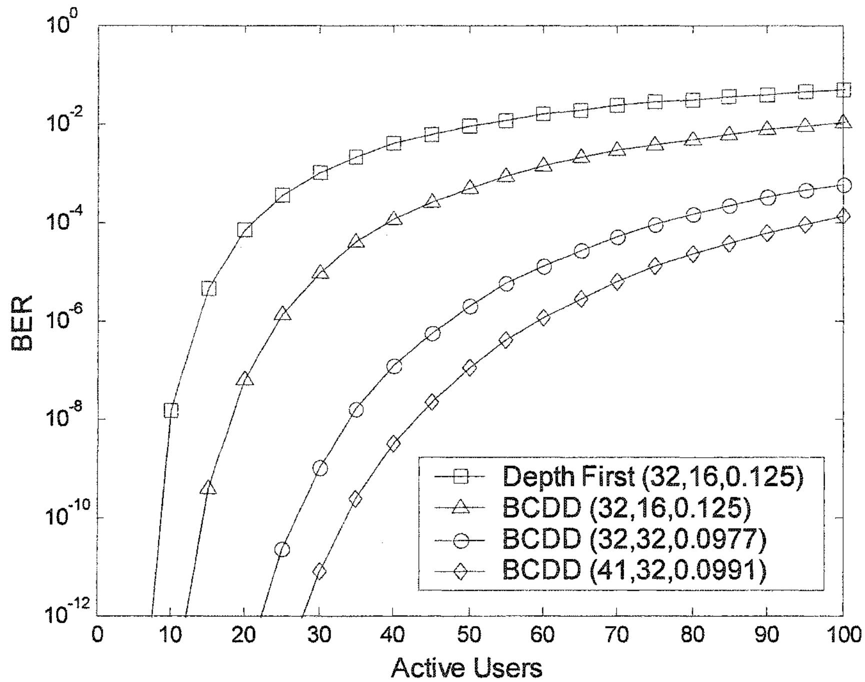

Fig. 4.4 Performance comparison of the BCDD and DFSC.

4.3.2 Binary Statistics Calculation

4.3.2.1 Mathematical Analysis

The same binary statistics analysis used for DFSC applies to BCDD, except that the cross-correlation and the maximum MAI for K active users ranges from $-\kappa_c$ to κ_c and $-(K-1)\kappa_c$ to $(K-1)\kappa_c$ respectively. When evaluating the BER performance, the expression to be used for BCDD is

$$BER = \Pr[b=1]\Pr[MAI < w] + \Pr[b=0]\Pr[MAI > w] = \frac{1}{2}\left(\sum_{\alpha=-(K-1)\kappa_c}^{-w} P(\alpha) + \sum_{\alpha=w}^{(K-1)\kappa_c} P(\alpha)\right) \quad (4.8)$$

4.3.2.2 Results

BCDD(41,32,0.0991) is used for analyzing the probability distribution of the MAI. Fig. 4.5 shows the MAI distribution when 10, 40, 80 and 120 users transmit on the network. A total of 15 samples are taken for each calculation, where users are randomly chosen from a total of 559 spreading codes available in the sequence generation. It is worth noting that the plots in Fig. 4.5 are discrete in nature, they only appear to be continuous due to the scale of the x-axis. Unlike DFSC, the MAI distribution for BCDD has a Gaussian-like shape even when there are only 10 active users online. The thickness of the distribution comes from the 15 different realizations of the calculation. One can expect from the pmf that the BER performance evaluated using (4.8) closely resembles the actual average BER of the channel. The differences in BER are shown in Table 4.1.

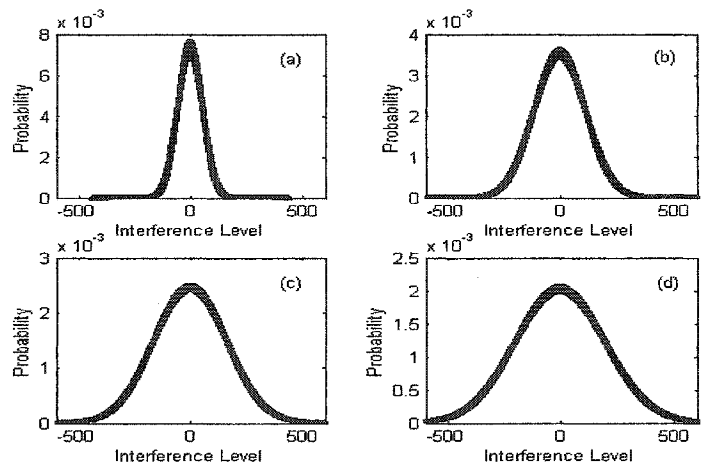

Fig. 4.5 MAI distribution from binary statistics for BCDD(41,32,0.0991) when the number of active users is (a) 10, (b) 40, (c) 80 and (d) 120.

Table 4.1 Differences between Gaussian approximated and calculated BER for BCDD.

Number of Users	Approx. BER	Calculated BER	% Difference
10	5.4×10^{-34}	0	--
40	3.1×10^{-9}	2.4×10^{-9}	-29.8%
80	2.2×10^{-2}	2.3×10^{-5}	3.9%
120	4.4×10^{-4}	4.5×10^{-4}	2.7%

For variance estimation, Fig. 4.6 shows a comparison between the estimated variance obtained from Monte-Carlo simulations (solid line) and the results obtained from considering the binary statistics (dots). As expected, the variance of the MAI increases linearly as function of the number of active users. It is worth noting that the MAI variance for BCDD is much higher than that of DFSC. The reason is that BCDD employs higher weight codes with higher cross-correlation. Nonetheless, due to the high weight nature of the code, the BER remains low as it requires a much higher MAI power to cause errors. For example, in Fig. 4.5(a), for 10 users, the MAI can take values in the range of 400. However, since the code weight for the system is 656, one can conclude that a 10-user BCDD(41,32) system will have a BER of exactly zero if receiver noise is neglected.

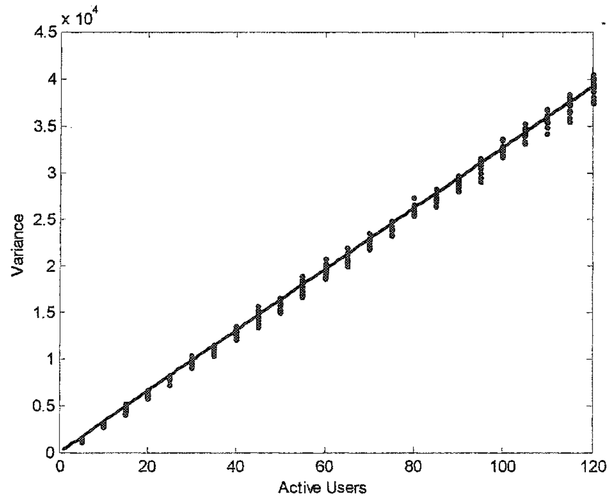

Fig. 4.6 Comparison between estimated MAI vairance (thick line) and results obtained from binary statistics (dots) for BCDD(41,32,0.0991).

The interference-limited BER performance as a function of active users is shown in Fig. 4.7. The thick solid line in the figure represents the BER performance obtained from variance estimation and the dots correspond to the results of the 15 trails. As we can see, for BCDD, the BER from variance estimation is an upper bound to the actual BER for low number of users. As the number of users increases, the two results converge.

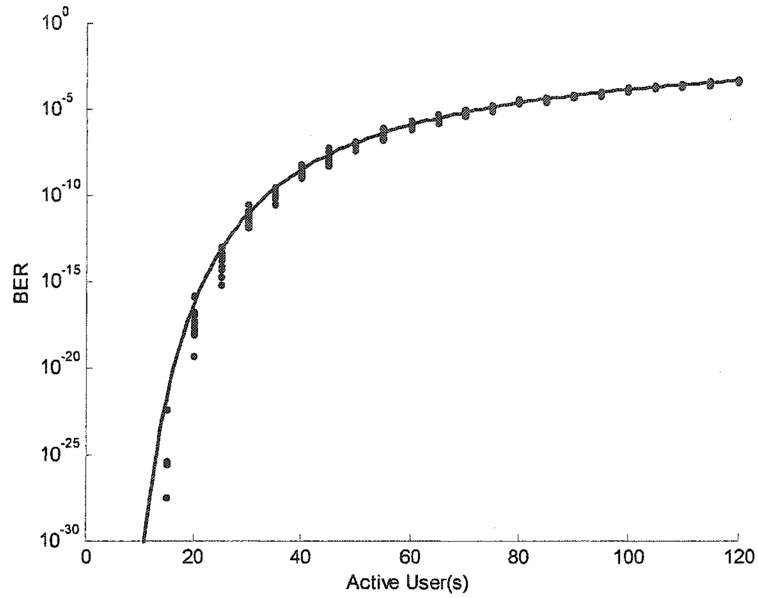

Fig. 4.7 Comparison of BER performance of BCDD(41,32,0.0991) using variance estimation (thick line) and binary statistics (dots).

4.3.3 Forward Error Correction

The use of FEC is demonstrated using the BCDD with 41 wavelengths and 32 time chips. In Fig. 4.8, the thick solid line represents the amount of codes that can be generated as a function of the normalized correlation. Below the line, five other lines show the maximum number of users that can simultaneously transmit with BER below 10^{-9} when various types of FEC are applied. The maximum number of users that can be supported with BER below 10^{-9} for an uncoded system is 37. The FEC used are RS(255,239), RS(255,233), and commercially available Turbo Product Codes (TPC) with rate 0.931 and 0.824. When such FEC codes are applied, the number of users that can be supported increases to 115, 151, 211 and 320 respectively.

When the cross-correlation of a BCDD system is relaxed, an increase in the maximum number of supported users can be achieved. When the correlation of the system is low, so is the average variance, resulting in a good BER performance. However, the code generation algorithm only provides a limited number of user codes. Although the average variance of the MAI increases with a higher normalized correlation, a larger number of codes can be generated. More importantly, the average BER performance is approximately constant for a range of normalized correlation. Thus, optimum operating conditions that provide good BER performance and a large number of codes can be found.

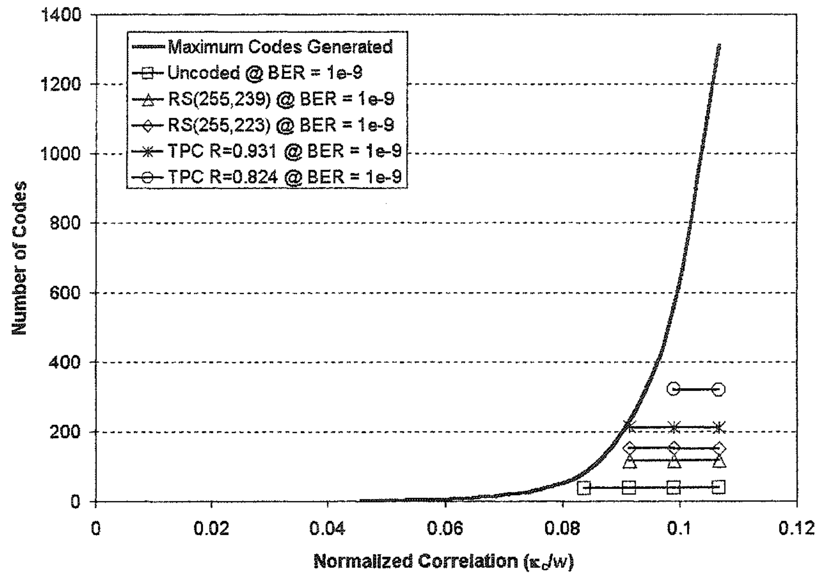

Fig. 4.8 BCDD(41,32) code generation and users supported at 10^{-9} with and without forward error correcting code.

4.4 Optical Simulation Results

Due to limitations of *Linksim*™, simulations of the BCDDs are performed in *MATLAB*™. However, the optical pulse is extracted from *Linksim*™ with proper rise and fall time (non-rectangular pulse). Nonetheless, the effect of fiber is not modelled in the following example.

4.4.1 Simulation Setup

BCDD(48,4,0.125) is employed for the purpose of this simulation. Note that the code size is 48x4 = 192, as supposed to 16x16 = 256 in the DFSC demonstration. The code generation algorithm finds 24 codes that satisfy the correlation constraints, and calculations predict that this system can support about 9 users with an average BER below 10^{-9}. Among the 24 codes, 8 codes are chosen at random. The codes are listed in Table 4.2. The spreading sequence shown in the table correspond to the hexadecimal representation of the chip that is actively transmitting when the bit "1" is sent. The four time chips are separated by a space in the representation. For bit "0", the complementary chip is sent. The network topology for this simulation is the same as in Fig. 3.12 for DFSC.

Table 4.2 Spreading sequence of BCDD(48,4,0.125) used in demonstration.

Code	Spreading Sequence
1	7322FA4242AC C0FD6531FE2A 72A227279BB2 A136F4E1317D
2	7FCC3678012D 09DAA7C07F7D A0C281A677C4 0A2C74C797F9
3	7C5454319EE1 32F176B1B5AC 38BF1F5BC5A3 54149D022B66
4	BFE568AC3E29 A4B479913F58 A9B9ED282765 D2E6D406A520
5	2D76BC1DB395 5B33E0E42B7A 353D34454FAD 0F9C0C2E6288
6	9A8EB08FF1AF 690877326DB7 D20C231C0D35 D9739F900DA3
7	8C5ABD0FEB93 BF3911030723 C99706F258BC B6276B8A807B
8	8A35B22BFDFD D1C97C832291 C1E4E28E124A 9559933F64B9

4.4.2 Simulation Results

For the simulation, an OC-3 data rate (155.52Mbps) is used, the asynchronism delays are randomly chosen to be 0.2773, 0.5566, 0.4844, 0.9512, 0.2305, 0.4788, 0.5254 and 0.7910 of a bit period respectively for the 8 users.

The decoded electrical signals for all users are shown Fig. 4.9. On the figure, the matched filter output of the PRBS signals are listed with the corresponding users. Similar to DFSC, the auto-correlation peak stands out among the MAI for this realization of 8-user BCDD system. Furthermore, it is easy to see that the threshold for this system can be set to zero, which is an advantage of BCDD. Fig. 4.10 further shows the decoder output of user 1 as the number of active users increases.

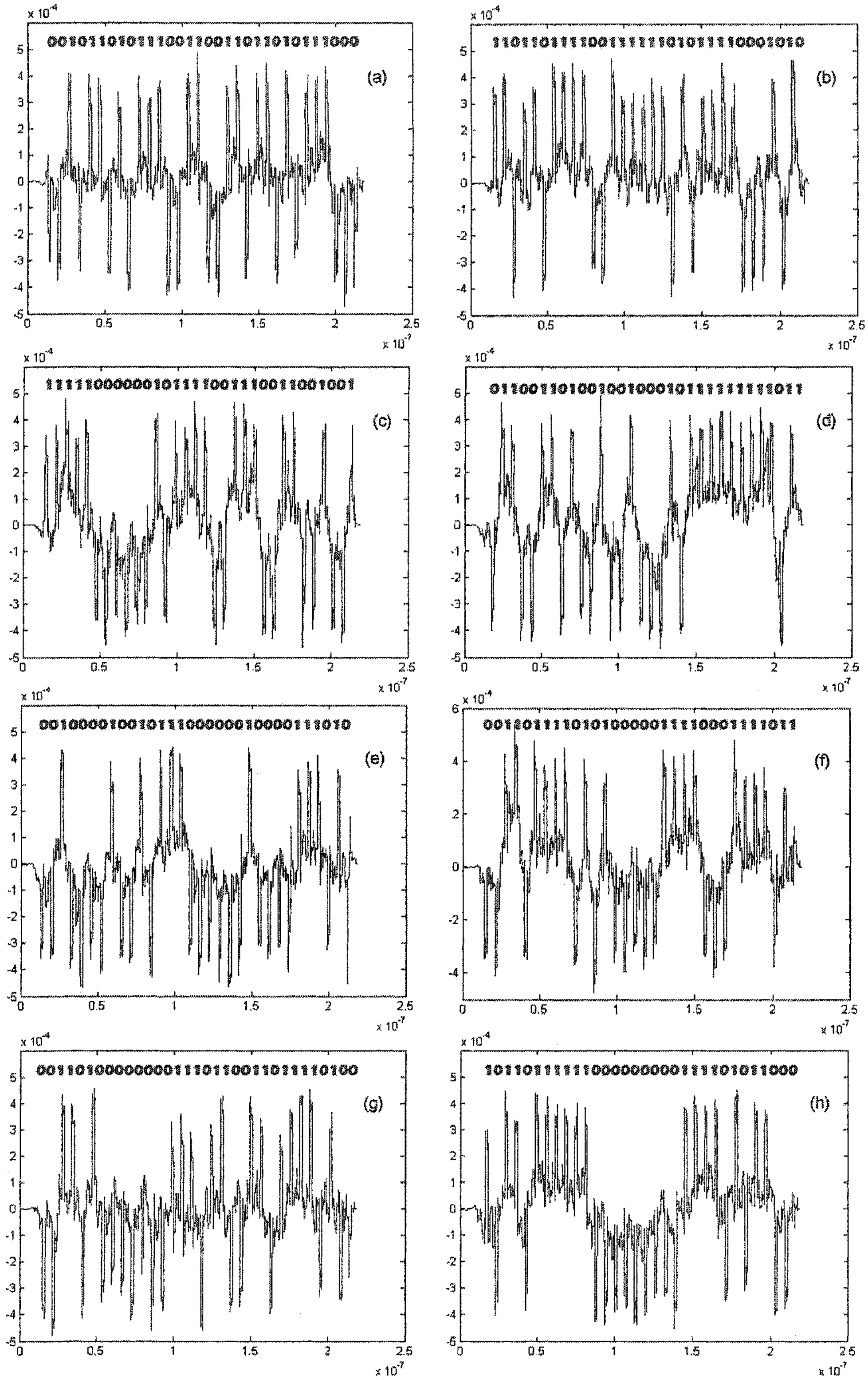

Fig. 4.9 Decoded electrical signal (voltage versus time) for 8-user OCDMA system: (a) code 1, (b) code 2, (c) code 3, (d) code 4, (e) code 5, (f) code 6, (g) code 7 and (h) code 8.

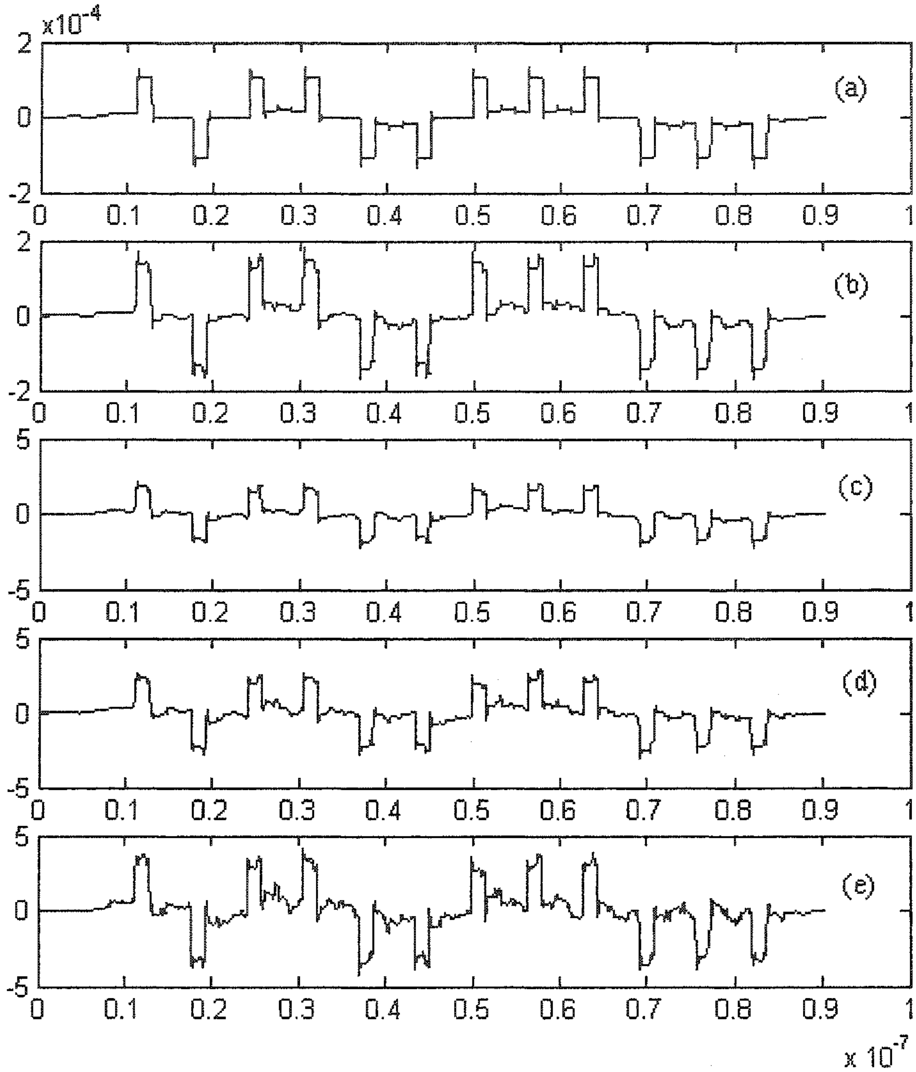

Fig. 4.10 Decoder output (voltage versus time) for user 1 with transmitted pattern "101100111000" and interference due to: (a) no other user; (b) 1 user; (c) 2 users; (d) 4 users; and (e) 7 users.

Chapter 5 Asynchronous OCDMA Channel Capacity

The use of DFSCs and BCDDs with FEC has shown great performance improvement over previously proposed OCDMA systems, both in terms of increasing the maximum number of codes that can be generated and the BER performance. However, the ultimate capacity of an OCDMA channel, and thus the performance gap of BCDD and DFSC, has not been investigated. This information is useful for designing proper error correction codes to be used in OCDMA, and it provides an upper bound on what can be achieved by OCDMA.

This chapter analyzes the OCDMA channel from an information theoretical viewpoint. Specifically, we assume that the decoder employs a SUD technique for recovering the user information bits, since the high-speed and bursty nature of the OCDMA channel makes even sub-optimal multi-user detection schemes too complex to implement. We begin by modelling the OCDMA channel and then investigate its capacity for three different cases: interference-limited transmission, transmission impaired by interference and AWGN noise, and a Gaussian approximation for the MAI.

5.1 System Model of Asynchronous OCDMA

We make the following assumptions for modeling an asynchronous OCDMA system in which K users transmit data concurrently over an optical network. Firstly, each user employs a 2-level binary signal to modulate the outgoing signal.

Secondly, SUD is employed at the receiver, which tries to recover the message sent by the i-th user from the received signal. Thirdly, assuming synchronization at the chip level, the received signal at time instant n can be described, at the chip level, as

$$y_n = \mathbf{b}_n \mathbf{s}_n^T, \quad (5.1)$$

where $\mathbf{b}_n = (b_{1,n}, b_{2,n}, \cdots, b_{K,n}) \in \{0,1\}^K$ are the data bits transmitted by users 1,2,..., K and $\mathbf{s}_n \in \{0,1\}^K$ is a row vector due to the different spreading sequences of the users. Finally, the transmission is assumed to be interference-limited, i.e., the effects of receiver and channel noise are negligible when compared to the interference of other users transmitting with equal power.

Consider the case of 3 users employing the same type of spreading sequences, i.e., all users transmit the chips "*1*" and "*0*" over the channel with probability q and 1-q, respectively. We can model such transmission using a Discrete Memoryless Channel (DMC) as shown in Fig. 5.1. At the output of the channel, the input signal is corrupted by interference due to other users, each operating independently with the same probability of transmitting bit "1" and "0". For a 3-user system, if a user transmits bit "0", the receiver will receive "0" if and only if the other two users also transmit a zero. Hence the transition probability is $(1-q)^2$. Similarly, the receiver takes the value 1 if one interfering user transmits the bit "1" and the other transmits "0", which occurs with probability $2q(1-q)$.

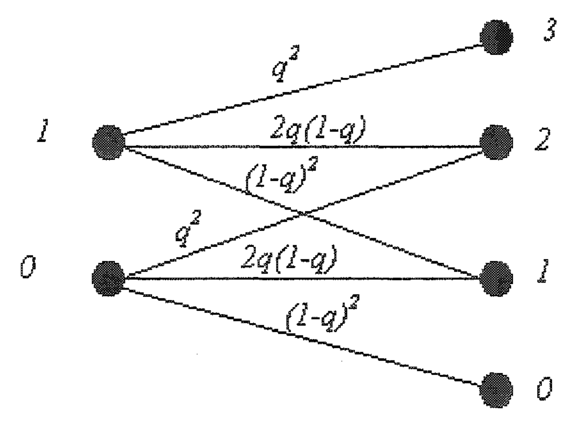

Fig. 5.1 Discrete memoryless channel model of a 3-user asychronous OCDMA system with SUD.

For the general case of K active users, the DMC has two inputs $X \in \{0,1\}$, K+1 outputs $Y \in \{0,1,\cdots,K\}$ and conditional probabilities given by

$$P_{Y|X}(y \mid x) = \binom{K-1}{y-x} q^{y-x} (1-q)^{K-1-y+x}, \qquad (5.2)$$

where for notational convenience $\binom{K-1}{-1} = \binom{K-1}{K} = 0$. The channel can also be described by a matrix of conditional probabilities

$$\mathbf{P}_{Y|X} = \begin{bmatrix} \beta_0 & \beta_1 & \cdots & \beta_{K-1} & 0 \\ 0 & \beta_0 & \cdots & \beta_{K-2} & \beta_{K-1} \end{bmatrix} \qquad (5.3)$$

where $\beta_i = \binom{K-1}{i} q^i (1-q)^{K-1-i}$.

5.2 Capacity of Asynchronous OCDMA Transmission

5.2.1 Interference-Limited Channel without Noise

With the model developed in the previous section, we now calculate the Shannon capacity of the DMC described by (5.2) and (5.3). Since the probability of output symbol Y is given by $P_Y(y) = \binom{K}{y} q^y (1-q)^{K-y}$, the mutual information of the DMC can be expressed as:

$$\begin{aligned} I_{noiseless}(X;Y) = & -\sum_{i=0}^{K} \binom{K}{i} q^i (1-q)^{K-i} \log_2\left(\binom{K}{i} q^i (1-q)^{K-i}\right) \\ & + \sum_{i=0}^{K-1} \binom{K-1}{i} q^i (1-q)^{K-1-i} \log_2\left(\binom{K-1}{i} q^i (1-q)^{K-1-i}\right) \end{aligned}. \qquad (5.4)$$

Since this calculation is done for transmission of a single user and under the assumption of independently operating users that utilize SUD, the aggregate throughput over the network by all K users is then limited by $C = K \sup_{q \in [0,1]} I(X;Y)$ bits per OCDMA chip. Specifically, an OCDMA chip is defined by the signal bandwidth and the time duration of the pulse; hence, bits per OCDMA chip can be converted to bits/sec/Hz using the knowledge of the two parameters.

The mutual information of such an asynchronous OCDMA channel is plotted as a function of input probability q in Fig. 5.2. When only one user is active in the system, the OCDMA channel reduces to a binary symmetric channel and the channel capacity is 1 bit per chip as in a binary TDMA system. Fig. 5.2 shows that as the number of users increases, the interference caused by asynchronism reduces the theoretical capacity limit. It is also worthwhile to note that the capacity limit does not occur for $q = 0.5$, but resides on a fairly unstable peak dependent on the number of users. For a system with 50 users, the optimum capacity of 0.8374 bits per chip is achieved when $q = 0.03$. Note that for $q = 0.5$, the limit is around 0.7288 bits per chip. For a sufficiently large number of users, the channel throughput limit varies slowly both as a function of q and the number of users. This is a highly desirable feature in a network with bursty traffic, since the channel throughput limit remains high even when the number of active users is misestimated.

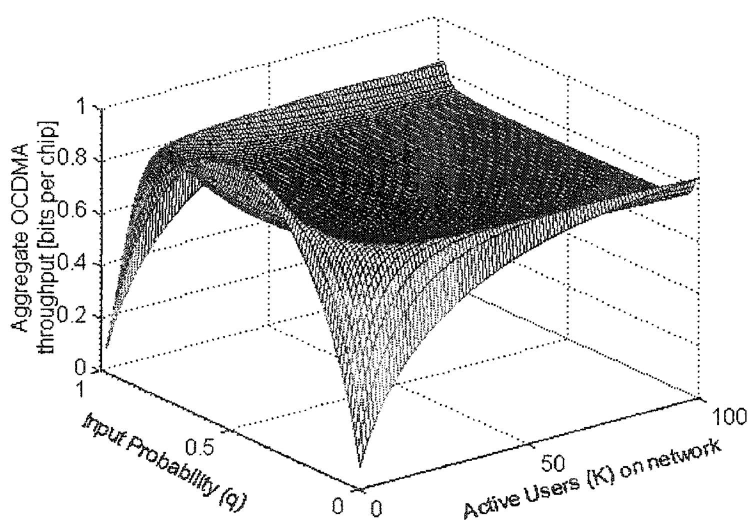

Fig. 5.2 Fundamental limits on asynchronous OCDMA transmission in a noise-free environment.

Fig. 5.3 further examines the system throughput as a function of input probability and the number of simultaneous users. Clearly, for $q = 0.5$, the system efficiency remains relatively constant as the number of users increases. The optimum capacity is achieved when there are 2 users in the system. As the number of users K increases, the optimum value of q decreases approximately as the reciprocal value of K. Nonetheless, any deviation from the optimal q results in a sharp drop of channel throughput efficiency (see Fig. 5.2). Ultimately, we conclude that the interference-limited throughput of an OCDMA system is practically limited by about 0.7 bits per chip for a variable number of users in the network.

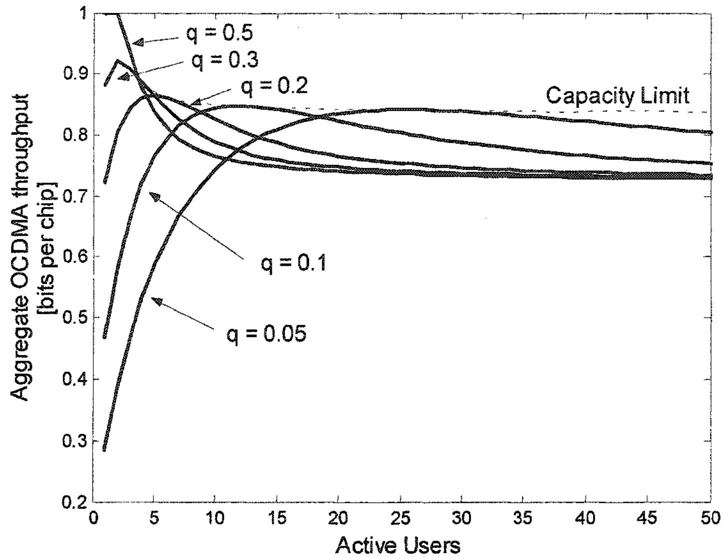

Fig. 5.3 Aggregate OCDMA throughput for different values of input probability.

5.2.2 Capacity in the presence of AWGN Noise

In the previous section, we omitted the presence of channel noise. Although this gives an upper bound on the capacity for OCDMA transmission under ideal conditions, noise should be included in the analysis to assess the robustness of the transmission scheme. Assuming additive white Gaussian channel noise and a binary input X with continuous output Y, the mutual information is given by

$$\begin{aligned} I_{AWGN}(X;Y) &= -\int_{-\infty}^{\infty}\left(\sum_{j=0}^{K}\binom{K}{j}q^j(1-q)^{K-j}N(y,j,\sigma^2)\right)\log_2\left(\sum_{j=0}^{K}\binom{K}{j}q^j(1-q)^{K-j}N(y,j,\sigma^2)\right)dy \qquad (5.5) \\ &+\int_{-\infty}^{\infty}\left(\sum_{i=0}^{K-1}\binom{K-1}{i}q^i(1-q)^{K-1-i}N(y,i,\sigma^2)\right)\log_2\left(\sum_{i=0}^{K-1}\binom{K-1}{i}q^i(1-q)^{K-1-i}N(y,i,\sigma^2)\right)dy \end{aligned}$$

where the Guassian probability density function mean μ and variance σ^2 is denoted by

$$N(y,\mu,\sigma^2)=\frac{1}{\sqrt{2\pi\sigma^2}}\exp\left(-\frac{(y-\mu)^2}{2\sigma^2}\right). \tag{5.6}$$

In Fig. 5.4, the maximum throughput of the OCDMA channel is plotted as a function of noise variance for different number of users when $q = 0.5$. It is clear that for low noise variance, a system with a small number of users can potentially accomplish a higher channel throughput. As the channel noise variance σ^2 increases, the system performance decreases as it switches from interference-limited to noise-limited. This effect is more apparent in systems with a small number of transmitting users. As the total number of users on the networks increases, the effect of noise is less dramatic, suggesting that the OCDMA system is robust, even when the signal power of a user is low compared to the noise level. This is due to the fact that the total amount of power used to transmit data over the network increases as the number of active users increases, hence the noise becomes less relevant compared to the effects of the MAI. Table 5.1 summarizes the channel characteristics for difference cases of noise and MAI variances.

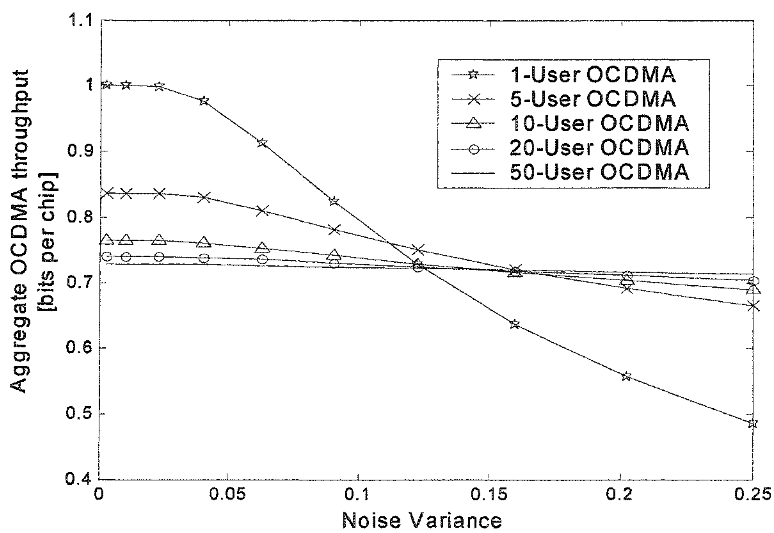

Fig. 5.4 Aggregate OCDMA throughput limits for equiprobable input distribution and different values of noise variance.

Table 5.1 Channel characteristics with respect to the noise and MAI variance.

		Number of Active users and σ^2_{MAI}	
		Large	Small
Noise Variance	High	Interference-Limited	Noise-Limited
σ^2_{Noise}	Low	Highly Interference-Limited	Depends on both

For the noiseless case, the optimal q that maximizes the channel mutual information is a function of the number of active users in the system. However, the same does not hold true for channel with high noise variance. In Fig. 5.5, the aggregate OCDMA throughput is plotted as a function of the input probability q and the number of active users K for two different noise variances. As the noise level increases, the aggregate OCDMA throughput decreases faster for input probabilities that are far from q = 0.5. This shows the robustness to noise of equiprobable input signaling for OCDMA channel.

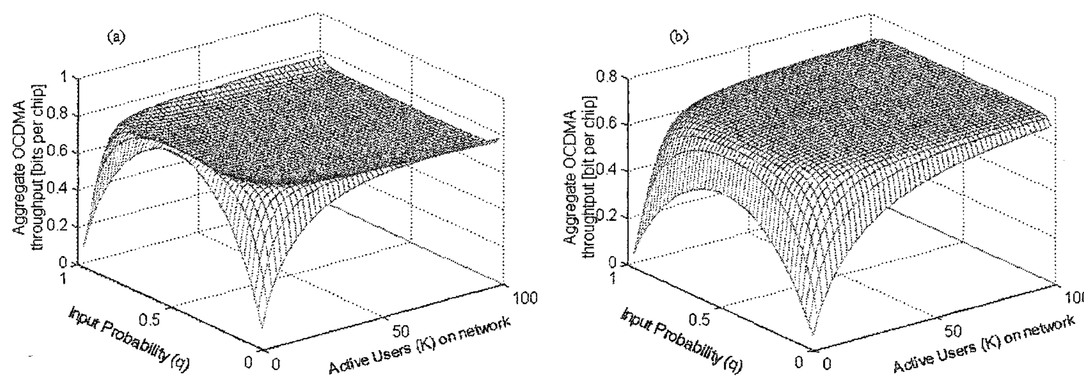

Fig. 5.5 OCDMA throughput at different noise variance with different input distribution for noise variance (a) σ^2 = 0.09 and (b) σ^2 = 0.25

5.2.3 Capacity under Gaussian Multiuser Interference Approximation

In practice, it is extremely difficult to distinguish the many output levels of the OCDMA channel. Thus, it is of interest to compute the modified maximum throughput of an OCDMA channel when the Gaussian approximation is employed to model MAI. Specifically, we assume each interfering user transmits bits "1" and "0" with probability q and $1-q$. Using the Central Limit Theorem

(CLT) with K active users on the network, the interference can be approximated by Gaussian distribution with mean $(K\text{-}1)q$ and variance $(K\text{-}1)(q\text{-}q^2)$. Graphically, the Gaussian approximated OCDMA channel is modeled as in Fig. 5.6.

The conditional probability density in this case is given by

$$p_{Y|X}(y\mid x)=N\left(y,x+(K-1)q,\sigma^2+(K-1)(q-q^2)\right), \tag{5.7}$$

and the mutual information takes the form

$$I_{Approx}(X;Y)=-\int p(y)\log_2 p(y)dy+\frac{1}{2}\log_2\left(2\pi e\left(\sigma^2+(K-1)(q-q^2)\right)\right), \tag{5.8}$$

where $p(y)=qN\left(y,1+(K-1)q,\sigma^2+(K-1)(q-q^2)\right)+(1-q)N\left(y,(K-1)q,\sigma^2+(K-1)(q-q^2)\right)$ and σ^2 represents the variance of additive white Gaussian noise present in the system. A comparison between the throughput limits of the actual and approximated channel for different noise variance are plotted in Fig. 5.7(a) for 20 and 50 active users assuming an equiprobable input distribution. Fig. 5.7(b) further shows the comparison for different number of active users for three different values of noise variances.

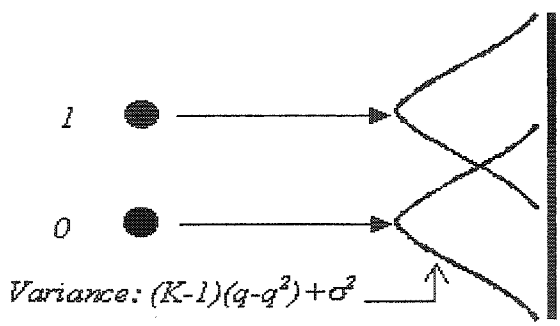

Fig. 5.6 OCDMA channel model using a Gaussian approximation for the MAI.

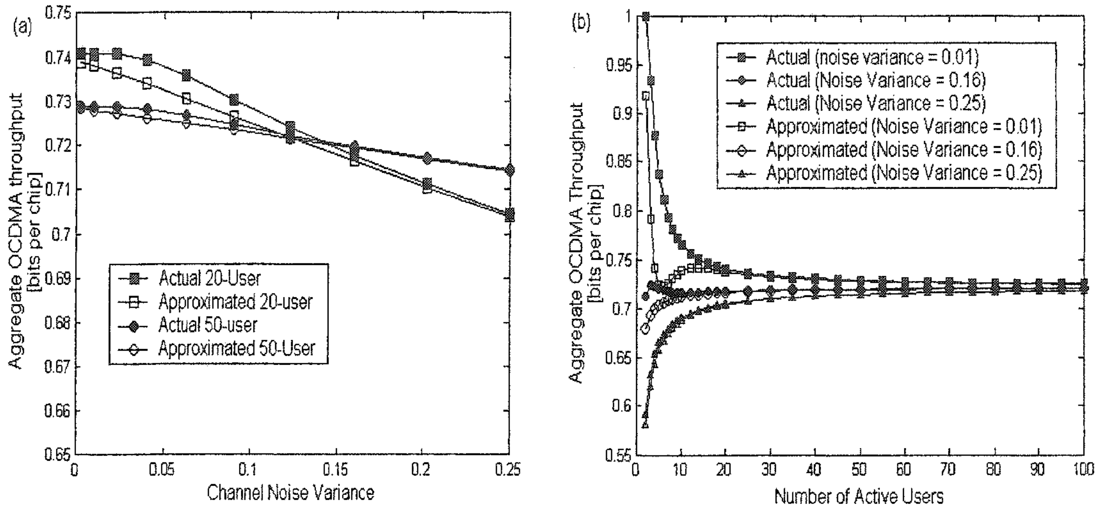

Fig. 5.7 Aggregate OCDMA throughput for actual and approximated channel at (a) different noise variance and (b) different number of active users.

From Fig. 5.7(a), we can see that as the number of active users increases, the difference between the theoretical limit of the exact channel and the approximated channel decreases. This can be intuitively explained using the CLT, i.e., the Gaussian approximation holds true only when enough random variables are added together. Furthermore, for high noise power, Fig. 5.7 suggests that it is less important to distinguish each output signal point in order to approach the capacity of a system.

It is also worthwhile to note that the difference between the output density of the approximated and the actual channel decreases when the noise level increases. This is due to the fact that the noise effectively turns the discrete density at the output into a continuous Gaussian-like distribution. Fig. 5.8 quantifies the likeness of the two probability density functions using the mean square difference. At high noise power, the mean square error decreases. Furthermore, the mean square error value is lower for a system with more users than with fewer users, confirming again the validity of Gaussian approximation for the OCDMA channel.

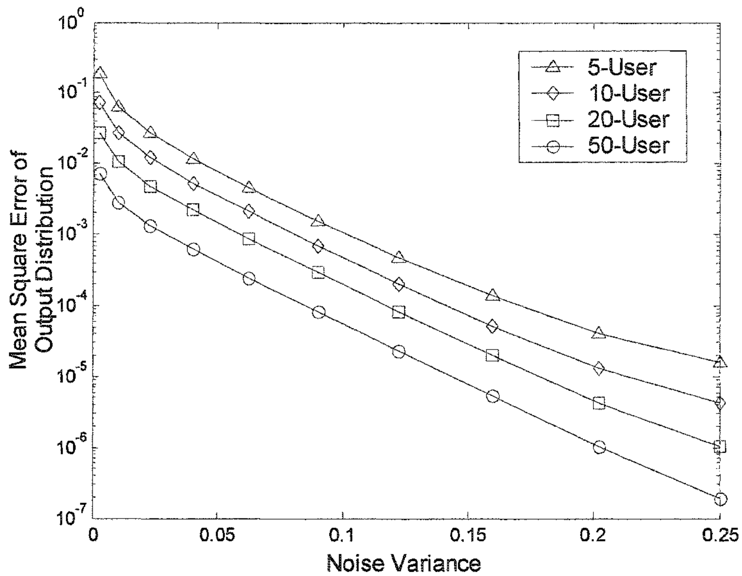

Fig. 5.8 Mean square error between the ideal OCDMA channel output density and the approximate output density.

5.3 Comparison of Proposed 2D-OCDMA Systems

Various OCDMA schemes proposed in the current literature are compared in Fig. 5.9. In the figure, the horizontal axis represents the ratio of the maximum number of codes generated by a particular scheme to the code size (the total number of wavelengths and time chips) used in the code generation. The diamond-shape symbols in the graph represent the number of supported users at a benchmark BER of 10^{-9}. The square symbols represent the rate-compensated (rate=7/8) number of users that can be supported at the same BER when a RS(255,223) is applied. The triangular symbols denote the number of users supported when a commercially available Turbo Product Code (TPC) is applied with rate 0.824 [81]. The considered 2D-OCDMA schemes presented here include: Prime/Hop [36], Yu-Park [37], Prime/OOC [53], FFH [35], and the proposed DFSC and BCDD spreading codes. These codes all have a suitable number of available wavelengths and time chips to permit hardware implementation, and they have shown good performance compared to other wavelength-time codes. In the presented codes, only BCDDs uses equiprobable channel input distributions; the others use sparse sequences.

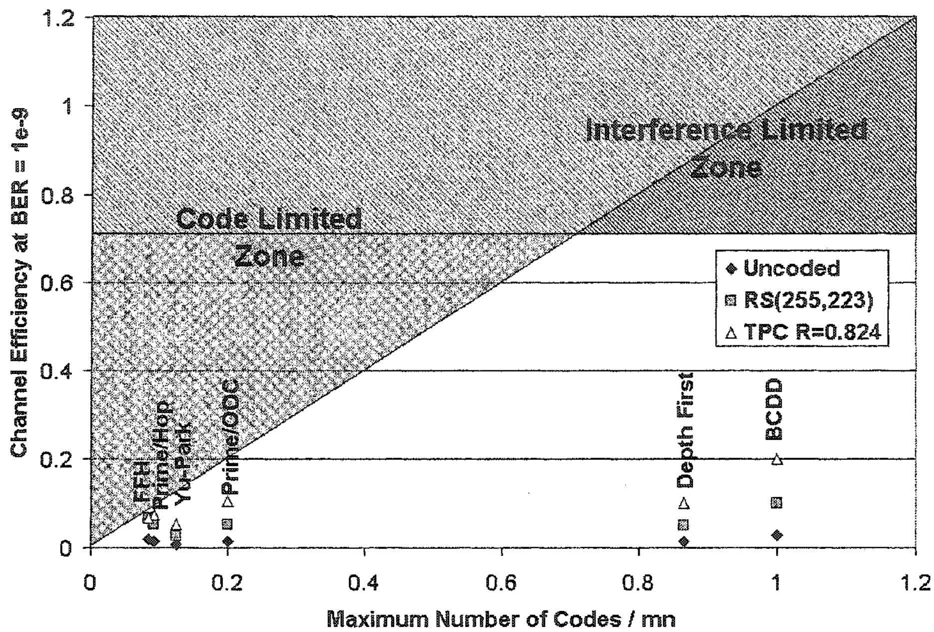

Fig. 5.9 Comparison of the performance and the bound for the proposed 2D-OCDMA schemes in the interference-limited case.

Fig. 5.9 divides the interference-limited channel efficiency plot into three regions: the code-limited zone, the interference-limited zone and the achievable zone. In the code-limited zone, the maximum number of supported users is limited by the maximum number of available spreading sequences that can be generated for a given code family. In the interference-limited zone, when enough spreading sequences are provided by the coding scheme, the maximum number of users that can be supported is limited by the channel capacity as calculated previously. These two zones constitute forbidden zones for an OCDMA network. The remaining represents the achievable region, in which clever coding and detection strategies can be employed to achieve the throughput. For the current existing systems, even after FECs are employed, most codes can achieve a compensated capacity of only 0.1 bits per chip. On the other hand, using the commercially available TPC, the BCDD can achieve a compensated rate of 0.2 bits per chip.

5.4 Spreading Sequence Specific Channel Capacity

The channel capacity that is obtained in the previous section corresponds to the optimum throughput that one can achieve using asynchronous OCDMA. However, depending on the coding scheme, this capacity may decrease. For example, in a normal AWGN channel, there is a difference between the channel capacity for Gaussian and antipodal signalling [59]. A similar phenomenon applies to the channel capacity obtained from considering the OCDMA chips and from considering the output of a matched filter in the bit period. Therefore, the channel capacity for DFSC and BCDD should be considered. At the output of the matched filter, the channel models for DFSC and BCDD are shown in Fig. 5.10. Gaussian approximation is assumed for calculating the distribution of the interference, and CLT is applied to obtain the total MAI variance $(K-1)\sigma^2_{MAI}$ when K users are online assuming equiprobable signalling for the input symbols. The interference-limited mutual information in bits per mn chips for this case is:

$$I_{MF}(X;Y) = -\int_{-\infty}^{\infty} p(y)\log_2 p(y)dy + \frac{1}{2}\log_2\left(2\pi e(K-1)\sigma^2_{MAI}\right), \qquad (5.9)$$

$$p(y) = \left[N\left(y, 1+\mu_{MAI}, (K-1)\sigma^2_{MAI}\right) + N\left(y, \mu_{MAI}, (K-1)\sigma^2_{MAI}\right)\right]/2 \quad \text{for DFSC}, \qquad (5.10)$$

$$p(y) = \left[N\left(y, 1, (K-1)\sigma^2_{MAI}\right) + N\left(y, -1, (K-1)\sigma^2_{MAI}\right)\right]/2 \quad \text{for BCDD}, \qquad (5.11)$$

where μ_{MAI} is the mean of the MAI, which does not affect the mutual information. The capacity of the K-user channel in bits per OCDMA chip in this case is:

$$C_{MF} = \frac{K}{mn}\max_{p(x)} I_{MF}(X;Y) \qquad (5.12)$$

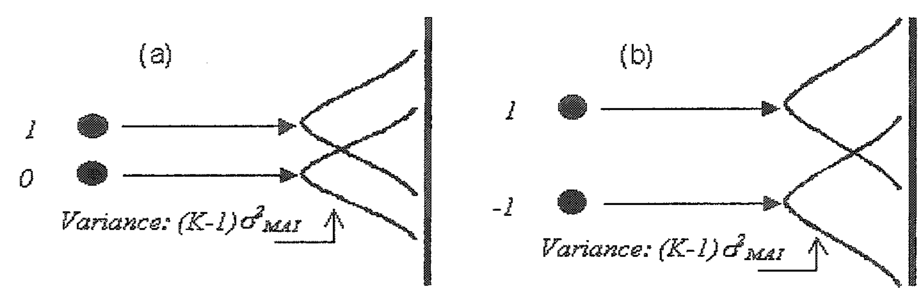

Fig. 5.10 Channel models for (a) DFSC and (b) BCDD.

5.4.1 DFSC Capacity

Since the spreading sequence specific capacity depends on the particular spreading sequence of choice, for illustration purposes, the capacity of DFSC(32,16,0.167) is calculated. The variance used in the DFSC capacity calculation is obtained from the pmf of every code pair in the spreading sequences when asynchronism is assumed. The calculated DFSC capacity is shown in Fig. 5.11. It can be seen from the figure that the maximum throughput of DFSC is approximately 0.275 bits per chip, which is much lower than the interference-limited capacity. For the interference-limited capacity, since DFSCs employ OOK with a Hamming weight of 6, the probability of transmitting a "1" at the chip level is $6/32/16/2 = 0.005860$. Also, DFSC(32,16,0.167) can generate a maximum of 332 codes, which defines the code limited zone. Finally, since each user can transmit a maximum of one bit in a bit interval regardless of the number of chip slots in use, the aggregate throughput is further limited when the number of active users is small. This constitutes the transmission limited bound for an OCDMA system. The fact that there is a large gap between DFSC and interference-limited capacity suggests that much improvement can be obtained if we change the channel coding scheme.

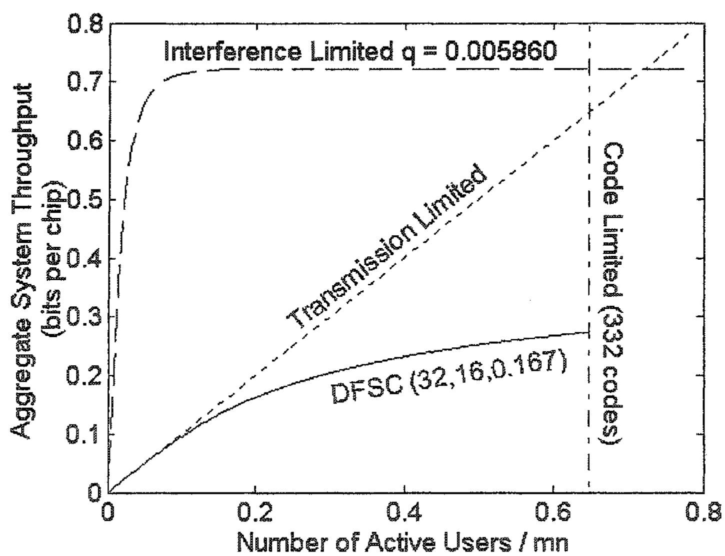

Fig. 5.11 DFSC capacity for DFSC(32,16,0.167).

5.4.2 BCDD Capacity

BCDD(32,16,0.156) is used for obtaining the BCDD capacity. In Fig. 5.12, we see that the BCDD capacity gradually approaches the interference-limited capacity as the number of users in the system increases. When 768 users are online, the BCDD capacity is about 0.55 bits per OCDMA chip. Comparing to the interference-limited capacity of 0.7 bits per chip, this corresponds to approximately a 1dB loss in the maximum throughput in terms of the number of user that can be supported after compensating for FEC. When the number of users in the network is small, the aggregate throughput remains bounded by the single bit transmission from each user.

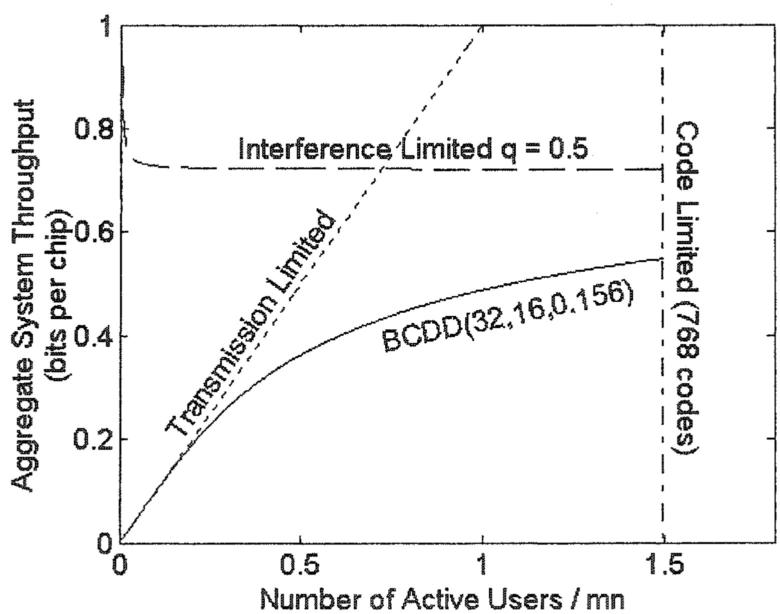

Fig. 5.12 BCDD capacity for BCDD(32,16,0.156).

5.5 Attempts to Reach the Channel Capacity

Due to the multiple advantages of BCDDs over DFSCs, we choose BCDDs in the attempts to reach the channel capacity. The objective is to find a coding scheme that can get close to the BCDD capacity with a BER below 10^{-9}. For channel coding, a serial concatenation of turbo codes and Reed-Solomon codes is employed to bring the BER below 10^{-9} as shown in Fig. 5.13. The reason for this comes from the fact that it is difficult to achieve performance near 10^{-9} using turbo codes unless an extremely long interleaver is used in the system. However, turbo codes can improve system performance when the original BER is as high as 10^{-1}; Reed-Solomon codes cannot achieve such coding gain. On the contrary, Reed-Solomon can lower the BER to virtually any value due to the inherent mathematical construction of the code.

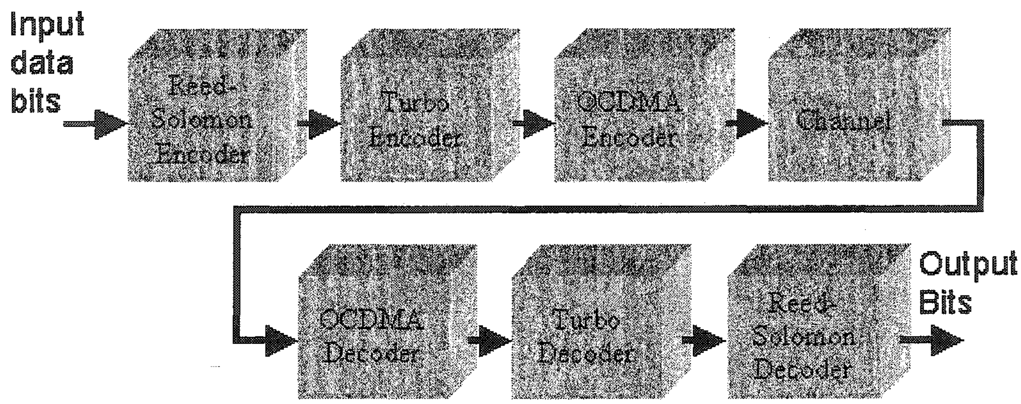

Fig. 5.13 Channel coding strategy for BCDD.

As discussed in Section 2.4.1, RS(255,239) maps a channel with a BER of 3.5×10^{-4} to 10^{-9}, and RS(255,223) maps a channel with a BER of 1.6×10^{-3} to 10^{-9}. Hence, it is desired to find a turbo code that can lower the BER to those values to meet the objective.

For turbo code, we use the original rate ½ turbo coding scheme proposed by Berrou *et al.* [65]. A 16-state recursive systematic code with generator (37, 21) is used for the convolutional encoder. A packet length of 10,000 bits with an srand interleaver is employed. We use the BCJR algorithm to perform turbo decoding. For the channel, discrete interference is generated with respect to the pmf of the MAI that is present in the system. The Gaussian approximation is assumed to estimate the soft output of the OCDMA decoder. A Monte-Carlo simulation with 100 packets of 10,000 bits each is done to obtain the BER performance. In Fig. 5.14(a), the BER performance of BCDD(32,16,0.156) is plotted as a function of the number of active users in the system. It is easy to see that after 8 iterations, this turbo code can lower the BER of a 400-user system to below 10^{-5}. For such

BER, as shown in Fig. 5.14(b), RS(255,239), which has a rate of 0.937, can be applied to further lower the BER to meet the benchmark specification.

With respect to the channel capacity, 400 users in a system that employs 32 wavelengths and 16 time chips with a concatenation of FEC at rate ½ and 0.937 corresponds to an aggregate throughput of 0.366 bits per OCDMA chip. For 400 users, the BCDD capacity is 0.446 bits per OCDMA chip. Our result corresponds to 0.86dB from the capacity limit. This result corresponds to the result obtained by Berrou. If each user transmits at OC-12 rate (622Mbps, chip rate at 9.95Gbps), this corresponds to an aggregate throughput of 117Gbps after compensating for FECs.

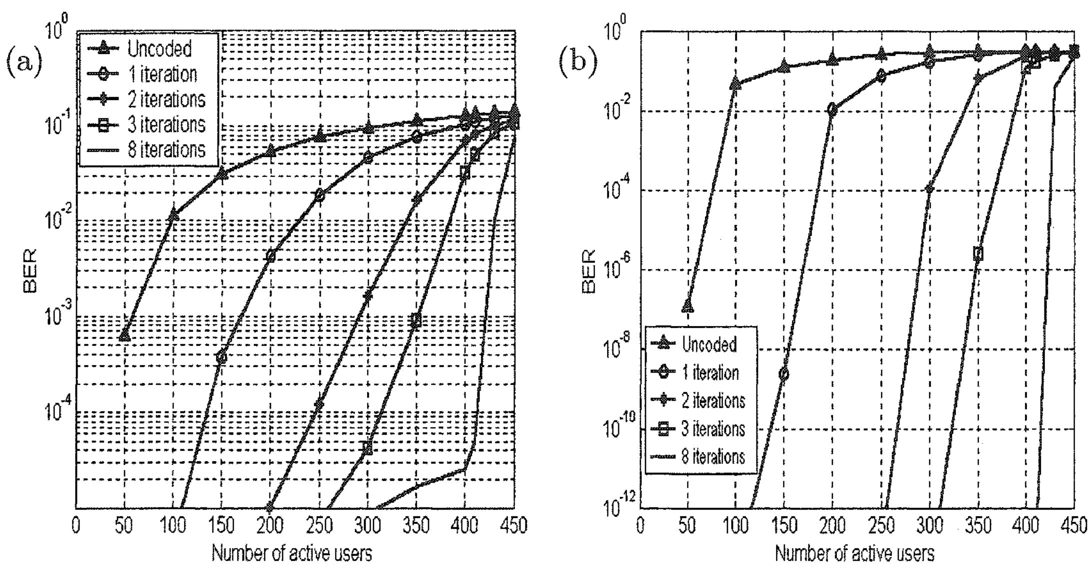

Fig. 5.14 BER performance of BCDD(32,16,0.156) as a function of active users using (a) Berrou's turbo code with rate 1/2, and srand interleaver of length 10000 bits; (b) Berrou's turbo code with RS(255,239).

Fig. 5.15 shows the BER of the same system as a function of the number of iterations. With 200 users, 3 iterations are required to lower the BER below 10^{-5}. However, for 400 users, it requires 8 iterations to achieve such performance. For this particular packet length and interleaver, the error floor occurs near 10^{-5}, meaning that this turbo code cannot push BER beyond this point.

Using the same turbo code scheme without puncturing, a rate 1/3 code is used to see the effect of the additional overhead on the BER performance. In Fig.

5.16, 700 users can be supported with a BER below 10^{-9} after 8 iterations, which is beyond the code size of 512 (32 wavelengths and 16 time chips). When used with RS(255,239), this corresponds to an aggregate throughput of 0.42 bits/chip, which is 1dB away from the BCDD capacity of 0.53 bits/chip at 700 users. If each user transmits at OC-12 rate, this corresponds to an aggregate throughput of 136Gbps after compensating for FECs.

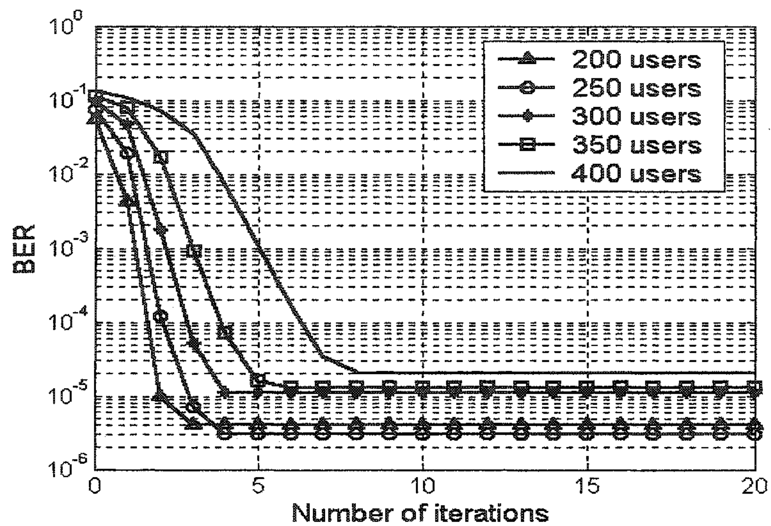

Fig. 5.15 BER as a function of the numbers of iterations for different numbers of active users.

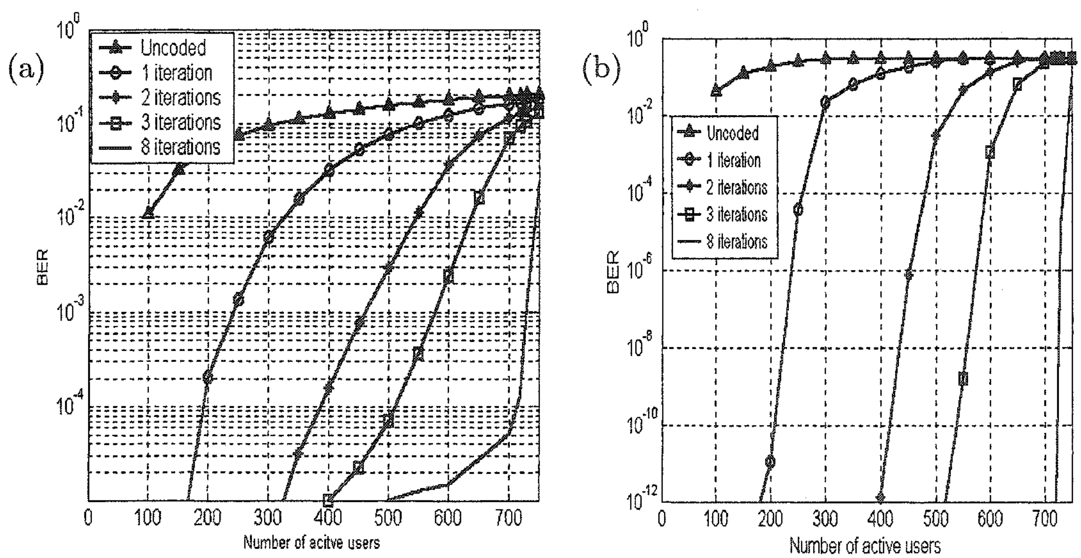

Fig. 5.16 BER performance of BCDD(32,16,0.156) as a function of active users using (a) Berrou's turbo code with rate 1/3, and srand interleaver of length 10000 bits; (b) Berrou's turbo code with RS(255,239).

5.6 Chapter Summary

In this chapter, we have obtained the chip synchronous (bit asynchronous) capacity for OCDMA under three scenarios: interference-limited transmission, interference with AWGN noise impaired transmission and a Gaussian approximation for the MAI. Empirically, we observe that input probability $q = 0.5$, the aggregate OCDMA throughput asymptotically approaches about 0.7 bits per chip as the number of users increases. Furthermore, equiprobable signaling can provide the best performance when the signal power is small compared to the channel noise. Moreover, the channel throughputs obtained from Gaussian approximation and from the exact model have very similar results. These results hint that Berrou's turbo code for AWGN channel [65] can possibly be employed to improve the OCDMA system performance under the interference-limited scenario. When this turbo code and RS(255,239) are used with BCDD(32,16,0.156), we were able to accommodate 450 users with an aggregate channel code rate of 0.4685, which corresponds to 0.366 bits/chip, or 117Gbps using OC-12 transmission (chip rate at 9.95Gbps). Alternatively, 700 users (out of a code size of 512) can be supported with an aggregate channel code rate of 0.3123, which corresponds to 0.42 bits/chip, or 136Gbps using OC-12 transmission. These results are less than 1dB away from the code-specific capacity for BCDD.

Chapter 6 Conclusion

6.1 Summary of Presented Work

This thesis has explored the design of spreading sequences for 2-dimensional (2D) wavelength-time Optical Code-Division Multiple Access for systems that employ direct detection and differential detection. Two new code families were presented: Depth First Search Codes (DFSC) and Balanced Codes for Differential Detection (BCDD). In order to form a basis of comparison and to get an idea of how much improvement one can expect from an asynchronous OCDMA system, the information theoretical capacity limit was obtained by modeling the channel in a single-user detection environment. This result was used to compare the performance of DFSC, BCDD and other previously proposed OCDMA systems to the capacity limit. BCDD clearly outperforms all other schemes, but it still requires clever channel coding in order to approach the capacity.

In direct detection, DFSC was introduced to generate low weight spreading sequences with multiple pulses per row (MPPR) and multiple pulses per column (MPPC) that have a maximum auto-correlation side lobe and cross-correlation of one. DFSC achieves a similar bit error rate (BER) performance as other 2D wavelength-time codes, but it can generate significantly more spreading sequences. This increase in the cardinality of codes is important when forward error correction (FEC) is applied. Furthermore, DFSC suggests that it is better to design spreading sequences with a high wavelength to time-chip ratio, since asynchronism of a wavelength-time OCDMA system only occurs in the time domain. Sequences designed with high wavelength to time-chip ratio can generate more codes for a given code size and Hamming weight, and are more suitable for use in high-speed optical communication systems.

BCDD was developed with a new set of constraints that take advantage of the antipodal signaling strategy enabled by optical balanced receiver. Specifically, it transmits complementary signals with a Hamming weight that is half of the code size for the "1" and "0" bits, and it further allows the auto- and cross-correlation constraints to vary. By choosing suitable parameters, BCDD can support almost twice the number of users at BER below 10^{-9} compared to systems proposed in the current literature. It can also generate a large number of spreading codes, so that FEC can be applied for further improvement of the system performance. As in the case of DFSC, BCDD should be designed with high wavelength to time-chip ratios.

In modeling the asynchronous OCDMA channel, it is found that the capacity decreases as the number of users increases in the system. For the interference-limited case, 0.7288 bits per OCDMA chip can be supported theoretically when 50 users are online. For a noisy system, it has been shown that a system with a high number of users is more tolerant to noise, since the noise is less relevant compared to the effects of interference, and the channel remains interference-limited. This implies that OCDMA is stable, even when signal power is low compared to the noise level. Finally, it has also been shown that the simplification obtained by using Gaussian approximation to the MAI can be used to approximate the OCDMA channel. With Berrou's turbo code of rate 1/3 and RS(255,239), BCDD(32,16,0.156) can accommodate 700 users with BER below 10^{-9}, which is beyond the code size of 512. After compensating for the FEC overheads, this system can support an aggregate throughput of 0.42 bits per OCDMA chip. This corresponds to a throughput of 136Gbps when 32 wavelengths and pulse duration of 100ps are used by the OCDMA system.

6.2 Future Research Directions

6.2.1 Enhanced Coding Strategy for OCDMA

Two aspects can be considered for the coding strategy for OCDMA: the improvement in the design of OCDMA spreading sequences and the proper use of channel coding. In this thesis, BCDD has defined a new set of constraints for generating 2D wavelength-time OCDMA codes with good BER performance. A greedy algorithm is implemented to generate the suitable codes. It is conceivable to use either an analytic technique or a more systematic algorithm to generate BCDD, thus obtaining a larger code set using the same constraints. The performance of such codes will be similar to the performance presented in this thesis, as the codes satisfy the same construction constraints. However, the extra codes generated will give more room for performance gain by the application of FEC.

Currently, using Berrou's turbo code, it is possible to achieve close to 0.8dB from the BCDD capacity. However, when the number of active users in the network is small, the BCDD capacity is limited by the maximum transmission of 1 bit per symbol interval for each user; hence, the BCDD capacity is several dB away from the ultimate OCDMA capacity. In particular, we would like to explore the possibility of removing the transmission-limited capacity of an OCDMA system: when the number of users on the network is small, how can a user transmit more than one bit in a single bit interval? Other challenges include the design of high rate (low redundancy) channel codes that can achieve this with minimal delay.

6.2.2 Multi Access Interference Cancellation and Detection

The performance of an OCDMA system is primarily limited by the MAI. However, unlike noise that is statistically independent from the received signal, MAI is governed by the cross-correlation from the different users. This suggests that something can be done to reduce its effect. In Fig. 6.1, MAI cancellation is shown in vector form. Since the original user and interfering signal do not have orthogonal spreading sequences, we can estimate and cancel the amount of correlation between the desired and interfering signal. In a noiseless environment, this method can optimize the signal-to-interference ratio, thus improving the BER performance at the receiver.

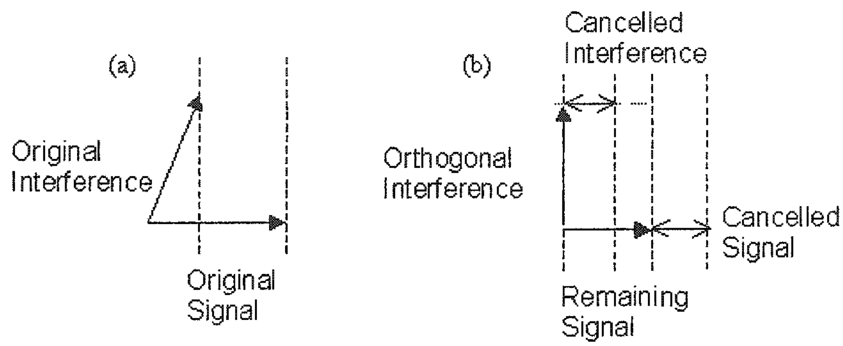

Fig. 6.1 Signal vector representation for MAI cancellation: (a) before cancellation; (b) after cancellation.

Example

Assume that three users are trying to transmit information in an interference-limited OCDMA system, let the cross-correlation between each user pair u and v be $\rho_{u,v} = \langle \mathbf{s}_u, \mathbf{s}_v \rangle$, $u \neq v$. When 3 users are transmitting, the received signal is $\mathbf{r} = b_1\mathbf{s}_1 + b_2\mathbf{s}_2 + b_3\mathbf{s}_3$. We modify the matched filter to be a linear combination of the input signal. The output for user 1 is then

$$\begin{aligned} out_1 &= \langle \mathbf{r}, a_1\mathbf{s}_1 + a_2\mathbf{s}_2 + a_3\mathbf{s}_3 \rangle \\ &= b_1(a_1 + a_2\rho_{12} + a_3\rho_{13}) + b_2(a_1\rho_{12} + a_2 + a_3\rho_{23}) + b_3(a_1\rho_{13} + a_2\rho_{13} + a_3) \end{aligned} \quad (6.1)$$

For cancelling the interference caused by users 2 and 3, one may set the first term in the above expression to one and the rest to zero:

$$\begin{bmatrix} 1 & \rho_{12} & \rho_{13} \\ \rho_{12} & 1 & \rho_{23} \\ \rho_{13} & \rho_{23} & 1 \end{bmatrix} \begin{bmatrix} a_1 \\ a_2 \\ a_3 \end{bmatrix} = \begin{bmatrix} 1 \\ 0 \\ 0 \end{bmatrix} \quad (6.2)$$

Solving the above matrix results in matched filter coefficients that can eliminate the MAI.

When noise is presented in the system, other optimization techniques have been developed for the wireless CDMA system. Namely, we can employ Minimum Mean Square Error (MMSE) and Minimum Variance Distortionless Response (MVDR) [83]-[84]. These two methods produce very similar results, differing only with a scalar factor. Basically, MMSE tries to minimize $E[|\mathbf{w}^T\mathrm{r}-\mathrm{b}_o|^2]$, and MVDR tries to find the vector $\mathbf{w}$ such that the output variance is minimized subject to $\mathbf{w}^T\mathbf{s}_1 = 1$. For MMSE, using results from adaptive filter theory, $\mathbf{w} = R^{-1}\mathbf{s}_1$ where $R = SS^T + \sigma^2 I$ is the input correlation matrix, $S = [\mathbf{s}_1,\ldots,\mathbf{s}_k]$ is the matrix of spreading sequences, and σ^2 is the variance of the noise. MVDR has similar results, but with an additional scaling factor.

The challenge for applying MAI cancellation in OCDMA resides in the implementation, and the need to deal with overloaded systems where the number of active users is beyond the number of dimensions in the transmission signal vector space. One must consider whether the interference cancelling operation should be conducted in the optical or electrical domain. This will have major implications on the speed and complexity of detection. Also, due to asynchronism, the autocorrelation matrix R will evolve over time. Techniques such as Least Mean Square (LMS) [84] estimation may be used for such purposes.

In addition to multi-user cancellation, one may consider the use of multiuser detection (MUD). Depending on the network topology, multiple users may be required to communicate with the central station. In such case, MUD may be employed to improve the system performance. Many MUD techniques have been developed in the context of wireless mobile communications. Some examples are the decorrelator [83], the MMSE [84] and the decision feedback receiver [85]. Basically, in the wireless context, these techniques required the use of matched filtering at the chip level for each actively transmitted user, and a linear transformation W is conducted before the decision is made. For the decorrelator, $W = (S^TS)^{-1}$ is the matrix inversion of the signature cross-correlation matrix; for the MMSE, $W = (S^TS+\sigma^2 I)^{-1}$. $S = [s_1,\ldots,s_k]$ is the matrix of spreading sequences, and σ^2 is the variance of the noise. For the decision feedback receiver, the Cholesky decomposition is done to the cross-correlation matrix, and outputs are obtained one after another.

According to information theory, the multiuser detector can achieve a higher capacity than SUD. Fig. 6.2(a) shows the equivalent signle user channel for 2-user binary erasure multiple access channel, and Fig. 6.2(b) shows the capacity region of such channel. For MUD, a capacity of two-user OCDMA channel is 1.5 bits per OCDMA chip. The challenge for implementing MUD resides in its complexity.

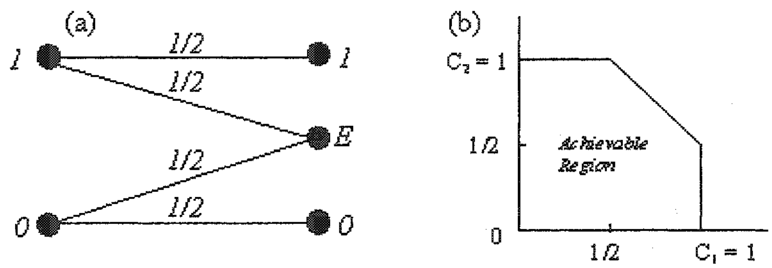

Fig. 6.2 Multiuser multiple access channel (a) channel model (b) capacity region [58]

6.2.3 Synchronous and Fully Asynchronous OCDMA Capacity

OCDMA has always been credited for its ability to accommodate asynchronous traffic among different users. However, the asynchronous channel capacity is only about 0.7 bits per OCDMA chip. Asynchronism has caused the design of orthogonal spreading sequences to be difficult. If synchronism is allowed, it is possible to increase the channel capacity. For instance, if a Hadamard spreading sequence [1] is employed, the interference-limited throughput of the system is at most 1 bit per OCDMA chip. It is interesting to find the Shannon capacity for synchronous OCDMA systems. It may be possible that, when proper coding is used, OCDMA can support error-free traffic beyond 1 bit per OCDMA chip. The challenge would be also to develop synchronization techniques that are robust to network changes, and that minimizes the use of network resources.

Instead of synchronization, one may take advantage of the asynchronism of the OCDMA channel one step further. In the analysis, if we remove the assumption of chip synchronization, we can technically use this additional asychronism to create parallel channel for each user chip transmitted. Fig. 6.3(a) diagrammatically shows this effect when two users are actively transmitting, and Fig. 6.3(b) shows the simplified channel model for this asynchronous system using SUD when memory between consecutive interference chips is ignored. A more detailed technique for analyzing the capacity of such symbol-asynchronous channel can be found in [71].

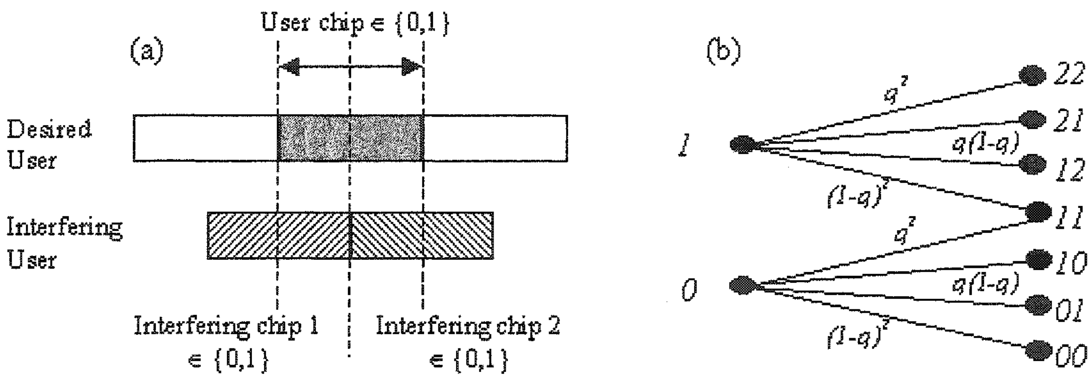

Fig. 6.3 Two-user fully asynchronous OCDMA model (a) physical meaning (b) channel model.

For a two-user system, this model gives an upper bound capacity of 1.5 bits per OCDMA chip in a noiseless environment. The challenge for achieving this fully asynchronous OCDMA system is the ability to sample signals at high speeds. Furthermore, signal processing will need to occur at sub-chip rate. However, this opens the possibility of transmitting signals beyond 1 bit per OCDMA chip.

Appendix A – Reed Solomon Codes

The encoding and decoding procedures of Reed-Solomon codes are presented based on the exposition in [72].

Encoding

For simplicity, assume a double symbol error correcting Reed-Solomon code RS(7,3). The generator polynomial is

$$\begin{aligned}\mathbf{g}(X) &= (X-\alpha)(X-\alpha^2)(X-\alpha^3)(X-\alpha^4) \\ &= \alpha^3+\alpha^1X+\alpha^0X^2+\alpha^3X^3+X^4\end{aligned} \qquad (\text{A.3})$$

Mathematically, for a message $\mathbf{m}(X)$, stored parity symbol $\mathbf{p}(X)=X^{n-k}\mathbf{m}(X) \bmod \mathbf{g}(X)$, the codeword can be described by the polynomial $\mathbf{U}(X)=\mathbf{p}(X)+X^{n-k}\mathbf{m}(X)$. The resulting codeword yields zero for any roots in $\mathbf{g}(X)$, thus $\mathbf{U}(\alpha)=\mathbf{U}(\alpha^2)=\mathbf{U}(\alpha^3)=\mathbf{U}(\alpha^4)=\mathbf{0}$.

Using linear feedback shift registers (LFSR), the Reed-Solomon encoder can be implemented as shown in Fig. A.1. All multiplications and additions are done in $GF(2^3)$ (3 bits at a time).

The procedure for encoding is listed below:

1. Switch 1 is closed during the first 3 clock cycles to shift message symbols into 4 registers. While doing so, switch 2 is in the up position, so that the message symbols are directly sent to the output.

2. After 3 clock cycles, switch 1 is opened and switch 2 moved to the down position. The stored parity symbols in the registers are flushed to the output in the following 4 clock cycles.
3. The process is repeated for the consecutive packets.

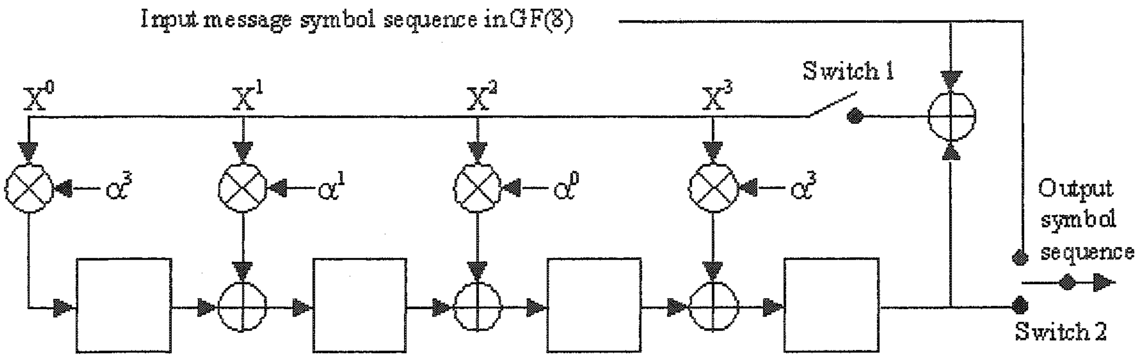

Fig. A.1 LFSR encoder for RS(7,3).

Decoding

Continuing the example above, assuming errors occur in the transmission so that the receive signal **r**(X) = **U**(X) + **e**(X) where **e**(X) is the error pattern. The decoding process requires the followings:

1. Compute the syndrome $S_j = \mathbf{r}(\alpha^j) = \mathbf{e}(\alpha^j)$ for $j = 1,2,3,4$.
2. If non-zero syndrome vector is computed, use the error locator polynomial $\Lambda(X) = 1 + \sum_{j=1}^{v} \Lambda_j X^j$, $v \leq 2$ (maximum correctable error in this example is 2) so that $\begin{bmatrix} S_1 & S_2 \\ S_2 & S_3 \end{bmatrix}\begin{bmatrix} \Lambda_1 \\ \Lambda_2 \end{bmatrix} = \begin{bmatrix} -S_3 \\ -S_4 \end{bmatrix}$ is largest dimensioned matrix that has a non-zero determinant.
3. The roots of $\Lambda(X)$ are the reciprocals of the error locations. Let $\beta_l = 1/\alpha^{j_l}$ where $l = 1,\ldots,\Psi$ and Ψ is the number of identified errors. For $\Psi = 2$, find error value e_l using $\begin{bmatrix} \beta_1 & \beta_2 \\ \beta_1^2 & \beta_2^2 \end{bmatrix}\begin{bmatrix} e_1 \\ e_2 \end{bmatrix} = \begin{bmatrix} S_1 \\ S_2 \end{bmatrix}$.
4. Compute the error polynomial $\mathbf{e}(X) = \sum_{l=1}^{\Psi} e_l X^{j_l}$ and $\hat{\mathbf{U}}(X) = \mathbf{r}(X) + \mathbf{e}(X)$.

Appendix B – Turbo Codes

The encoding and decoding procedures for turbo code [65] is described in this appendix section. For decoding, the BCJR algorithm is also described [73].

Encoding

A parallel-concatenated turbo code is composed of two identical convolutional encoders (output **s** and **t**) separated by an interleaver (π) and systematic information sequence (output **r**). Fig. B.1 shows diagrammatically the composition of a turbo encoder.

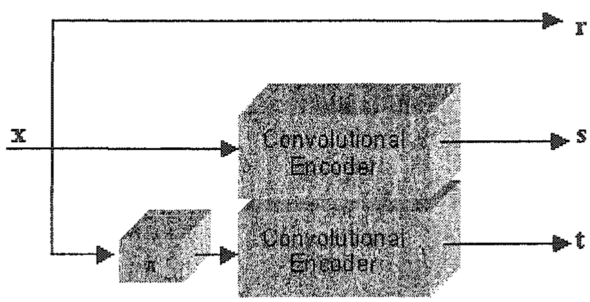

Fig. B.1 Turbo encoder.

For a convolution encoder, the original turbo code by Berrou [65] employs a (37,21) recursive systematic code in octal representation. This is shown in Fig. B.2.

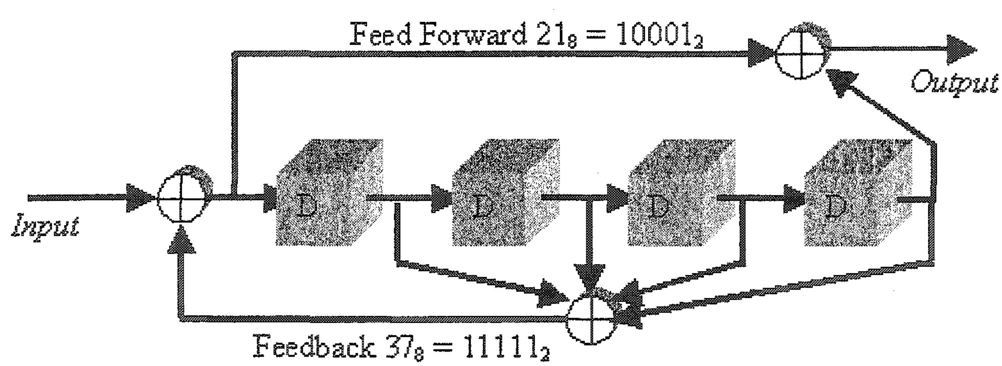

Fig. B.2 (37,21) recursive systematic code convolutional encoder.

Decoding and BCJR Algorithm

Essentially, the decoding of a turbo code involves an iterative process that uses two soft decision convolutional decoders. This process is achieved by exchanging extrinsic information $\mathbf{z}_i$ and $\mathbf{w}_i$ at iteration i, and using algorithm such as BCJR or SOVA. Only the BCJR algorithm is described in this appendix. Diagrammatically, the turbo code decoder is shown in Fig. B.3.

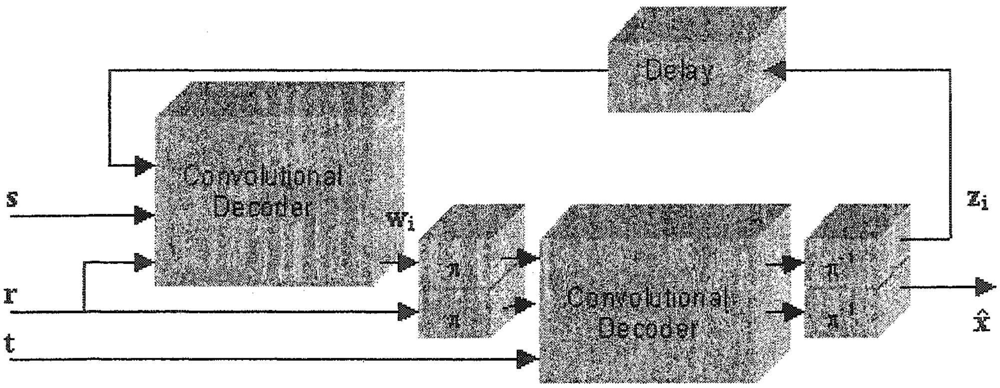

Fig. B.3 The iterative turbo decoder.

The key to understand the BCJR algorithm involves the estimation of the *a posteriori* probabilities using the trellis structure. Specifically, the trellis can be viewed as a Markov source with M distinct states, and let S_t denote the state at time t. Using the knowledge of the received sequence $Y_1^\tau = Y_1, Y_2, \ldots, Y_\tau$ (this may be $\underline{s}$ or $\underline{t}$ depending on the decoder), the quantity γ_t is defined to denote the sum of all the weighted branches going from state m' at time t-1 to state m at time t:

$$\gamma_t(m',m) = \Pr\{S_t = m; Y_t \mid S_{t-1} = m'\} = p_t(m \mid m')q_t(Y \mid m',m) \qquad (\text{B.4})$$

where p_t denotes the transition probability of the trellis governed by the extrinsic information ($\underline{z}_i$ or $\underline{w}_i$) and the systematic message bit ($\underline{r}$), and q_t denotes the probability of the observed output code bit resulting from the state transition in the trellis. Furthermore, two new quantities are defined:

$$\alpha_t(m) = \Pr\{S_t = m; Y_1^t\} = \sum_{m'} \alpha_{t-1}(m')\gamma_t(m',m) \qquad (\text{B.5})$$

$$\beta_t(m) = \Pr\{Y_{y+1}^{\tau} \mid S_t = m\} = \sum_{m'} \beta_{t+1}(m')\gamma_{t+1}(m',m) \tag{B.6}$$

Physically, α_t denotes the sum of all weighted branches coming from time 0 and state 0 into state m at time t. β_t denotes the sum of all weighted branches coming from time τ, time at the last trellis stage, and state 0 into state m at time t. Finally, we further employ matrices to represent the three quantities α, β and γ.

$$\alpha_t = [\alpha_t(0) \quad \alpha_t(1) \quad \cdots \quad \alpha_t(M-1)] \tag{B.7}$$

$$\beta_t = [\beta_t(0) \quad \beta_t(1) \quad \cdots \quad \beta_t(M-1)]^T \tag{B.8}$$

$$\gamma_t = \begin{bmatrix} \gamma_t(0,0) & \gamma_t(1,0) & \cdots & \gamma_t(M-1,0) \\ \gamma_t(0,1) & \gamma_t(1,1) & \cdots & \gamma_t(M-1,1) \\ \vdots & \vdots & \ddots & \vdots \\ \gamma_t(0,M-1) & \gamma_t(1,M-1) & \cdots & \gamma_t(M-1,M-1) \end{bmatrix} \tag{B.9}$$

From the definitions, it is easy to observe that

$$\alpha_0 = [1 \quad 0 \quad 0 \quad \cdots \quad 0] \tag{B.10}$$

$$\beta_\tau = [1 \quad 0 \quad 0 \quad \cdots \quad 0]^T \tag{B.11}$$

Using the above initial conditions, the BCJR algorithm computes γ_t and α_t as the decoder receives data. When the whole encoded sequence is received, the decoder recursively calculates β_t. Once all the matrices have been calculated, the BCJR algorithm obtains the probabilities of the message bits using the following:

$$\Pr\{X_{t-1} = 0 \mid \underline{r}, \underline{s}, \underline{z}\} = \frac{\alpha_{t-1}\gamma_t^0\beta_t}{\alpha_{t-1}\gamma_t\beta_t} \tag{B.12}$$

$$\Pr\{X_{t-1} = 1 \mid \underline{r}, \underline{s}, \underline{z}\} = \frac{\alpha_{t-1}\gamma_t^1\beta_t}{\alpha_{t-1}\gamma_t\beta_t}, \tag{B.13}$$

for the top decoder where $\Pr\{X_{t-1} = 1 \mid \underline{r}, \underline{s}, \underline{z}\}$ is the conditional probability that the message bit with index t-1 is equal to one. In the equation, γ_t^1 is obtained by masking the γ_t matrix, so it only contains the transitions resulting from the message bit equal to one. Similarly, γ_t^0 is obtained by masking the γ_t matrix, so it only contains the transitions resulting from the message bit equal to zero. For the bottom decoder, everything is the same except replacement of $\underline{s}$ by $\underline{t}$ and $\underline{z}$ by $\underline{w}$.

Once the probability estimate is obtained, the soft decision output will be sent to the next stage of the iterative decoder for further processing. After a specified number of iterations, decisions are formed on the message bits by thresholding the soft outputs of the last decoder.

References

[1] T. S. Rappaport, *Wireless Communications: Principles and Practice.* Upper Saddle River, New Jersey: Prentice Hall, 2002.

[2] A. Leon-Garcia and I. Widjaja, *Communication Networks: Fundamental Concepts and Key Architectures.* Toronto, Ontario: McGraw Hill, 2000.

[3] J. A. Salehi, "Emerging optical code-division multiple access communication system," *IEEE Network*, vol. 3, pp. 31-39, March 1989.

[4] L. L. Peterson and B. S. Davie, *Computer Networks: A Systems Approach.* Beijing: China Machine Press, 2001.

[5] R. M. H. Yim, L. R. Chen, and J. Bajcsy, "Design and performance of 2D codes for wavelength-time optical CDMA," *IEEE Photon. Technol. Lett.*, vol. 14, pp. 714-716, May 2002.

[6] R. M. H. Yim, L. R. Chen and J. Bajcsy, "2D wavelength-time codes for optical code-division multiple-access with differential detection," presented at *5th Int. Conf. on Application of Photon. Technol.*, Quebec City, June 2002.

[7] R. M. H. Yim, J. Bajcsy and L. R. Chen, "A new family of 2D wavelength-time codes for optical CDMA with differential detection," submitted to *IEEE Photon. Technol. Lett.*

[8] R. M. H. Yim, J. Bajcsy and L. R. Chen, " On the capacity limit of asynchronous OCDMA with single user detection," *Proc. 21st Biennial Symp. on Commun.*, pp. 485-489, June 2002.

[9] A. A. Shaar and P. A. Davis, “Prime sequences: quasi-optimal sequence for Or channel code division multiplexing,” *Electron. Lett.*, vol. 19, pp. 888-889, October 1983.

[10] S. V. Maric, M. D. Hahm and E. L. Titlebaum, “Construction and performance analysis of a new family of optical orthogonal codes for CDMA fiber-optic networks,” *IEEE Trans. Commun.*, vol. 43, pp. 485-489, February 1995.

[11] D. Zaccarin and M. Kavehrad, “An optical CDMA system based on spectral encoding of LED,” *IEEE Photon. Technol. Lett.*, vol. 4, pp. 479-482, April 1993.

[12] L. Chen, S. Benjamin, P. Smith and J. Sipe, “Ultrashort pulse reflection from fiber gratings: A numerical investigation,” *IEEE J. Lightwave Technol.*, vol. 15, pp. 1503-1512, August 1997.

[13] A. Kirk, *Course notes for 304-527 Optical Engineering,* McGill University, 2002.

[14] A. Gameiro, “Synchronous and quasisynchronous optical CDMA with balanced complementary receivers,” *IEE Procs. Optoelectronics*, vol. 147, pp. 370-376, October 2000.

[15] S. Tamura, S. Nakano and K. Okazaki, “Optical code-multiplex transmission by Gold sequences,” vol. 3, pp.121-127, February 1983.

[16] F. R. K. Chung, J. A. Salehi and V. K. Wei, “Optical orthogonal codes: desing, analysis and applications,” *IEEE Trans. Inform. Theory*, vol. 35, pp. 595-604, May 1989.

[17] J. A. Salehi, “Code division multiple-access techniques in optical fiber networks – Part I: Fundamental principles,” *IEEE Trans. Commun.*, vol. 37, pp. 824-833, August 1989.

[18] J. A. Salehi and C. A. Brackett, “Code division multiple-access techniques in optical fiber networks – Part II: System performance analysis,” *IEEE Trans. Commun.*, vol. 37, pp. 834-842, August 1989.

[19] H. Chung and P. V. Kumar, "Optical orthogonal codes – new bounds and an optimal construction," *IEEE Trans. Inform. Theory*, vol. 36, pp. 866-873, July 1990.

[20] W. C. Kwong, P. A. Perrier and P. R. Prucnal, "Performance comparison of asynchronous and synchronous code-division multiple-access techniques for fiber-optic local area networks," *IEEE Trans Commun.*, vol. 39, pp. 1625-1634, November 1991.

[21] P. R. Prucnal, M. A. Santoro and T. R. Fan, "Spread spectrum fiber-optic local area network using optical processing", *IEEE J. Lightwave Technol.*, vol. LT-4, pp.547-554, May 1986.

[22] M. Y. Azizoglu, J. A. Salehi and Y. Li, "Optical CDMA via temporal codes," *IEEE Trans. Commun.*, vol. 40, pp. 1162-1170, 1992.

[23] S. V. Maric, "New family of algebraic designed optical orthogonal codes for use in CDMA fibre-optic networks," *Electron. Lett.*, vol. 29, pp. 538-539, March 1993.

[24] S. V. Maric, Z. I. Kostic, E. L. Titlebaum, "A new family of optical code sequences for use in spread-spectrum fiber-optic local area networks," *IEEE Trans. Commun.*, vol. 41, pp. 1217-1221, 1993.

[25] A. M. Weiner, J. P. Heritage and J. A. Salehi, "Encoding and decoding of femtosecond pulses," *Opt. Lett.*, vol. 13, pp. 300-302, April 1988.

[26] J. P. Heritage, A. M. Weiner and R. N. Thurston, "Synthesis of phase coherent, picosecond optical square pulses," *Opt. Lett.*, vol. 10, p. 609, 1985

[27] A. M. Weiner, J. P. Heritage and R. N. Thurston, "Analysis of picosecond pulse shape synthesis by spectral masking in a grating pulse compressor," *IEEE J. Quantum Electron.*, vol. QE-22, p. 682, 1986.

[28] J. A. Salehi, A. M. Weiner and J. P. Heritage, "Coherent ultrashort light pulse code-division multiple access communication systems," *IEEE J. Lightwave Technol.*, vol. 8, pp. 478-491, March 1990.

[29] R. A. Griffin, D. D. Sampson and D. A. Jackson, "Modification of optical coherence using spectral phase coding for use in photonic code-division

multiple access systems," *Electron. Lett.*, vol. 29, pp. 2214-2216, December 1993.

[30] K. Kitayama, "Novel spatial spread spectrum based fiber optic CDMA networks for image transmission," *IEEE J. Select. Areas Commun.*, vol. 12, pp. 762-772, May 1994.

[31] G. C. Yang and W. C. Kwong, "Two-dimensional spatial signature patterns," *IEEE Trans. Commun.*, vol. 44, pp. 184-191, February 1996.

[32] J. Hui, "Pattern code modulation and optical decoding – a novel code-division multiplexing technique for multifiber networks," *IEEE J. Select. Areas Commun.*, vol. 3, pp. 916-927, November 1985.

[33] E. Park, A. J. Mendez and E. M. Garmire, "Temporal/spatial optical CDMA networks – design, demonstration, and comparison with temporal networks," *IEEE Photonics Technol. Lett.*, vol. 4, pp. 1160-1162, October 1992.

[34] A. A. Hassan, J. E. Hershey and N. A. Riza, "Spatial optical CDMA," *IEEE J. Select. Areas Commun.*, vol. 3, pp. 603-613, April 1995.

[35] H. Fathallah, L. A. Rusch and S. LaRochelle, "Passive optical fast frequency-hop CDMA communications system," *IEEE J. Lightwave Technol.*, vol. 17, pp.397-405, March 1999.

[36] L. Tancevski and I. Andonovic, "Wavelength hopping/time spreading code division multiple access systems," *Electron. Lett.*, vol. 30, pp. 1388-1390, August 1994.

[37] K. Yu and N. Park, "Design of new family of two-dimensional wavelength-time spreading codes for optical code division multiple access networks," *Electron. Lett.*, vol. 35, pp.830-831, May 1999.

[38] J. Proakis, *Digital Communications.* New York: McGraw Hill, 1989.

[39] M. E. Maric and Y. L. Chang, "Pulse coding and coherent decoding in fibre-optic ladder networks," *Electron. Lett.*, vol. 25, pp. 1535-1536, October 1989.

[40] D. D. Sampson and D. A. Jackson, "Spread-spectrum optical fibre network based on pulse coherent correlation," *Electron. Lett.*, vol. 26, pp. 1550-1552, 1990.

[41] Y. L. Chang, "Fiber-optic ladder networks for inverse decoding coherent CDMA," *IEEE J. Lightwave Technol.*, vol. 10, pp. 1952-1962, December 1992.

[42] R. A. Griffin, D. D. Sampson, D. A. Jackson, "Optical phase coding for code-division multiple access networks," *IEEE Photon. Technol. Lett.*, vol. 4, pp. 1401-1404, December 1992.

[43] D. Zaccarin and M. Kavehrad, "Performance evaluation of optical CDMA systems using non-coherent detection and bipolar codes," *IEEE J. Lightwave Technol.*, vol. 12, pp. 96-105, January 1994.

[44] W. Huang, I. Andonovic and M. Tur, "Decision-directed PLL for coherent optical pulse CDMA systems in the presence of multiuser interference, laser phase noise, and shot noise," *IEEE J. Lightwave Technol.*, vol. 16, pp.1786-1794, October 1998.

[45] W. Huang, I. Andonovic and M. Nakagawa, "PLL performance of DS-CDMA systems in the presence of phase noise, multiuser interference, and additive Gaussian noise," *IEEE Trans. Commun.*, vol. 46, pp. 1507-1515, November 1998.

[46] W. Huang, M.H.M. Nizam, I. Andonovic and M. Tur, "Coherent optical CDMA (OCDMA) systems used for high-capacity optical fiber networks – system description, OTDMA comparison, and OCDMA/WDMA networking," *IEEE J. Lightwave Technol.*, vol. 18, pp. 765-778, June 2000.

[47] D. Zaccarin and M. Kavehrad, "New architecture for incoherent optical CDMA to achieve bipolar capacity," *Electron. Lett.*, vol. 30, pp. 258-259, February 1994.

[48] M. Kavehrad and D. Zaccarin, "Optical code-division-multiplexed systems based on spectral encoding of noncoherent sources," *IEEE J. Lightwave Technol.*, vol., 13, pp. 534-544, March 1995.

[49] L. Nguyen, T. Dennis, B. Aazhang and J. F. Young, "Experimental demonstration of bipolar codes for optical spectral amplitude CDMA communication," *IEEE J. Lightwave Technol.*, vol. 15, pp. 1647-1653, September 1997.

[50] T. Dennis and J. F. Young, "Optical implementation of bipolar codes," *IEEE J. Quantum Electron.*, vol. 35, pp. 287-291, March 1999.

[51] L. Nguyen, B. Aazhang and J. F. Young, "All-optical CDMA with bipolar codes," *Electron. Lett.*, pp. 469-470, March 1995.

[52] J. F. Huang and D. Z. Hsu, "Fiber-grating-based optical CDMA spectral coding with nearly orthogonal m-sequence codes," *IEEE Photon. Technol. Lett.*, vol. 12, September 2000.

[53] S. P. Wan and Y. Hu, "Two-dimensional optical CDMA differential system with prime/OOC codes," *IEEE Photon. Technol. Lett.*, vol. 13, pp. 1373-1375, December 2001.

[54] N. Karafolas, "Optical fiber code division multiple access networks: A review," *Opt. Fiber Technol.*, vol. 2, pp. 149-168, 1996.

[55] G. C. Yang and W. C. Kwong, "Two-dimensional spatial signature patterns," *IEEE Trans. Commun.*, vol. 44, pp.184-191, February 1999.

[56] S. Kim, K. Yu and N. Park, "A new family of space/wavelength/time spread three-dimensional optical code for OCDMA networks," *IEEE J. Lightwave Technol.*, vol. 18, pp.502-511, April 2000.

[57] C. E. Shannon, "A Mathematical theory of communication", *Bell System Technol. Journal*, vol. 27, pp. 379-423 and 623-656, 1948.

[58] T. M. Cover and J. A. Thomas, *Elements of Information Theory.* New York, New York: John Wiley and Sons, Inc., 1991.

[59] R. G. Gallager, *Information theory and reliable communication.* New York, New York: John Wiley and Sons, Inc., 1968.

[60] R. W. Hamming, "Error detecting and error correcting codes", *Bell System Technol. Journal*, vol. 29, pp. 147-160, 1950.

[61] I. S. Reed and G. Solomon, "Polynomial codes over certain finite fields," *J. SIAM*, vol. 8, pp. 300-304, June 1960.

[62] P. Elias, "Coding for noisy channels," *IRE Conv. Rec.*, vol. 3, pt. 4, pp.37-46, 1955.

[63] A. J. Viterbi, "Error bounds for convolutional codes and an asymptotically optimum decoding algorithm," *IEEE Trans. Inform. Theory*, vol. IT-13, pp. 260-267, April 1967.

[64] A. J. Viterbi, "Convolutional codes and their performance in communication systems," *IEEE Trans. Commun.*, vol. COM-19, pp. 751-772, October 1971.

[65] C. Berrou, A. Glavieux and P. Thitimajshima, "Near Shannon limit error-correcting coding and decoding: turbo-codes (1)", *Proc. of ICC '93*, Geneva, Switzerland, pp. 1064-1070, May 1993.

[66] International Telecommunication Union, ITU-T G.991.1, "High bit rate digital subscriber line (HDSL) tranceivers," http://www.itu.int/rec/recommendation.asp?type=products&lang=e&parent=T-REC-G.

[67] International Telecommunication Union, ITU-T G.992.1, "Asymmetrical digital subscriber line (ADSL) transceivers," http://www.itu.int/rec/recommendation.asp?type=products&lang=e&parent=T-REC-G.

[68] International Telecommunication Union, ITU-T G.975, "Forward error correction for submarine systems," http://www.itu.int/rec/recommendation.asp?type=products&lang=e&parent=T-REC-G.

[69] International Telecommunication Union, ITU-T G.709, "Interfaces for optical transport network (OTN)," http://www.itu.int/rec/recommendation.asp?type=products&lang=e&parent=T-REC-G.

[70] M. R. Dale and R. M. Galiardi, "Channel coding for asynchronous fiberoptic CDMA communications," *IEEE Trans. Commun.*, vol. 43, pp. 2485-2492, September 1995.

[71] S. Verdú, "The capacity region of the symbol-asynchronous Gaussian multiple-access channel," *IEEE Trans. Inform. Theory*, vol. 35, pp. 733-751, July 1989.

[72] B. Sklar, *Digital Communications: Fundamentals and Applications.* Upper Saddle River, New Jersey: Prentice Hall, 2001.

[73] L. Bahl, J. Cocke, F. Jelinek and J. Raviv, "Optimal decoding of linear codes for minimizing symbol error rate," *IEEE Trans. Inform. Theory*, vol. 20, pp. 278-284, March 1973.

[74] G. D. Forney Jr., "The Viterbi algorithm", *Proc. of IEEE.*, vol. 61, pp. 268-278, March 1973.

[75] J. Hagenauer and P. Hoeher, "A Viterbi algorithm with soft-decision outputs and its applications," *Proc. Global Telecommun. Conf.*, vol. 3, pp. 1680-1686, 1989.

[76] J. Y. Kim and H. V. Poor, "Turbo-coded optical direct-detection CDMA system with PPM modulation," *J. Lightwave Technol.*, vol. 19, pp. 312-323, March 2001.

[77] T. Ohtsuki and J. M. Kahn, "BER performance of turbo-coded PPM CDMA systems on optical fiber," submitted to *J. Lightwave Technol.*, 2002.

[78] J. Boutros, G. Caire, E. Viterbo, H. Sawaya and S. Vialle, "Turbo code at 0.03dB from capacity limit," *Proc. IEEE Int. Symp. on Inform. Theory*, Lausanne, p.56, July 2002.

[79] P. Azmi, M. Nasiri-Kenari and J. A. Salehi, "Low-rate super-orthogonal channel coding for fiber-optic CDMA communication systems," *IEEE J. Lightwave Technol.*, vol. 19, pp. 847-855, June 2001.

[80] P. Azmi, M. Nasiri-Kenari and J. A. Salehi, "Internally bandwidth efficient channel coding for fiber-optic CDMA communication systems with soft-input decoding," *Proc. of ICC '02*, New York, pp. 2922-2926, April-May 2002.

[81] E. Hewitt, "Introduction to forward error correction: Reed-Solomon and turbo product codes," Advanced Hardware Architectures, http://www.aha.com, 2001.

[82] G. M. Schneider and S. C. Bruell, *Concepts in Data Structures and Software Development.* St. Paul, MN: West Publishing Company, 1991.

[83] S. Verdu, *Multiuser Detection.* New York, NY: Cambridge University Press, 1998.

[84] S. Haykin, *Adaptive Filter Theory.* Upper Saddle River, New Jersey: Prentice Hall, 1996.

[85] Y. H. Li, M. Chen and S. X. Cheng, "Decision feedback partial parallel interference cancellation for DS-CDMA," *Proc. the 21st Century Military Commun. Conf.*, vol. 1, pp. 578-582, 2000.